Modelling and Simulation of Groundwater Flow and Radionuclide Transport in Aquifers of Dahomeyan System of the Accra Plains in Ghana

Kafui Tsoeke Agbevanu

Department of NUCLEAR ENGINEERING

GRADUATE SCHOOL OF NUCLEAR AND ALLIED SCIENCES

COLLEGE OF BASIC AND APPLIED SCIENCES

UNIVERSITY OF GHANA

MPhil

July, 2015

Modelling and Simulation of Groundwater Flow and Radionuclide Transport in Aquifers of Dahomeyan System of the Accra Plains in Ghana

A Thesis presented to the:

Department of NUCLEAR ENGINEERING
GRADUATE SCHOOL OF NUCLEAR AND ALLIED SCIENCES
COLLEGE OF BASIC AND APPLIED SCIENCES
UNIVERSITY OF GHANA

By

Kafui Tsoeke Agbevanu (ID No.:10008512)
BSc (Ghana), 1999

In partial fulfilment of the requirement for the award of the degree of

MASTER OF PHILOSOPHY

in

COMPUTATIONAL NUCLEAR SCIENCES AND ENGINEERING

July, 2015

DECLARATION

This is to certify that this thesis is the result of the research undertaken by KAFUI TSOEKE AGBEVANU towards the award of the Master of Philosophy in the Department of Computational Nuclear Sciences and Engineering, University of Ghana, Legon, under the supervision of DR. BARNABAS AMISIGO of Council for Scientific and Industrial Research, Ghana (CSIR) and DR. THOMAS TETTEH AKITI of Graduate School of Nuclear and Allied Sciences (GSNAS), University of Ghana, Legon.

I hereby declare that apart from references which have been duly acknowledged, this Thesis work is the result of my own research work and that no part of it has been presented for another degree in this University or elsewhere.

…….. DATE ……

KAFUI TSOEKE AGBEVANU

(**STUDENT**)

We hereby declare that the preparation and presentation of this thesis work were supervised in accordance with the guidelines on supervision of Thesis laid down by University of Ghana, Legon.

……..…. ……...……

DR. BARNABAS AMISIGO DR. THOMAS TETTEH AKITI

(**PRINCIPAL SUPERVISOR**) (**CO-SUPERVISOR**)

DATE …… DATE ……

DEDICATION

To My two Daughters, Selma and Sheena.

To My Motivators, Dr. W. K. Agbevanu and Mr. E. K. Agbevanu.

ACKNOWLEDGEMENTS

This thesis work benefited from knowledge, experience and guidance of my supervisors. I am grateful to Dr. B. Amisigo for his intellectual contributions, objectivity and criticisms in this research work. I sincerely thank Dr. T. T. Akiti for his immense contributions and planting in me this important intellectual journey. I very much appreciate the expert contributions in achieving this thesis work.

My special thanks go to Nana Prof. A. Ayensu Gyeabour I, for his excellent contributions and incessant guidance in the production of this thesis work and mapping my academic journey. I thank Prof. S. B. Dampare for the interest and assistance offered during this research work. I am indebted to Dr. E. Ampomah-Amoako, for his advice and the urge in the completion of this research.

Further, I am grateful to Dr. S. Y. Ganyaglo, Dr. W. A. Agyekum, Mr. E. T. Glover and Miss R. Tetteh for their support in data collection and readiness in supplying solutions to my questions. My thanks also go to Dr. S. Yamoah for assisting me in ANSYS FLUENT 13.0, and Dr. S. K. Debrah and Dr. V. Y. Agbodemegbe for their guidance and criticisms. I thank my colleagues, Francis, Sidique and Collins for their fruitful comments and friendship.

Most of all, I thank my father, Emmanuel; my siblings, Wisdom, Dzifa and Mawusi as well as my wife Patience, for their support, love, care and encouragement and for being inspirational in my life. Also, my appreciations go to all whose names were not mentioned and institutions (Ghana Atomic Energy Commission, Council for Scientific and Industrial Research, School of Nuclear and Allied Sciences, Community Water and Sanitation Agency and Abokobi Municipal Assembly) who in one way or the other supported me in the accomplishment of this thesis work.

TABLE OF CONTENTS

Titles **Pages**

LIST OF FIGURES

LIST OF TABLES

SYMBOLS

$\bar{v}_x$	Pore water flow rate in x direction
$\bar{C}$	Contaminant concentration that is sorbed
η_L	Longitudinal dispersivity
η_T	Transverse dispersivity
b	Aquifer thickness
C	Contaminant concentration dissolved
D	Domain
D*	Apparent diffusion coefficient of porous media
d/dt	Derivative with respect to time
d/dx	Derivative with respect to x direction
d/dy	Derivative with respect to y direction
dh/dx	Hydraulic gradient with respect to x-direction
dh/dy	Hydraulic gradient with respect to y-direction
dh/dz	Hydraulic gradient with respect to z-direction
d_{iiii}	Aquifer's dispersivity
Dij	Coefficient of dispersion
Do	Diffusion coefficient for aqueous solution
δp	Small change in pressure
δx	Small change in x
δy	Small change in y
$\delta \sigma_e$	Small change in stress-strain
g	Acceleration due to gravity
h	Total hydraulic head
K	Hydraulic conductivity

K_d	Equilibrium distribution coefficient (L^3/M)
k_f	Rate constant for forward reaction
k_r	Rate constant for reverse reaction
K_x	Hydraulic conductivity in the x direction
K_y	Hydraulic conductivity in the y direction
K_z	Hydraulic conductivity in the z direction
N	Natural recharge
n	porosity
^oC	Degree Celsius
P	Discharge through pumping
Q	Discharge rate
R	Artificial recharge
R_d	Retardation factor
S	Storativity
Sc	Specific capacity
Ss	Specific storage of an aquifer
T	Aquifer transmissivity
$T_{1/2}$	Half-life
T_x	Aquifer transmissivity in the x direction
T_y	Aquifer transmissivity in the y direction
T_z	Aquifer transmissivity in the z direction
V	Volume of the REV (control volume)
V_w	Fluid/water volume/ (void) in the REV
v_x	Apparent groundwater flow rate in the x-direction
v_y	Apparent groundwater flow rate in the y-direction

W_L	Weighting function
z	Elevation head
α	Expansion or compression of porous medium
β	Expansion or compression of fluid
Γ	Flow boundary
λ	Decay constant
μ	Dynamic viscosity of fluid
ν	Kinematic viscosity of fluid
ρ	Fluid mass density
P	Fluid pressure
ρ_b	Bulk density
Ψ	Pressure head

ABBREVIATIONS

AMA	Abokobi Municipal Assembly
CSIR	Council for Scientific and Industrial Research
CWSA	Community Water and Sanitation Agency
DS	Dahomeyan System
DWL	Dynamic Water Level
EPM	Equivalent Porous Medium
GAEC	Ghana Atomic Energy Commission
GEM	Ga East Municipality
GSD	Geological Survey Department
GWF	Groundwater Flow
IAEA	International Atomic Energy Agency
PDE	Partial Differential Equation
REV	Representative Elemental Volume
SNAS	School of Nuclear and Allied Sciences
SWL	Static Water Level
WHO	World Health Organization
ADDE	Advection-Dispersion-Decay Equation
BC	Boundary Condition
IC	Initial Condition
TS	Togo Series
GPS	Global Positioning System

ABSTRACT

Locating a suitable radioactive waste disposal site in the Dahomeyan System of the Accra Plains has become necessary in isolating radionuclide waste from the biosphere to reduce risk to human and environment. Radionuclide as leaked from canister into the groundwater is carried by groundwater through fractured domain in space and time lead to groundwater contamination that poses threat to humans and the environment. Previous researches carried out in the study area modelled radionuclide flow in unsaturated and saturated zones used published hydraulic properties. Modelling and simulation of groundwater flow and radionuclide transport in the Dahomeyan System was used to better understand the aquifer system. Detailed site characterisation was done as prerequisite for accurate modelling results using pumping test and borehole logs data. Effective porosity and hydraulic properties (e.g. T, K, S) were estimated using field methods. The flow path and flow rate were also determined for the domain. The groundwater flow was simulated using ANSYS FLUENT 13.0 software to validate the field flow rate estimated and the range of storativity values estimated for the domain. Analytical and numerical solutions developed for 1D ADDE were simulated using MATLAB R2013a codes. 2D ADDE solution was also simulated to show the behaviour of groundwater flow and radionuclide spread in aquifers of the domain. C-14 and Sr-90 contaminants simulations showed that for a simulation time far less than half-life of the radionuclide the error between analytical and numerical solutions are negligible. The flow path determined was in SSE direction and dispersion was faster initially transversally than longitudinally due to preferential flow paths. The low values of the hydraulic parameters determined qualify Accra Plains as a host rock for radionuclide waste repository especially where transmissivity and storativity values were smallest.

CHAPTER ONE

INTRODUCTION

This Chapter presents the background to the research including a general description of groundwater flow and radioactive contaminant transport in hard rock aquifers of the Accra Plains. An outline of the research problem statement, justification, goal and objectives, and scope of the study are presented.

1.1 Background of the Research

Radioactive wastes generated from nuclear research reactor, gamma irradiation facility, radiotherapy and nuclear medicine facilities in Ghana need to be safely managed [1]. As Ghana aspires to generate electricity from nuclear power, the radioactive waste from the nuclear reactor (spent fuel) cannot be avoided but need to be properly and safely managed or isolated from the biosphere. Spent fuel contains large amounts of fission products (90Sr and 137Cs) as part of the radioactive waste that undergo radioactivity to produce daughter elements [2].

The long-term solution to nuclear power generation is to permanently store nuclear waste generated safely in a borehole disposal system. The International Atomic Energy Agency (IAEA) promotes acceptance of some basic tenets on security and safety of human health and environment by all countries in radioactive waste management [3]. The radioactive waste generated consist of: (i) the low and intermediate level radioactive waste that need to be isolated permanently for hundreds of years from the biosphere, and (ii) the high-level spent fuel that contains transuranium, and requires hundreds of thousands of years to isolate them permanently, can be temporarily stored for tens of years before permanent disposal in a suitable geological formation [2].

Crystalline hard rock underlying the study area is impermeable with fractures, joints and faults that permit groundwater flow [4] and a suitable geological formation required to retard the flow of radioactive waste in case of damage or corrosion to the canisters (radioactive contaminant storage) [5]. Accurate description of fracture flow will continuously improve based on the research in fracture flow and advancement in computational technology [6]. Indeed, the geological stratum of interest is complex and very expensive to study and field experiments though accurate but very much expensive to carry out [7]. The only alternative way of understanding the behaviour of groundwater in the crystalline formation is through modelling.

Modelling groundwater flow is a technique of increasing importance for analyzing hydrologic response to groundwater resource planning. Modelling groundwater flow and radionuclide transport in the crystalline hard-rocks underlying study area was to contribute to locating suitable radioactive waste disposal site. However, detailed site characterization is a prerequisite to accurate modelling results to better understand the groundwater flow and radionuclide transport processes in the Dahomeyan System.

Fortunately, some researches were carried out on the geology, hydrogeology, hydrogeochemical and geophysical processes of rocks and groundwater interaction in Ghana as a whole and in the Accra Plains in particular. Akiti [8] studied environmental isotopes in groundwater and [9] worked on origin of saline waters in Accra Plains. Research carried out by [10] on a radioactive waste disposal site at Kwabenya, an area underlain by both Togo Series and Dahomeyan System concluded that apart from some few discontinuities, the rest of the areas was good for nuclear waste disposal.

However, little knowledge exist on modelling to determine groundwater flow and radioactive contaminant transport in the crystalline hard rock of the study area with required site specific aquifer parameters, flow path, and flow rate. Field data on pumping test of boreholes drilled in the study area taken from Community Water and Sanitation Agency (CWSA) Accra, Ghana, will be analyzed using available methods in the estimation of hydraulic properties [7] as inputs for simulation.

1.2 Research Problem

Radioactive waste generated by Ghana Atomic Energy Commission (GAEC) and some institutions in Ghana are stored in temporary storage need to be disposed of safely. The study area as part of the Accra Plains underlain by crystalline rocks is suitable for radioactive waste repository [5]. However, groundwater in the Accra Plains is noted to be saline [9, 11]. This saline groundwater may cause the canisters of the radioactive waste to corrode and cause leakage into the groundwater. Understanding groundwater flow and radionuclide transport in the study area can contribute to locating radioactive waste repository. Previous modelling research carried in the study area used assumed hydraulic parameters. However, the accuracy of modelling result in a geologic domain is dependent on detailed site characterization. Although some studies on aquifer characterization and modelling were carried out in the Dahomeyan System, more similar studies are needed for better understanding. This research shall determine and use the actual aquifer hydraulic properties (i.e., porosity, transmissivity, hydraulic conductivity, storativity, etc) as input in modelling and simulating groundwater flow and radionuclide (i.e., Carbon-14 and Strontium-9) distributions in the study domain.

1.3 Justification

The increase in radioactive waste generation in Ghana called for a safe management or isolation of radioactive waste from the environment by GAEC through borehole disposal facility. According to [12], groundwater vulnerability based on geology and layering of rocks, hydrological conditions in terms of flow direction, flow rate and aquifers properties as well as the economic importance of groundwater were some of the areas for consideration in the selection of radioactive waste disposal sites. Crystalline hard rock as suitable geologic formation for radioactive waste repository has been studied in detail however, site specific characterization and modelling can contribute to understanding groundwater flow and contaminant transport in aquifers [13]. The hydraulic properties estimated will contribute to existing knowledge of hydraulic properties database in Accra Plains and shall be used as input data in the simulation of groundwater flow model to determine the flow rate required as input to the simulation of the radionuclide transport model in aquifers of the study area. The results of the simulated models in this research will show the behaviour of groundwater flow and radioactive contaminant/radionuclide transport in space and time in a confined saturated Dahomeyan System and shall contribute to GAEC's quest in locating radioactive waste disposal site in the Accra Plains.

1.4 Research Goal

The goal of the research was to model and simulate the behaviour of groundwater flow and radioactive contaminant transport as a contribution to locating radioactive waste repository in aquifers of the crystalline formation of the Accra Plains.

1.5 Objectives

The research objectives were to:

1. estimate aquifer parameters (e.g. porosity, transmissivity, hydraulic conductivity, storage coefficient for confined aquifer) for modelling the groundwater flow,
2. estimate groundwater flow path and flow rate,
3. formulate and solve transient groundwater flow and radioactive contaminant transport equations,
4. simulate the behaviour of groundwater flow and radioactive contaminant transport models and predict contaminant concentrations at points of interest.

1.6 Scope of Research

The research work was conducted to model and simulate groundwater flow and radionuclide transport in aquifers of the Dahomeyan System of the Accra Plains. The thesis was organised to present the literature review, research methodology, results and discussions, conclusions and recommendations as well as references and appendices.

Chapter One dealt with the background to the research, problem statement, justification, research goal and objectives. Chapter Two consists of basic concepts and definitions, review of pertinent literature on groundwater flow and transport models, fractured models, pumping test characteristics and some basic concepts on hydraulic properties, sources of radioactive wastes, models solutions methods, boundary and initial conditions, and modelling errors. Chapter Three covered the location, geology, geomorphology, hydrogeology, geohazard, geophysics, climate, vegetation and land use. Further, data collection and analysis, aquifer characterization, hydraulic properties determination, determination of groundwater flow direction, flow rate, physical domain conceptualization, formulation of transient groundwater flow and radioactive transport equations, analytical and numerical solutions of ADDEs,

development of flow chart algorithm for ANSYS Fluent 13.0 and MatLab R2013a simulation of the groundwater flow and radionuclide movement. Chapter Four dwelt on the results and discussions. Chapter Five presented the conclusions and recommendations.

CHAPTER TWO

LITERATURE REVIEW

2.1 Aquifer System

Subsurface water describe water found below the ground surface. However, hydrologists restrict the use of groundwater to denote water in the saturated zone of the subsurface [14].

The term aquifer refers to porous geologic formation that contains water at full saturation and can permit water to flow through. In other words, aquifer stores and transmits water in relation to other geologic formations in the area and sometimes, referred to as groundwater reservoir or basin. The term aquitard describes a semi-permeable geologic formation that is thin in relation to aquifer and permits water to flow through it at a very slow rate. Aquitard sometimes referred to as leaky aquifer (e.g., clay loam and shales) extends over a large horizontal area and has permeability smaller than that of the aquifers below and above it. An aquiclude (aquifuge) refers to an impervious geologic formation, which neither holds nor transmits water e.g., dense un-fractured metamorphic or igneous rocks [15].

2.1.1 Confined, Unconfined and Leaky Aquifers

The subsurface hydrogeologic units are grouped into confined, unconfined or leaky aquifers. The confined aquifer is bounded above and below by aquiclude. The water pressure of a well tapped in confined aquifer is often higher than that of the atmospheric. When the water level is at top of the aquifer, it is called artesian well and when the water level is above the ground surface it is called free flowing well. The unconfined aquifer is bounded at the bottom by an aquiclude but the water table which moves freely marks its top. A well tapped in this aquifer has its water level as

that of the water table where the pressure is at atmospheric pressure. The leaky aquifer also known as semi-confined aquifer is bounded at top and bottom by aquitards or one boundary is an aquitard, and the other is an aquiclude. In leaky aquifers, water can move freely up or down the aquitards and a hydraulic equilibrium occurs when the water level in this aquifer coincide with the water table [16]. In this research, the aquifers are confined and in saturated zone.

2.1.2 Anisotropy and Heterogeneity of Aquifers

Anisotropy and heterogeneity are properties of a hydrogeologic system that determine the permeability of water. If the hydraulic conductivity of an aquifer is the same throughout the geological formation, the aquifer is referred to as being homogeneous. However, if the hydraulic conductivity is the same in all directions, the geologic formation is referred to as isotropic. Also, if the hydraulic conductivity is not the same in the geological formation, it is said to be heterogeneous. It is worth noting that, the lithology of most geological formations varies greatly vertically and horizontally making the formation to be mainly heterogeneous. The heterogeneity may be caused by grain size, clay lenses, and discontinuities. Additionally, if the hydraulic conductivity is different in different direction in the geologic formation, the domain is said to be anisotropic. The common property of fractured rock is anisotropy. Knowing the principal directions of anisotropy can lead to transforming the anisotropic system to isotropic system by change of coordinates and the new coordinate system has the well flow equations to be isotropic [14]. This transformation was employed in the study area.

2.2 Groundwater System in Accra Plains

Groundwater is an important natural resource that needs protection from contamination. The increasing human population and urbanization have resulted in the usage of groundwater resources worldwide. In Ghana, different communities rely heavily on river, streams, lakes, and underground water as source of water supply. The analysis of groundwater by [17] in the Ga East Municipality revealed the pH of the sampled hand-dug wells to be between 5.4 – 5.6 which is below World Health Organization (WHO) recommended limit of 6.5 – 8.5. They also indicated that the hardness of the water was between 5.7 – 4.9 and concluded that these two parameters led to rusting and scale formation in fittings of boreholes in the study area.

Kankam-Yeboah et al. [18] studied the sustainable yield of groundwater exploitation and concluded that groundwater resource potential of 1.6 l/s/km^2 be used as threshold value in Pra river basin and other river basins in south-west Ghana. Based on the reliance of many rural communities and urban centres on groundwater as an economic source of potable water, the water quality have been assessed generally in Ga East Municipality and in Ghana as a whole and it was concluded that most of the groundwater analyzed were within national and international guidelines [19, 20]. In the study area, the water quality has been moderately good with some level of salinity.

A suitable geological formation surrounding the radioactive repository acts as barrier and retards radioactive waste away from the repository. Environmentally stable isotope studies of groundwater in the Accra Plains showed that groundwater recharge takes place in fractures [5]. The geochemical processes were studied in Accra Plains and it was found that groundwater was in equilibrium with kaolinite and montmorillonite [21]. The necessity to understand groundwater flow and composition

of groundwater was further indicated since mechanisms of transport of radionuclides from waste repositories was dissolution or suspension in the groundwater and migration through the rock matrix and permeable fractures of the bedrock [21]. The evolution of groundwater systems might be affected by sorption behaviour of the radionuclides that might be released from the repository [22]. In this research sorption processes were considered as groundwater flows and contaminants are transported in the study area.

Essel et al., [23] modelled solute transport for radioisotope in an unsaturated layered soil of Kwabenya, an area near GAEC. In their research, the spillage of Tritium on the surface of the ground will take two years for it to get to the groundwater and 15 years to completely leave the unsaturated zone. Their research looked at the vertical flow of radioactive contaminant from the surface through the unsaturated zone to the water table. Yeboah et al. [24] numerically modelled the migration of radionuclide in a borehole disposal site and found that differences in hydraulic conductivities due to heterogeneity affected the direction of flow and that the fracture medium created preferential pathways through which radionuclides migrate from the radioactive waste repository.

2.2.1 Dahomeyan System

The Dahomeyan System (DS) attributed to Meso to Neoproterozoic age covers the flat lying terrain to the east of the Togo Series of the study area. The rock types found in the DS are quartz-schist, amphibolites and metamicrogabbro, orthogneiss and marble. The DS of the study area consists mainly of quartz-schists with variable amount of quartz, white mica, chlorite or biotite. The amphibolites and metamicrogabbro form dikes and sills, and may be massive black and coarse–

crystalline [4]. The primary porosity and fracturing in the paragneiss is low and creates a low yielding aquifer. The DS has low permeability due to clayey/loam overburden that makes recharge to be low. Depth to groundwater table is between 5-15 m. Aquifers in the DS are confined with low infiltration rate which makes it less vulnerable. Groundwater in the DS system is saline and not good for drinking but good for livestock and poultry with electrical conductivity of 500 S/cm. However, further to the east of the DS, the electrical conductivity of groundwater is more than 5000 µS/cm and unsuitable for human and animal consumption [11, 12].

2.3 Aquifer Characterization

In Figure 2.1, A, B, C represent semi-log plots of drawdown versus time for unconsolidated aquifers and D, E, F represent semi-log plots of consolidated fractured rock aquifers [15].

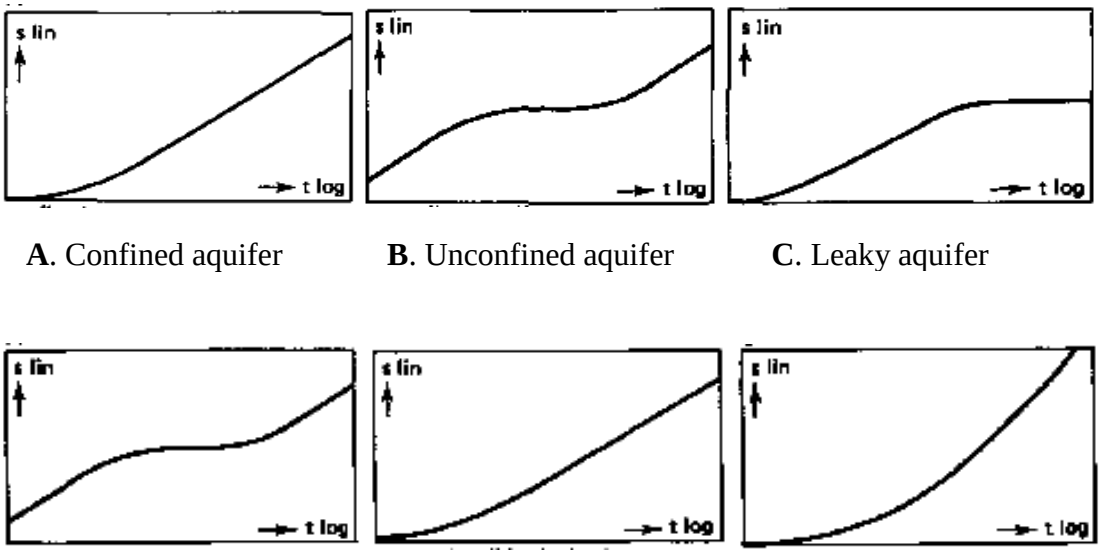

A. Confined aquifer **B**. Unconfined aquifer **C**. Leaky aquifer

D. Confined fracture aquifer – double porosity **E**. Pumped well in single plane, vertical fracture **F**. Pumped well in fractured dike

Figure 2.1: Semi-log plots of theoretical time-drawdown of unconsolidated (A, B, C) and consolidated fractured aquifers (D, E, F) [15]

The Figure 2.1 D refers to confined, densely fractured, consolidated fractured aquifer with double porosity. Two interpretations drawn on Figure 2.1 D are that it has: (i) fractures of high permeability and low storage capacity and (ii) matrix blocks of high permeability and low storage capacity. Part E of Figure 2.1 shows a curve for a borehole that pumps a single vertical fracture in a confined, homogeneous and isotropic aquifer of low permeability. Part F of Figure 2.1 refers to a borehole in a densely fractured, highly permeable dike of infinite length and finite width in a confined, homogeneous, isotropic, consolidated aquifer of low hydraulic conductivity and high storage capacity. The theoretical curves are mainly affected by recharge and impermeable boundaries [15]. In fractured formations accuracy of groundwater flow and contaminant transport modelling is greatly dependent on the accuracy and extent of data from site characterization. Generally, the more detailed the site characterization the greater the probability of characterizing the site [25]. The real aquifer type curves will be plotted in this research to show the aquifer types of the study area.

To understand the hydrogeologic system, groundwater flow models were employed in the simulation of groundwater movement through the subsurface. Hydrogeologic system characterization include: the distribution and magnitude of groundwater recharge, pumping and leakage from sources and sinks; steady state and transient hydraulic head; thickness and extent of aquifers and confining units; boundary and initial conditions that control the flow and hydraulic properties of the aquifer [16].

The effectiveness of aquifers is characterized by formation factors (hydraulic properties), transmissivity, storativity and specific capacity. Transmissivity is the rate at which water flows through a vertical column, 1 m wide that spans through the

complete saturated thickness of the aquifer under a hydraulic gradient of 1 unit [26]. Driscoll [26] pointed out that when the aquifer transmissivity is lower than 12.4 m^2/day, the borehole could supply water for domestic use. Otherwise, for transmissivity values of aquifer higher than 12.4 m^2/day, the borehole yield is enough to support industrial, municipal and irrigation use. The specific capacity of a well can be determined from the pumping rate (yield) divided by drawdown [27].

2.3.1 Theis Recovery Method

Theis [28] derived and solved equation for analyses of pumping test data shown in Figure 2.2, and the non-equilibrium equation was expressed as;

$$\frac{\partial^2 h}{\partial r^2} + \frac{1}{r}\frac{\partial h}{\partial r} = \frac{S}{T}\frac{\partial h}{\partial t} \quad (2.1)$$

where, *h* is hydraulic head, *r* is radial distance from monitoring well, H is static water level, b is the aquifer thickness, *T* is aquifer transmissivity, and *S* is aquifer storativity.

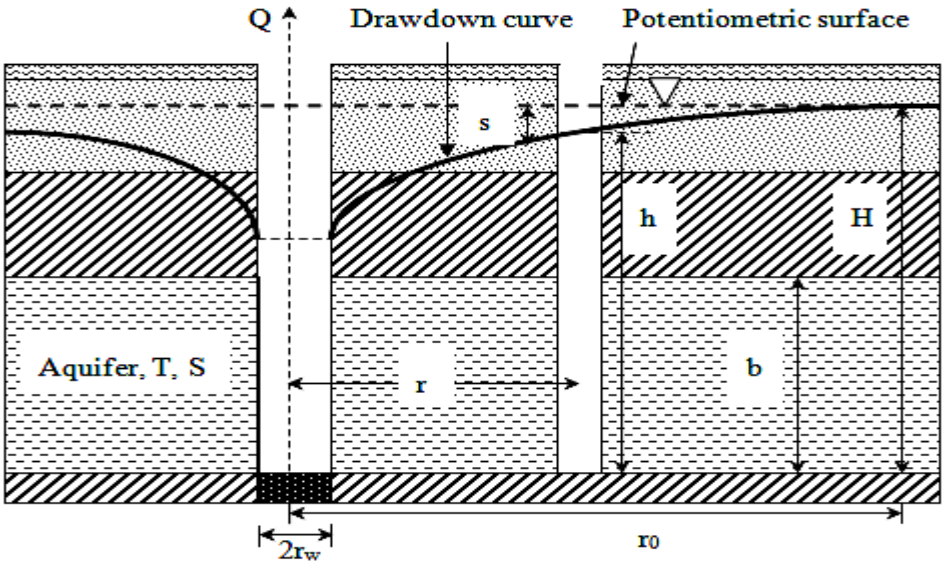

Figure 2.2: Unsteady radial flow during pumping in a confined aquifer.

The hydraulic properties (transmissivity T and hydraulic conductivity K) of non-leaky confined aquifers can be determined using Theis mathematical solution of equation

(2.1) for recovery tests. The analysis involves matching the Theis recovery solution to water-level recovery (residual drawdown) data collected after a pumping test. Theis then derived an approximate linear equation to predict residual drawdown in a homogeneous, isotropic and non-leaky confined aquifer assuming a fully penetrating line sink that discharged at a constant rate prior to recovery [29]. Thus,

$$s' = \frac{2.303Q}{4\pi T}\left[\log_{10}\left(\frac{t}{t\prime}\right) - \log_{10}\left(\frac{S}{S\prime}\right)\right] \quad (2.2)$$

where s' is residual drawdown [L], Q is the pumping rate [L^3/T], T is transmissivity [L^2/T], S is storativity during pumping [-], S' is storativity during recovery [-], t is elapsed time since start of pumping [T] and t' is elapsed time since pumping stopped [T]. Plot of s' versus $\log_{10}(t/t')$ gave T from the slope as

$$T = \frac{2.303Q}{4\pi\Delta s'} \quad (2.3)$$

The intercept of the line on $\log_{10}(t/t')$ axis gave the storativity ratio S/S' that should be close to 1 in the absence of boundary effect. However, for $S/S' > 1$, the aquifer is unconfined or semi-confined and recharge occurs during the pumping test, and $S/S' < 1$, the aquifer is said to be confined and suggest no-flow boundary exist [29].

The assumptions for Theis recovery solution were:

(i) aquifer had infinite areal extent

(ii) pumping (control) well was fully penetrating

(iii) flow to pumping (control) well was horizontal

(iv) aquifer was homogeneous, isotropic and of uniform thickness

(v) flow was transient (unsteady)

(vi) water was released instantaneously from storage with decline of hydraulic head

(vii) diameter of pumping (control) well was very small so that storage in the well can be neglected [29].

In determining the aquifer parameters, Theis' assumptions were applied to the aquifer system study area.

2.3.2 Cooper-Jacob Method

If the late time data from pumping tests are not influenced by well bore storage, the Cooper-Jacob method of pumping test analysis could be employed in estimating the hydraulic properties of the aquifer [30]. The Cooper-Jacob method stems from the work of Theis and similar to the recovery method [31]. Due to well losses, pumping wells become inefficient therefore, observation well was required to calculate the coefficient of storage. When the drawdown was plotted against the logarithm of time, a straight-line curve is fitted to the data after sufficient/ late time of pumping. The value $(H - h) = \Delta s$ for one log cycle of time and the intercept on the time axis were used to estimate the formation factors of the aquifer as

$$T = \frac{2.3Q}{4\pi\Delta s} \tag{2.4}$$

and

$$S = \frac{2.25Tt_0}{r^2} \tag{2.5}$$

where, T is transmissivity, S is storativity, Q is discharge, Δs is drawdown over one log cycle, t_0 is time intercept, r is radial distance from the pumping well to the monitoring well. The Cooper Jacob method was used in determining the field the storage coefficient in the research work.

2.3.3 Groundwater Recharge and Discharge

The movement of water through the vadose zone to the water table coupled with the flow away from the water table is termed groundwater recharge [32]. Groundwater

recharge occurs locally, from surface water bodies or, in diffuse form, from precipitation via the unsaturated soil zone. Long-term average diffuse groundwater recharge is the part of precipitation that does not evapotranspirate and does not run off to a surface water body on the soil surface or within the unsaturated zone [33].

Groundwater resources in crystalline rock have been associated with weathered and fracture zones, which are well connected to the surface [34]. Gaspa [35] found that recharge represents about 15% of the average annual precipitation in the case of a less compacted study area. In the study area, this percentage value of the annual precipitation is small which reflects in the small amount of yield in most wells. As groundwater flows from a higher head level to a lower head level, the discharge zones are mainly streams, rivers and sea. Groundwater that leaves the saturated zone is referred to as discharge water.

2.3.4 Aquifer Yield and Cone of Depression

The yield of an aquifer is necessary in the management of the aquifer. Aquifer yield concerns not only the water quantity but also water quality and reliability of good water in terms of quantity and quality [14]. Figure 2.3 shows the cone of depression created as the aquifer has been disturbed.

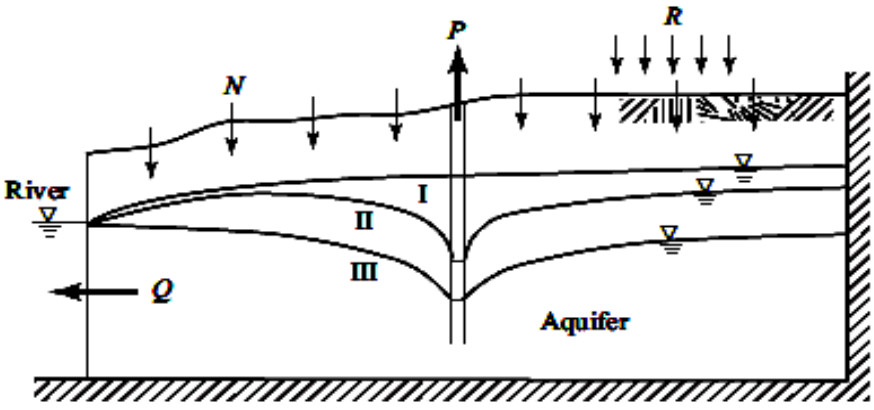

Figure 2.3: Cone of depression distribution of a disturbed aquifer [14].

The simple case of steady state flow of aquifer being replenished naturally at an annual rate of N and artificial rate of R were considered. The water balance of the aquifer was given by: *mass of water recharging aquifer to be equal to mass of water leaving it*. Therefore, for steady state

$$N + R = Q + P \tag{2.6}$$

where, N is natural recharge, R is artificial recharge, Q is flow out to river and P is flow out through pumping. For no artificial recharge and no pumping, the natural recharge equals discharge which gives the water level at level I. Pumping the water, brings the water level to II. Further withdrawal brings the water level to III and the cone of depression deepens as Q reverses (river water entering the aquifer). This undesirable situation may lead to intrusion of poor quality water into the aquifer known as seawater intrusion which pollutes the aquifer.

2.4 Pumping Test, Tracer Test and Isotopes

Pumping test and tracer test were used in the determination of aquifer hydraulic properties and these hydraulic properties enable the understanding of groundwater flow and contaminant transport in the hydrogeologic domain.

2.4.1 Pumping Test

Hydraulic properties of rocks can be estimated using laboratory and field methods. However, the laboratory estimation of the hydraulic properties does not truly represent the aquifer [36]. Pumping tests give adequate information on aquifer systems. The principle of pumping test involves applying a stress to an aquifer by extracting groundwater from a pumping well and measuring the aquifer response to that stress by monitoring drawdown as a function of time. De Smedt [37] noted that the most reliable method for ascertaining well yield or capacity was pumping test.

Pumping test is done to determine the average hydraulic properties of the aquifer among others [38]. Constant rate pumping tests commonly used in unconsolidated porous media can provide information on hydraulic conductivity and anisotropy for fractured formations [25]. This research partly looks at the determination of the average hydraulic properties of the aquifer by incorporating the pumping data into an appropriate well flow equation to calculate the hydraulic parameters of the aquifer.

2.4.2 Tracer test

The tracer test involves injecting a tracer (conservative substance that mixes with the groundwater) into a well and documenting its movement in the aquifer around the well or between two or more wells for a period. Tracer tests are used to determine groundwater flow paths, flow rate and provide contaminant transport parameters and also in groundwater contamination studies at hazardous waste site. However, tracer tests are rarely used because of their expensiveness and possible pollution of groundwater by additional introduction of other chemicals and the higher possibility of not finishing the process [39].

2.4.3 Environmental Isotopes

In regional groundwater movement, environmental isotopes are considered and the use of these isotopes is mainly confined to stable isotopes (i.e., hydrogen, deuterium, and oxygen-18) and radioactive isotopes (i.e., tritium and radiocarbon). Studies of stable and radioactive isotopes in groundwater yield among others; (i) mean flow velocity and direction; (ii) mean field coefficient of permeability; (iii) distribution of anisotropy; (iv) degree of homogeneity; (v) spatial extent and order of flow systems; and (vi) the spatial and temporal distribution of recharge events [40].

2.4.4 Radioisotopes

Radioisotopes in groundwater come from natural and/ or artificial processes. Tritium and Carbon-14 as environmental radioisotopes are used in groundwater studies. When homogeneity is established using stable isotopes, the radioisotope Tritium and Carbon-14 analysis of groundwater system follows [41]. In local flow systems of short residence time less than 50 years, Tritium with a short half-life of 12.26 years can be used [42]. Carbon-14 is not a conservative tracer and may be lost through dilution and decay. The half-life of carbon-14 is 5730 years and it is used in regional groundwater flow systems. Strontium-90 has a half-life of about 29 years and a product of nuclear spent fuel. Knowing the flow pattern permits the radiocarbon determination of age, velocity, permeability, and anisotropy in a flow system among others. On a small scale, Tritium and Carbon14 are used to develop and test both steady state and transient flow models [43]. The research used Carbon-14 and Strontium-90 as radioactive contaminants in the transport model simulation. In this research the word radionuclide and radioactive contaminant are used interchangeably.

2.4.5 Radioactive Waste Sources in Ghana

About 15 institutions in Ghana generate radioactive wastes in the field of research, medicine and industry. National Nuclear Research Institute (NNRI) of Ghana Atomic Energy Commission (GAEC) is the largest radioactive waste generator. The main activities of NNRI include radiotherapy and nuclear medicine, neutron activation analysis, radiopharmacy, pesticide research and gamma irradiation all of which result in radioactive waste generation [1]. The activities of radioactive waste generated in Ghana are between Bq to GBq [44].

Radioactive waste generation in Ghana will increase due to increasing use of radioactive materials and the quest for installation of nuclear power plant to produce electricity. The radioactive waste from existing and the expected nuclear reactor will include spent ion exchange resins from the nuclear reactor water purification system, incompatible solid waste from mechanical filters, liquid and organic waste, spent fuel and spent sealed sources made up of between 185 GBq to 1.85 PBq of Co-60. Seven 200 litres drums are required annually in conditioning radioactive waste generated in Ghana [45]. Therefore, safe management of the radioactive waste using the borehole disposal system will help reduce the risk it posed to human and environment.

2.5 Fractured Rock Models for Groundwater Flow

Fractured rock media are made of the two rock formations of fracture zone and porous media [46]. The crystalline rocks in the study area are fractured and weathered [21]. Fracture zones have low mean porosity and good lateral continuity. However, the matrix porous media have larger porosity and shorter continuity. Porosity and permeability of rocks are estimated from interconnections, aperture size, spacing and orientation of the rocks. Groundwater movement mainly occurs along the discontinuities in fracture zones (i.e., joints, faults and fractures). Fractures which are not filled by weathered materials permits groundwater flow but permeability is restricted when the fractures are filled with clayey materials (i.e., smecite or montmorillonite) [46]. Three boreholes drilled in the study area were having low yields attributed to the fractures not pronounced or blocked by weathered materials.

Fracture formations can be classified according to their porosity and permeability as shown in Figure 2.5. In purely fractured rock, groundwater flows through the major fractures and the micro fractures.

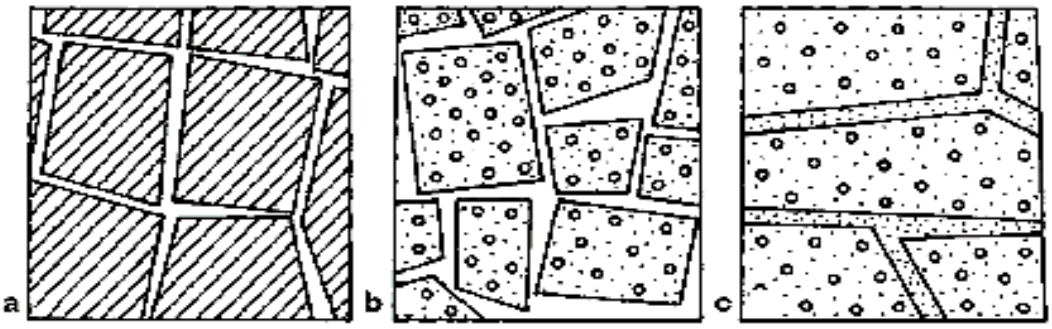

Figure 2.4: Fracture types (a) purely fractured (b) double porosity (c) heterogeneous media [47].

The porosity and permeability in purely fractured domain is mainly secondary porosity due to the interconnected fractures and the impermeable matrix block in the domain. However, the fractures and matrix blocks in double porosity medium contribute to flow of groundwater with fractures being main contributors. Groundwater flow in double porosity medium is largely through fractures of secondary porosity and also through pores in the matrix with primary porosity. Heterogeneous medium is that in which groundwater flows through the matrix block where the fractures are mostly blocked. The permeability of groundwater flow is reduced in a heterogeneous medium as fractures are filled with weathered materials [46]. The aquifer yield in heterogeneous domain is small compared to the purely fractured medium and the double porosity medium.

In modelling contaminant transport, so much accuracy is needed since the heterogeneity of a fracture domain greatly affects the travel times and contaminant concentration. Fractures parallel to the maximum compressive stress as shown in studies tend to be open and those perpendicular to this direction tend to be closed [48]. These three fracture domains were encountered in the study area and led to variations in the hydraulic conductivity in the study area.

Fracture models describe flow in fractured medium. These fracture models are: (a) Parallel plate model, (b) Double porosity model, (c) Equivalent porous medium model, (d) Discrete fractured network model, and (f) Equivalent parallel plate model.

2.5.1 Parallel Plate Model

Parallel plate model employs single fracture and groundwater flows in this single fracture using Darcy's law [46] as

$$v = K_f I \tag{2.7}$$

where, K_f is the fracture hydraulic conductivity given as

$$K_f = \frac{\gamma_w a^2}{12\mu} \tag{2.8}$$

and a is the fracture aperture, μ is the viscosity of water and γ_w is the unit weight of water. The relationship between the hydraulic conductivity (K) and permeability (k) is

$$K = \frac{\gamma}{\mu} k \tag{2.9}$$

The permeability of the fracture k_f is given as

$$k_f = \frac{a^2}{12} \tag{2.10}$$

The average velocity v in the fracture for a single parallel plate model is [46]

$$v = \frac{\gamma a^2}{12\mu} \frac{dh}{dl} \tag{2.11}$$

where, dh/dl is the hydraulic gradient.

For even small hydraulic gradients, the groundwater velocity in discrete fractures is very high in relation to velocities in porous medium [49] as indicated in Figure 2.5.

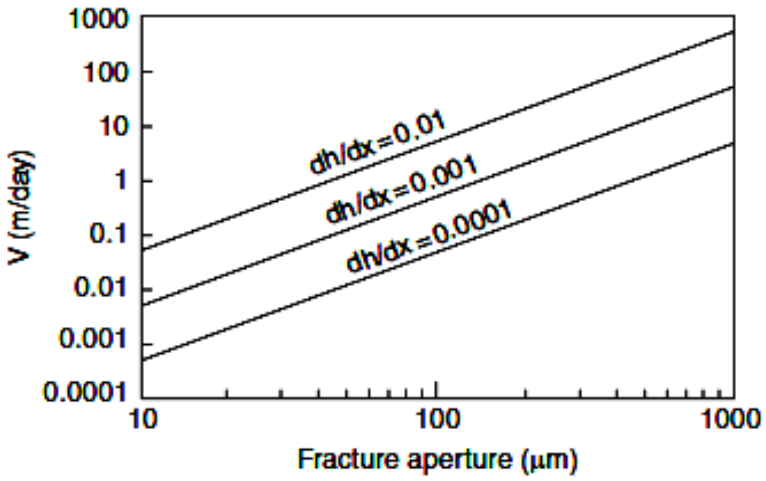

Figure 2.5: Cubic law predictions of groundwater velocities in a single fracture [49]

For permeable fracture walls, the average velocity is given in [50] as:

$$v = \frac{\gamma a^2}{12\mu + 2a\rho ql}\frac{dh}{dl} \tag{2.12}$$

where ql is the rate of leakage into the wall of fracture. Thus, if $v \gg a\rho ql/6$, then the conductivity K_f can be predicted as above knowing the fracture aperture.

Bear [50] and many researchers defined transmissivity of fracture T_f as

$$T_f = K_f a = \frac{\gamma a^3}{12\mu} \tag{2.13}$$

The volumetric flow rate Q_f per unit plate (fracture width) is

$$Q_f = \frac{\gamma a^3}{12\mu} I \tag{2.14}$$

This is referred to as the cubic law [50, 51, 52] valid for laminar flow between parallel plate fractures with smooth surfaces. It is very difficult to determine the representative distance between fracture walls under field studies since fracture spacing is difficult to determine and therefore will not be employed in this research work.

Channelling occurs in fractured rocks and refers to preferential flow paths applicable in both single fracture and fracture networks. The application of tracer in natural fractures in laboratory experiments and computer simulations reveals the effect of

channelling [53]. Many researchers have questioned the ability of parallel plate model in nature as channelling effect showed preferred paths in these studies that is difficult to predict. The channelling concept in practice is rarely used in interpreting hydraulic or tracer tests as constant aperture is assumed for the fracture medium [46]. The channelling effect may be seen in this research as a result of preferential flow path for contaminant transport.

2.5.2 Double Porosity Model

Double (dual) porosity model in regional groundwater investigation best describes the behaviour of groundwater in fractured rocks. The dual porosity model was first developed by [54] and several researchers have contributed to it including [55]. These porosities are primary and secondary. The primary (matrix) porosity occurs during the rock formation such as the voids between the mineral grains or bedding planes. However, secondary porosity occurs after the rock formation and mainly due to tectonic forces resulting in micro or macro fissures, fractures, faults and fault zones in rocks (e.g. brittle rock as limestone).

The porous block and the fracture zone are two regions with different hydraulic and hydrodynamic behaviours. The differences in permeability of fractures and matrix blocks results in different flow mechanism during early, intermediate and long time of pumping. During early times the flow from matrix block is zero as initially the fluid flow mainly from fractures which have high permeability. The fractured reservoir behaves equivalently as a homogeneous porous medium with permeability that is equal to fissure permeability at late times. Midway during the flow, there is a transition from fracture flow to flows from fractures and matrix block [46]. Most of

the aquifers in the study domain do not exhibit dual porosity but mainly secondary porosity.

2.5.3 Discrete Fracture Network Models

The network models employ fracture characteristic properties and heterogeneity of rock mass from field data. These fracture properties are fracture aperture, length, orientation, connectivity, density and filling materials that determine the hydraulic behaviour of discrete fracture network. Numerical techniques to differentiate discrete fracture networks from fracture system that uses equivalent continuum model were developed [56]. Fracture network models have been suggested to use two-dimension and three-dimension for the model representation [50, 56].

The discrete fracture network models simulate flow in fractures or fracture set with artificial distributions of fracture spacing, aperture, orientations and dimensions considering surface roughness, flow channelling and mixing pattern at fracture intersections. Though discrete fracture network models are minimally used on natural fracture systems, they are useful in small geological formations where nuclear waste repository is studied over long time period [46]. Two main disadvantages on the use of the discrete fracture network models are that (a) it is difficult to get statistical information on fracture properties and (b) there is no guarantee the model will capture its main flow or transport features of the domain [48]. This model therefore is not suitable in this research work.

2.5.4 Equivalent Porous Medium Model (EPM)

The Equivalent Porous Medium (equivalent continuum) model is conceptually simple and used in the estimation of groundwater flow and contaminant transport in fractured media where fracture characterization properties (i.e., fracture aperture, length etc) are

not known. Several researchers maintained that groundwater flow in large volume of fractured medium represent the flow through porous medium using the equivalent continuum model. This model is based on the following assumptions that: (a) fracture density is high (b) apertures are not varying (c) sample sizes are large (d) fracture orientations distributed (e) flow is volumetric (groundwater supplies) and (f) joint sets relatively oriented [46]. This model approach shall be applied in this research work based on the assumptions enumerated above among others.

Groundwater flow equations developed for granular porous medium can be adopted in such cases as expressed in EPM [46] to represent the study domain of this research work. Flow modelling employ geological heterogeneity and code developed for EPM simulations in new ways due to increasing computer-processing efficiency [56]. Shapiro, [57] used an EPM and endorsed it for describing fluid flow in fractured rock. Investigations carried out by [57] using EPM pointed out that, only very few cases showed evidence in early transient flow responses of the effect of fractures. The equivalent hydraulic conductivity in the models investigated accounts for all fracture sets and the matrix void spaces which is mainly anisotropic.

Berkowitz et al. [58] studied flow and transport in a fracture network consisting of two orthogonal sets of equally spaced parallel-plate fractures aligned along and diagonal to the flow direction. The resulting S-shaped breakthrough curves suggested single continuum behaviour. Schwartz and Smith [59] modelled anisotropic dispersion in fractured rock using a continuum approach. Neuman [60] suggested that the scale dependence of the dispersivities of fractured media and of porous media follow the same scaling rule. Streltsova [61], in her book on aquifer tests, uses the EPM approach repeatedly for analyses of hydraulic properties of fractured rocks, as

do other books in the petroleum industry. In the conceptual and numerical model development for groundwater EPM was used to model the heterogeneity of a fractured rock system in a small number of regions [34]. It is clear that EPM model can be used to model fractured domain to represent the behaviour of the domain. This research shall adopt EPM model to model groundwater flow and radioactive contaminant transport in the aquifers of the study area.

2.6 Radioactive Contaminant Transport in Fractured Aquifer

Transport models simulate the groundwater movement and chemical alteration of contaminants as they move through the subsurface. Fate and transport models used to model transport within a ground water zone require the development of a calibrated flow model or, at a minimum, an accurate determination of the flow velocity based on field data as this research sought to achieve. Figure 2.6 shows a schematic diagram of various processes of contaminant transport in an idealized fractured porous medium [62]. The transport processes illustrate the (a) movement of contaminants by advection, diffusion, and dispersion, (b) removal or release of contaminants by sorption or desorption from soil or rock (adsorption), (c) alteration of contaminants by biological or physical processes, or by chemical reactions.

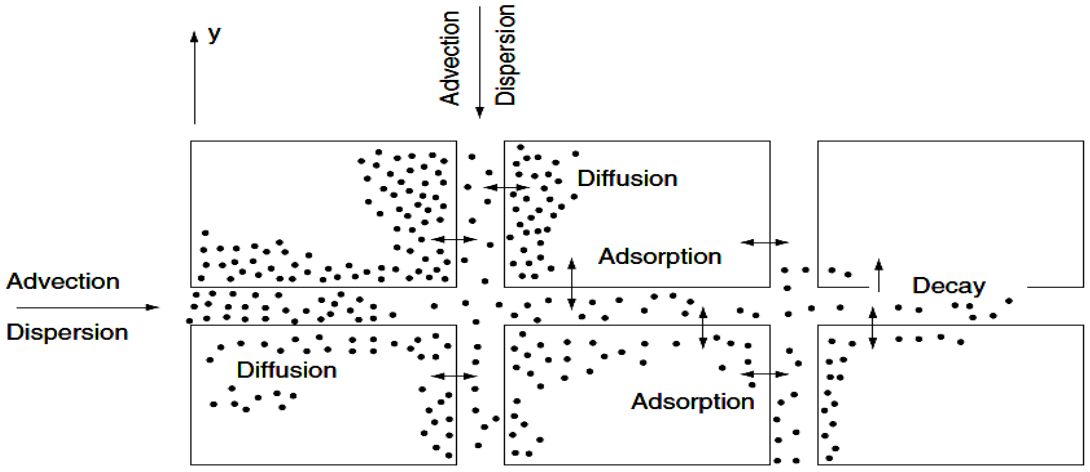

Figure 2.6: Idealized fracture schematic showing transport processes [62].

The simulation of transport processes through hydrogeological investigations would require the following inputs: (i) horizontal and vertical distribution of average linear groundwater velocity (direction and magnitude) determined by a calibrated flow model or through accurate determination from field data (ii) initial distribution of contaminant (iii) location, history and mass loading rate of chemical sources or sinks (iv) effective porosity (v) soil bulk density (vi) fraction of organic carbon in soils; (vii) density and viscosity of non-aqueous fluid (viii) longitudinal and transverse dispersivity (ix) diffusion coefficient (x) chemical decay rate or degradation constant and (xi) possibly, equations describing chemical transformation processes [62].

The outputs from transport model simulations are contaminant concentrations that are in equilibrium with the groundwater flow system and geochemical conditions for the modelled area. As with flow models, fate and transport models should be calibrated and verified by adjusting values of the different hydrogeologic or geochemical properties to reduce any disparity between the simulations and field data. Fate and transport model simulation may predict the expected concentrations of contaminants as a means to the implementation of a remedial action [46].

2.7 Groundwater Flow Model

Groundwater flow is governed by a set of partial differential equations derived using laws that govern the flow, mass and momentum balance, constitutive equations and simplifying assumptions [63]. Groundwater flow models are important in the development and management of groundwater resources. Groundwater flow and transport models have been used widely as: (i) interpretive tools for investigating groundwater system dynamics and understanding the flow patterns; (ii) predictive tools for predicting future impacts of anthropogenic activities; (iii) simulation tool for

analyzing groundwater systems responses to stresses; and (iv) visualization tools for communicating key messages to public and decision-makers among others [13]. The advent of computers and increase in computation powers of modern computers make groundwater modelling become an important tool for hydrogeologists.

The characteristic features affecting groundwater flows are; location, extent of recharge and discharge, flow direction, flow rate, and the depth of penetration in an aquifer system [64]. Toth [64] indicated that the irregular geological environment (lithological changes, faults etc), cause changes in the flow system and of the spatial arrangement of the flow patterns. For the first time [65] found analytical solution to investigate groundwater flow in a hypothetical small drainage basin and pointed out that the topography, geology and climate were some of the factors for the formation of three flow systems. These are the local flow, intermediate flow and regional groundwater flow systems Figure 2.7.

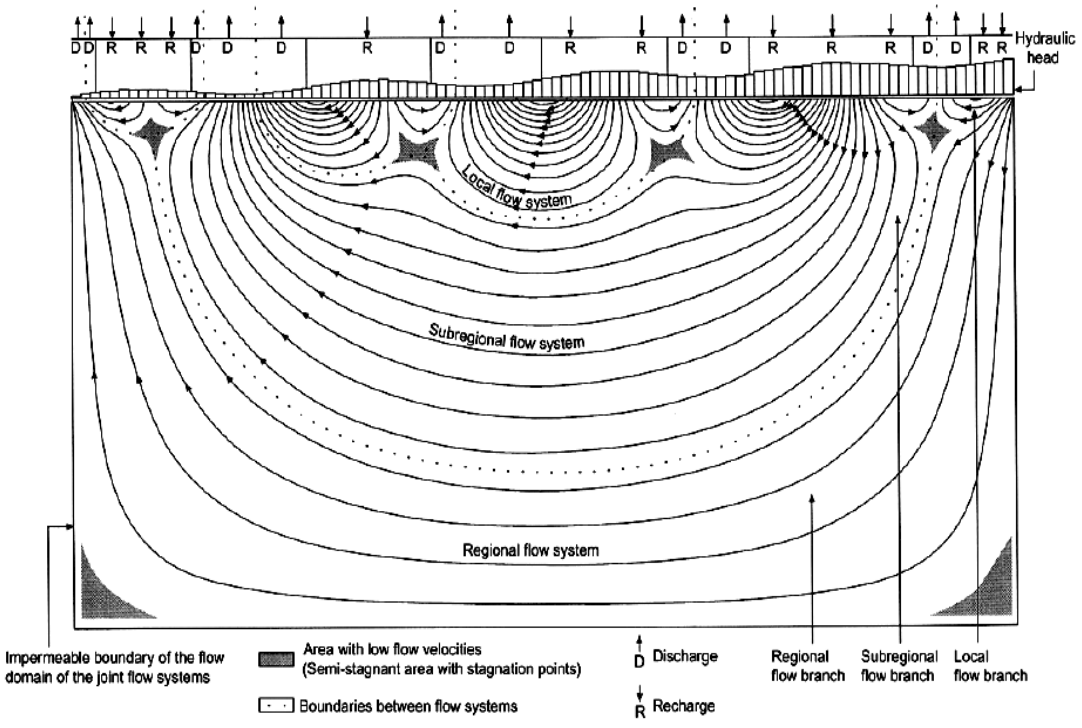

Figure 2.7: Toth's groundwater flow pattern [66]

These three patterns of groundwater flow results from changes in groundwater levels with depth, environmental isotopes, recharge and discharge, climate and vegetation of the study area [67, 68, 69].

Numerical models were first simulated to show a steady state regional flow patterns in a hypothetical layered aquifer systems [70, 71]. The numerical models of simulation have the advantage of simulating 3D groundwater flow in heterogeneous and anisotropic groundwater basins [13]. Numerical modelling of groundwater flow and transport procedures and some computer software tools available were presented by [72]. Report on a study of three basins with confined aquifers showed different shapes and peculiar features of flow systems [73]. This means that aquifers in different geological settings may exhibit different behaviour and properties and that site specific hydraulic properties are necessary in the determination of the behaviour of groundwater flow and contaminant transport in the domain. This research established the isotropy in hydraulic conductivity and the heterogeneity of the study area but shall model a simple case of 2 dimensional homogeneous flows and anisotropic coefficient of dispersion of radioactive contaminant in the Dahomeyan System.

In recent years, large-scale transient groundwater flow models were analyzed because of high processing computer availability and ease to use modelling systems and Geographic Information Systems (GIS). Regional groundwater flow modelling in view of significant advances was reviewed to predict regional impacts of human effects on groundwater systems [13]. Models help in understanding groundwater system in specific geological settings as this research seeks to find out the effect of human activity of radionuclide repository on the groundwater flow and any leaked contaminant transport in the study area.

Models can be used to predict the hydraulic head and groundwater flow rates in the aquifers [74]. Groundwater flow models in a saturated porous domain are well developed and confidence in model validity is high [75, 76]. Although mechanism of groundwater flow through porous media is well understood, many uncertainties exist about the flow of water and transport of contaminant in fractured rocks. Singhal and Gupta [46] were of the view that low permeability rock formations are potential repositories for high-level radionuclide waste. Though models are important in predicting the behaviour of groundwater flow and contaminant transport, the major limitation on model application in predictions is the adequacy of the database for the specific site, and which is addressed by parameter estimation [76]. In this case hydraulic properties are estimated from field data to represent the real parameters of the study area.

2.7.1 Darcy's Law in Porous Medium

Darcy (1856) demonstrated experimentally the percolation of water through soil for laminar flow in saturated porous media. The flow rate or discharge per unit time was found to be proportional to the hydraulic gradient and given as:

$$Q = -KAI \tag{2.15}$$

or

$$v = \frac{Q}{A} = -KI \tag{2.16}$$

where, Q is volume rate of flow, I is hydraulic gradient, K is hydraulic conductivity, A is cross-sectional area of soil mass normal to the direction of flow, v is flow velocity (Darcy's velocity or apparent water velocity).

Darcy's law indicates a linear relationship between discharge velocity and hydraulic gradient. This law represents statistical macroscopic equivalent of the Navier-Stokes

equation of motion for viscous flow of groundwater [77]. The law is valid only for laminar flow with small pore dimensions (fine-grained soils). For coarse grained soils the flow is turbulent. The validity of the law is based on particle size, hydraulic gradient and the flow velocity. It has been shown that the flow through sands remains laminar and Darcy's law is valid when Reynold's number is less than one. Thus,

$$Re = \frac{\rho v d}{\mu} \leq 1 \qquad (2.17)$$

where, ρ is mass density, v is velocity of flow, d is diameter of porous medium or particle size and μ is dynamic viscosity. The law is within its validity limits for groundwater flow occurring in nature. However, in unconsolidated rock aquifers with steep hydraulic gradients or large diameter grains the law may not be applicable. In the immediate vicinity of wells, Darcy's law is not applicable since there is a steep hydraulic gradient [77].

2.7.2 Range of Validity of Darcy's Law

Reynolds number is a measure to whether a flow is laminar or turbulent. Darcy's law is valid for only laminar flow. Experiments have shown that, Darcy's law is valid for Reynolds number Re < 1 where the head loss is linear. The upper validity limit Re = 10 for Darcy's law is also accepted where no serious errors are created. Turbulence occurs gradually from around this upper limit to Re < 100, where the head loss varies close to the second power of velocity rather than linearly. However, rocks with wide openings, where steep hydraulic gradients exist (e.g. near a well), laminar flow is not satisfied and Darcy's law is not valid [15, 77]. Darcy's law is also invalid at low hydraulic gradients as in the case of clays and therefore the relation between v and I is non-linear. It is not possible to give a unique lower limit to the hydraulic gradients

for which Darcy's law is still valid, since *I* varies with the type and structure of the clay with the mineral content of the water also playing a role [78].

2.7.3 Conceptual Model

Groundwater conceptual model gives qualitative, quantitative and pictorial description of groundwater system, delineating, hydrogeologic units, system boundaries, inputs/outputs, and soils/rock types and their properties. Hydrogeological conceptual models are simplified conceptual representations of part of real hydrogeological, hydrological and hydrochemical processes in a geological formation and aquifer system. Conceptual models are used for understanding and prediction of hydrologic processes. Also, hydrologists use conceptual model to investigate and understand regional flow system and define strategies for detailed investigation of component needed by the model using classical methods of geology, hydrogeology, and hydrology in addition to relevant science fields including geophysics, geochemistry, soil science and isotope physics [79].

2.7.4 Physical Domain

Figure 2.8 shows schematic representation of the boundaries of 2D physical geometry of regional groundwater flow system [64]. The rectangular problem domain of the mathematical model approximately represents the exact shape of the saturated flow region. The geometry was a cross section of a small watershed with boundaries specified. The aquifer was assumed to be porous, isotropic, homogeneous and underlain by an impermeable rock. No flow boundaries were taken to be groundwater divides and basement rock indicating impermeable boundary. Groundwater flows away from either side of the topographic high and also groundwater and left of the valley bottom discharge at point A [64, 65].

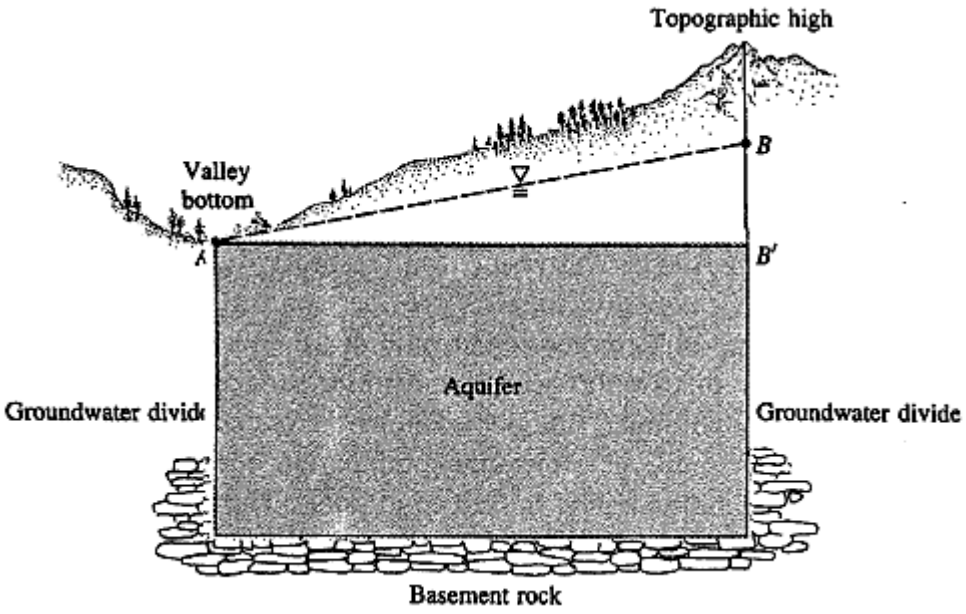

Figure 2.8: Schematic boundaries for two-dimensional regional groundwater flow system [63].

2.8 Formulation of Mathematical Models

The mathematical model formed can be one, two, or three dimensional, steady-state or transient, saturated or unsaturated flow or transport equations [80, 81]. Two main mathematical problems relate to groundwater flow and contaminant transport. These are boundary value problems and initial value problems.

2.8.1 Flow Equations

Governing groundwater flow equations are formulated using Darcy's law, continuity or conservation of mass principle and simplifying assumptions. Regional field problems mostly simulate anisotropic and heterogeneous aquifers. Three dimensional models are rarely used due to data unavailability. One dimensional models mostly do not represent the field situation but give the idea of the behaviour of flow in geological domain. However, two dimensional models in the form of areal model assume flow in vertical component to be negligible or profile model (where flow is

assumed to be zero in one horizontal axes) is adequate to model field problems. The two dimensional transient groundwater flow with heterogeneity and anisotropy is [63];

$$\frac{\partial}{\partial x}\left(T_x \frac{\partial h}{\partial x}\right) + \frac{\partial}{\partial y}\left(T_y \frac{\partial h}{\partial y}\right) = S\frac{\partial h}{\partial t} - R(x, y, t) \quad (2.18)$$

where, h is the hydraulic head, T_x is the transmissivity in x direction, T_y is the transmissivity in y direction, S is the storativity, and R is a source/sink (recharge or discharge) term. The research will model and simulate 2D homogeneous and isotropic groundwater flow equation with uniform flow in x-direction for the study area.

2.8.2 Solute Transport Equations

Advection is the transport of dissolved solids at the same velocity as groundwater. Transport equations are formulated with the assumption that dispersive mass is proportional to the concentration gradient using Fick's law. Continuity or conservation of mass principle was also used in the derivation of the governing equation of contaminant transport considering advection and dispersion processes of transport. The assumption of uniform flow in the x direction means that total mass flux in x-direction is the sum of advection and dispersion fluxes and the total mass flux in y-direction is just dispersive. The generalised 2D Advective-dispersive equation is given in [63] as;

$$\frac{\partial}{\partial x}\left(nD_L \frac{\partial C}{\partial x}\right) + \frac{\partial}{\partial y}\left(nD_T \frac{\partial C}{\partial y}\right) - \frac{\partial}{\partial x}(nCv_x) = n\frac{\partial C}{\partial t} \quad (2.19)$$

where, n is the effective porosity, C is the solute concentration, v_x is the apparent flow velocity in x-direction, D_L is the longitudinal dispersion coefficient, and D_T is the transversal dispersion coefficient. The research would model Advective dispersive equation in addition to decay term in the study area.

2.8.3 Boundary Value Problem and Initial Value Problem

Mathematical problems with one or more PDEs and a set of boundary conditions are known as Boundary Value Problem (BVP). Steady state mathematical models form part of this category. The field variable or the unknown quantity (i.e., hydraulic head, concentration) can be specified at some portions of the aquifer boundaries. The derivatives of the field variables (i.e., rates of groundwater flow) can be specified also at portions of the aquifer boundaries to represent groundwater recharge at some points in the aquifer known as point sources or sinks to represent groundwater withdrawal from wells. For boundary value problems, the boundary conditions and the computed values of the field variables are independent of time, with the maximum or minimum values of the field variable occurring all the time at the boundaries of the aquifer or at point sources or sinks [81].

Initial value problems (IVP) are groundwater flow and contaminant transport models that are time dependent. The specified values of field variable, hydraulic head or contaminant concentration and the derivatives (i.e., rates of groundwater flow or contaminant flux) are specified along portions of the aquifer boundaries and at special points (point source or sink) within the aquifer boundaries. Further, the values of the field variable are specified at all points within the aquifer at some initial time t_0 and these specified values are together called initial conditions. A mathematical model is solved for values of the field variables at any point in the aquifer at any time $t > 0$ when combined with the initial conditions and the boundary conditions. For initial value problems, the boundary conditions and the computed values of the field variables can change with time with the maximum and minimum values of the field variable at time t occurring at any point within the aquifer [81].

2.8.4 Analytical Solution

The algebraic solution of model PDE of the groundwater problem obtained with simplifying assumptions gives the analytical solution also known as the exact solution of the problem. Analytical methods seek to obtain functional representation of the solution of the PDE (i.e., mathematical expressions that give hydraulic head or concentration as a function of position and time in the aquifer). The analytical solutions are used to study the behaviour of groundwater flow and contaminant transport processes under hypothetical conditions and help to: (i) determine the sensitivity of the computed values of the hydraulic head to values of the saturated hydraulic conductivity (ii) interpret data from field experiment and laboratory and (iii) accurately verify solutions obtained by numerical methods by comparing computed contaminant concentrations obtained using analytical and numerical methods for a wide range of apparent groundwater velocities and dispersion coefficients [81]. In this research, analytical solution will be used to simulate the radioactive contaminant transport model and compare with the numerical solution.

2.8.5 Laplace Transform

Differential equations have unknown integration constants in the solution. However, for some type of differential equations an algebraic solution can be obtained with the unknown integration constants evaluated whiles performing the solution process using Laplace transform method. For a semi-infinite domain, thus for a given function $f(x)$ in the x direction, where $x \geq 0$, Laplace transform is represented as

$$\mathcal{L}\{f(x)\} = \int_{x=0}^{\infty} e^{-sx} f(x) dx \tag{2.20}$$

where, the variable s chosen is positively large in order to make the semi-infinite integral converge [82]. The Laplace transform technique has the advantage of

incorporating the boundary and initial conditions in the solution process and is suitable for functions that are discontinuous [83].

2.9 Numerical Solution Methods

Numerical models (e.g., finite difference, finite element or finite volume) solve the partial differential flow or contaminant transport equations through numerical approximations using matrix algebra and discretization of the modelled domain. Numerical solutions are employed mainly in problems with complex geometry and time-dependent boundary condition with anisotropic and inhomogeneous aquifer properties. The model domain is discretized to represent a network of grid cells or elements and time of simulation represented by time steps. The accuracy of numerical models depends on the model input data, the size of the space and time discretizations, and the numerical method used to solve the model equations.

Numerical models generally model groundwater problems with irregular boundaries, variations in input parameters such as hydraulic conductivity and recharge, vertical flow gradients at recharge and discharge areas, transient flow conditions, multilayered hydrogeologic framework, and other complexities. Numerical models are best used when: (i) field data shows relatively complex groundwater flow or transport processes (ii) groundwater flow direction, hydrogeologic or geochemical conditions, and hydraulic or chemical sources and sinks vary in time and space, and (iii) input data available is for the model [81]. ANSYS Fluent 13.0 numerical software will be applied in the ground water flow simulation and the solution compared with that from field method.

2.10 Numerical Discretization Methods

Three main numerical methods of discretization are used in groundwater flow and transport modelling. These are Finite Difference Method (FDM), Finite Element Method (FEM) and Finite Volume Method (FVM).

2.10.1 Finite Difference Method

The Finite Difference Method (FDM) initially was applied to petroleum reservoirs but in mid-1960's it was employed in solving groundwater flow and contaminant transport problems. Though the FDM is good for simple problems e.g. one-dimensional steady state, transient, homogeneous, isotropic aquifers and it is efficient and accurate groundwater solutions; the FDM works best for rectangular or prismatic aquifers with uniform composition and has the difficulty in handling irregular and curved aquifer boundaries with anisotropic or homogeneous aquifer properties, and rock layers. To be able to solve complex problems complexities are encountered leading to inaccuracies in solute transport problems [63, 81].

2.10.2 Finite Element Method

Finite element method (FEM) application to groundwater modelling is a recent development [63]. FEM was first used to solve groundwater flow and contaminant transport problems in the early 1970's. Its advantages are that; (i) it can handle irregular or curved aquifer boundaries, anisotropic and inhomogeneous aquifer properties and rock layers can be easily incorporated into the model, (ii) it has accurate and very good solutions (mainly exact solutions) to groundwater flow and transport problems and (iii) its computer programming is modular [81].

A set of algebraic equations with unknown variables (i.e., head or concentration) are determined at the nodal points using this method. Different element types are

employed in finite element dicretization but triangular element is the basic element. Triangular elements have three nodes at the corners at which unknown heads/ concentrations are calculated within the problem domain. Basis function or interpolation function is used to define the head/concentration in each element. Throughout the problem domain the head/concentration is defined in a piecewise manner over individual elements. The finite element method allows the use of variational or residual principles in defining the head throughout the problem domain. Additionally, the flexibility of finite element enables it to be employed in coupled problems, contaminant transport, moving water table or moving boundary problems [84].

2.10.3 Finite Volume Method

The Finite Volume Method (FVM) was originally well documented and used by Evans and Harlow (1957) at Los Alamos. It is mainly used for problems where the unknown variable may not be continuously differentiable including discontinuities in mass, momentum and energy conserved. It is memory efficient and has good speed for large problems and applied in laminar, and turbulent flows. In the late 70s, it was used in solving body fitted grids and in the early 90s the unstructured grid methods emerged. The advantages of FVM are: (i) it uses efficient solvers (ii) cell shape can vary and (iii) mass, momentum and energy conserved on varying grids. The main disadvantage of FVM is the false diffusion when used for simple problems.

The governing PDE is integrated over domain divided into control volumes and a set of linear algebraic equations for each control volume is solved iteratively using simplifying assumptions. This method is applicable for 2D and 3D grids and can handle triangular, quadrilateral, tetrahedral and hexahedral elements. Information on

FVM can be found in [85]. ANSYS Fluent 13.0 solvers use this technology and which shall be used in this research to model groundwater flow in 2D using triangular element assuming a very thin aquifer thickness with respect to the width and length of the physical geometry.

2.11 Transient Groundwater Flow to Pumping Well

As a well is pumped, cone of depression results that fluctuates with time. The continuous extraction of water leads to the cone gradually approaching a steady state and the cone deepens with time. The amount of water released from storage from a column of an aquifer through a unit cross section for a unit decline of head is storage co-efficient (storativity) [77]. The pumping of a well in a confined aquifer at a constant rate influences the discharge and extends outwards with time. Theis [28] developed an equation for an unsteady state flow from the analogy of groundwater and conduction of heat. The equation for unsteady state or transient flow in a well show that drawdown s of the piezometric surface is related to the time of pumping in a confined aquifer [77]. Unsteady flow starts from the moment of pumping until steady state is reached. Unsteady state results when an infinite horizontal, confined aquifer of constant thickness is pumped at a constant rate. During the unsteady state flow, the changes in water level in the pumped well and piezometers can be measured and the changes in hydraulic gradient can be measured [15].

2.11.1 Well Loss of a Well in Confined Aquifer

As water is pumped out of a well Figure 2.9, the total drawdown caused is the sum of the logarithmic drawdown curve at the well face and the flow through the well screen and axial movement inside the well.

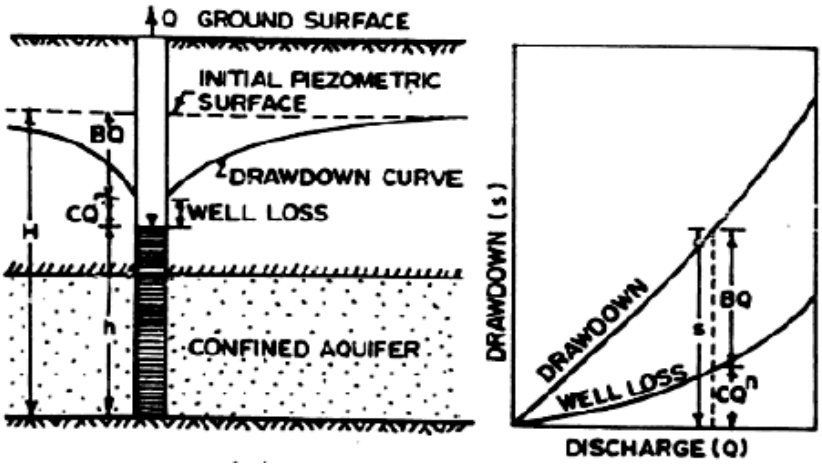

Figure 2.9: Well loss and aquifer loss as drawdown and drawdown versus discharge in confined aquifer [77].

The term well-loss is used to denote the latter drawdown. As turbulence is normally experienced near the well face, the well-loss is taken to be proportional to Q^n. It must be noted that if the screen is not clogged and its size is compatible to the surrounding porous media then the well-loss caused by water entering the well is small as compared to that from axial movement inside the well to the pump intake [77].

2.11.2 Specific Capacity (S_c) of a Well in Confined Aquifer

The specific capacity of a well is defined as the yield of the well per unit time per unit drawdown and is a measure of its effectiveness. Thus, specific capacity S_c is given as

$$S_c = \frac{Q}{s} \tag{2.21}$$

The total drawdown of a well of Figure 2.8 in the aquifer is,

$$s = BQ + CQ^n \tag{2.22}$$

where, BQ is aquifer loss and CQ^n is well loss, the specific capacity

$$S_c = \frac{Q}{BQ+CQ^n} = \frac{1}{B+CQ^{n-1}} \tag{2.23}$$

where, $B = [\ln(R/r)]/2\pi T$, C is a constant determined from factors such as well radius and n is an integer greater or equal to 1. Equation (2.26) shows that the specific capacity of a well is not constant but decreases as discharge increases.

2.12 Simulation Softwares

Code selection is very important in modelling and simulation. In this research, ANSYS Fluent 13.0 and MatLab R2013a softwares were selected for the simulations.

2.12.1 ANSYS Fluent 13.0

ANSYS Fluent 13.0 is a Computational Fluid Dynamics (CFD) code [86], robust and efficient software for modelling all physical models and flow types, steady state or transient, compressible and incompressible flows, laminar or turbulent flows, Newtonian or non-Newtonian flows, ideal or real gases and many more. The ANSYS Fluent 13.0 software has the capability of solving 2D and 3D flow and transport models. The mesh types supported include triangular, quadrilateral, tetrahedral, hexahedral, pyramid, prism and polyhedral meshes [78]. Triangular meshing will be used in this research work.

2.12.2 MatLab R2013a

MatLab means Matrix Laboratory; a multi-paradigm numerical computing environment and fourth generation language (4GL). It is a high-performance language for technical computing. It combines computation, programming, and visualization in an easy-to-use environment where problems and solutions are expressed in mathematical notation. MatLab is an interactive system that makes use of arrays and matrices data [87].

2.12.3 Model Calibration, Verification and Validation

Generally, calibration is the process of finding acceptable values for parameters of a physical model [63]. Model calibration involves tuning parameters and coefficients to get the best matching output to the observed or field values. Verification is the process by which a model is capable of simulating some historical hydrologic event for which field data is available [63]. Validation is the process of gaining confidence in the model embodied in a computer program as a correct representation of system for which it is intended. The process of validation involves comparing model predictions with independent field/experimental observations [72].

2.12.4 Errors in Modelling

It is difficult to represent exactly a real system with a model. Therefore simplifying assumptions are used since all field behaviours may not be fully understood. The inability to completely understand the field process and incorporate them in the model leads to *conceptual error*. Other sources of errors in numerical model are *truncation error*, *round-off error* and *data error*. Firstly, truncation error occurs as the exact solution differs from the partial differential equations formulated due to Taylor's series approximation. Secondly, round-off error occurs when the solution obtained from finite accuracy of computer calculations differs from the exact solution from field method or from algebraic equations. Thirdly, data error occurs because the aquifer description data (hydraulic properties) are rarely accurately and completely known [72, 75].

CHAPTER THREE

MATERIALS AND METHODS

This chapter describes the study area in terms of location, geology, geomorphology, hydrogeology, geohazard, geophysics, geochemistry, climate, vegetation and land-use. The chapter further dwells on aquifer characteristics; input data for models (porosity, hydraulic parameters, flow path, flow rate); conceptual model; assumptions; physical domain; groundwater flow; contaminant transport; mathematical formulation; 1D analytical and numerical for ADDE; 2D analytical solution for ADDE, boundary and initial conditions, and model errors.

3.1 Study Area

3.1.1 Location and Geomorphology

The study area forms part of Ga East District and Adenta District and located between latitude $5^0$40’0” N – $5^0$45’0” N and longitude $0^0$9’10” W – $0^0$15’0” W as shown in Figure 3.1.

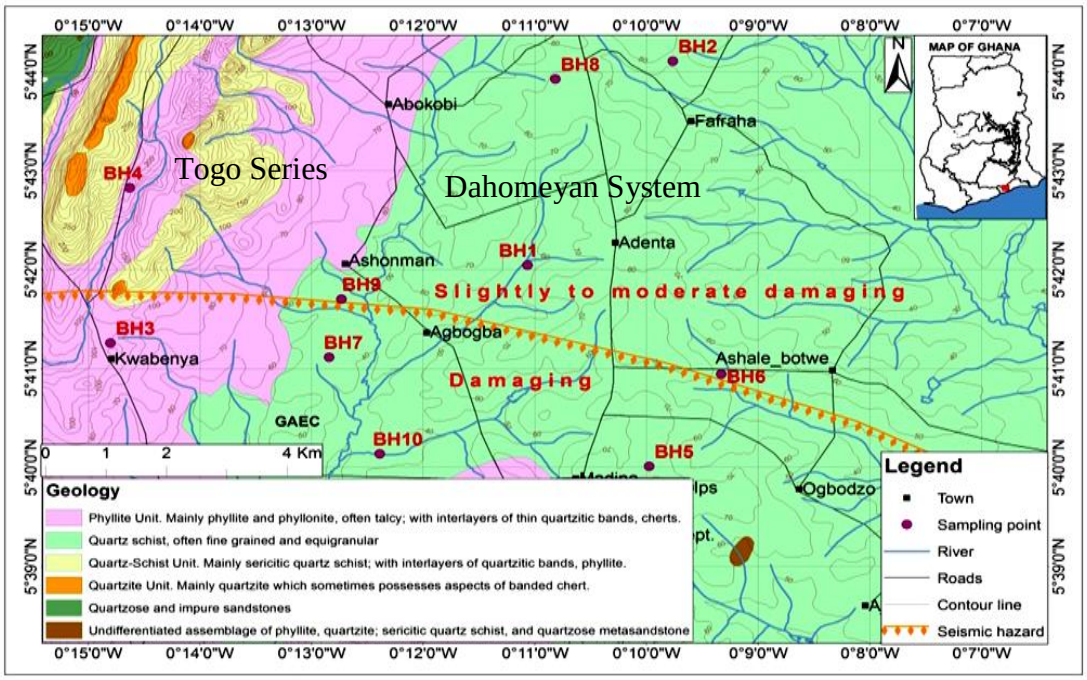

Figure 3.1: Hydrogeological map showing boreholes and seismic hazard line.

The study area covers an area of about 102.80 km^2 and has a rapid growth of population. The choice of this study area was informed by the location of Ghana Atomic Energy Commission (GAEC) being the major producer of radionuclide waste in Ghana in this environment. GAEC in order to locate an engineered radionuclide waste disposal site considered this domain for low to intermediate radionuclide waste repository due to the suitability of the crystalline hard rock underlying the domain.

The study area often called Eastern Lowlands/Coastal Plains/Accra Plains occupies the eastern part of the Akwapim Range and underlain by gentle, mature topography which slightly slopes towards the ocean [4]. The Eastern Lowlands as recognized by [88] has a pedimented surface and forms a low-lying terrain with no pronounced topography and rare outcrops. The directions of main rivers are recognized as lineaments in aerial photographs and they possibly present zones of weakness in the rocks, which are due to steeply dipping faults, preferred directions of dike intrusions, joint or shears [89].

3.1.2 Geology and Hydrogeology

The geological units underlying the Greater Accra Region are mainly Granitoids, Dahomeyan System, Togo Series, Voltaian System, and Accraian Series [11, 90]. However, the Togo Series (TS) and the Dahomeyan System (DS) that are of Precambrian age underlie the study area. The Togo Series occupied about 30% of the study area consists of siliciclastic sediments and moderately weathered. The rock mainly contains phyllites and phyllonites and possesses Upper Proterozoic age [4]. The rocks are highly folded, jointed and fractured with secondary porosity. It has a high recharge capacity with a depth to groundwater table between 0-20 m. Clay materials which are less permeable form the overburden as well as highly permeable

sand and rock fragments. The TS has moderately good water potential suitable for small scale water supple my mechanized boreholes [4, 11]. The Dahomeyan formation occupied about 70% of the study area and consists mainly of schists with variable amounts of quartz. The DS of the study area consists mainly of quartz-schists with variable amount of quartz. Aquifers in the DS are confined with low infiltration rate which makes it less vulnerable. Borehole yield ranges between 1 – 3 m^3/hr with borehole depths range between 45 – 70 m with a mean of 55 m. The mean transmissivity of the Dahomeyan rocks is 4.5 m^2/day [91]. Generally, fracture occurrence has been found to decrease with depth [92]. Geological map of eastern Greater Accra Region reveals faults in the study area [90].

The rock formations underlying the study area are impermeable with groundwater occurrence associated with secondary porosity resulting from fracture and weathering [11, 93]. There are three aquifers with good groundwater potentials in these rock formations. The borehole yields of both the confined and unconfined aquifers range between 0.41 - 29.8 m^3/hr [19, 94]. Nine out of ten borehole yields of the study area considered were all below 12.4 m^2/day that shows the borehole can serve at least domestic purpose and therefore need protection. The pumping test data collected on study area indicated that boreholes depths vary between 55 – 90 m and the boreholes yields vary from 5 – 60 L/min (i.e., 0.3 – 3.6 m^3/hr) indicating low yield.

3.1.3 Geohazard and Borehole Geophysics

The extract of geohazard map of Greater Accra Region, indicates the seismic hazard of the study area. The macro-seismic intensity shows the effects of earthquake on men, buildings and landscape. The intensity classification was based on international

scale MSK-1964 and the study area lies between iso-seismal intensity of VI-VII, indicating a range of slightly - moderately damaging effects [95].

Borehole geophysics investigation gives good vertical profile data on the lithology, and flow components (production zones). Similarly, it provides good profile data structure, permeability, porosity and water quality of the groundwater system. However, the lithology of the study area was extracted and depicted in the bore logs **Appendix A**.

3.1.4 Hydrogeochemistry

Geochemistry contributes enormously to the understanding of groundwater systems since 1950 [96]. Groundwater undergoes hydrochemical processes as it moves from the recharge areas to the discharge areas. Deep groundwater in central Region of Ghana was noted to have high Total Dissolves Solutes (TDS) or more mineralized due to longer trip from recharge to discharge area [97] indicative of the slow movement of groundwater in saturated zones. Hydrogeochemical and isotope studies on groundwater in the Accra Plains showed that the domain has poor water quality and mainly saline [5, 21, 93, 98].

3.1.5 Climate, Vegetation and Land Use

The study area lies in the coastal savannah zone, which is the driest climatic zone in Ghana. There are two rainy seasons: April to June and September to October with the first being the stronger. The mean annual rainfall is about 730 mm, which occurs mainly within the two rainy seasons from May to July and from August to October. The highest mean monthly temperature of 28.4ºC occurs during February, and the lowest mean monthly temperature of 25.1ºC occurs during August [89].

The vegetation is of the typical Savannah type. Grassland and clusters of shrub occupy the Western and Eastern Lowlands. Urban agriculture plays a very important role in supplying food to the metropolitan population, but as the agricultural plots are situated along heavily polluted urban streams and drainage channels, the vegetable farming is not without its health hazards. Land use pressure due to expanding metropolitan areas may in the future reduce the space used for agricultural purposes in the urban and peri-urban areas [12].

3.2 Estimation of Aquifer Hydraulic Parameters

Pumping test, recovery test and borehole logs data of boreholes drilled in March 2012 in ten communities in the study area were collected from the Community Water and Sanitation Agency (CWSA), Accra. The data include static water level (SWL), dynamic water level (DWL) and well depths. Site visits were made to collect coordinate/well location and the well elevation above mean sea level. These wells were pumped for a maximum period of 6 hours and a maximum recovery period of 3 hours and the information used to estimate the aquifer hydraulic parameters (e.g., porosity n, transmissivity T, and hydraulic conductivity K). A hydrogeolgic chart was drawn to reflect the well location, elevation, water level before and after pumping, aquifer top and well depth in relation to mean sea level.

3.2.1 Stratigraphy and Lithology of Aquifers

Figure 3.2 is a simplified representation of borehole logs of the study area. The lithology of the individual boreholes is presented in the **Appendix A**.

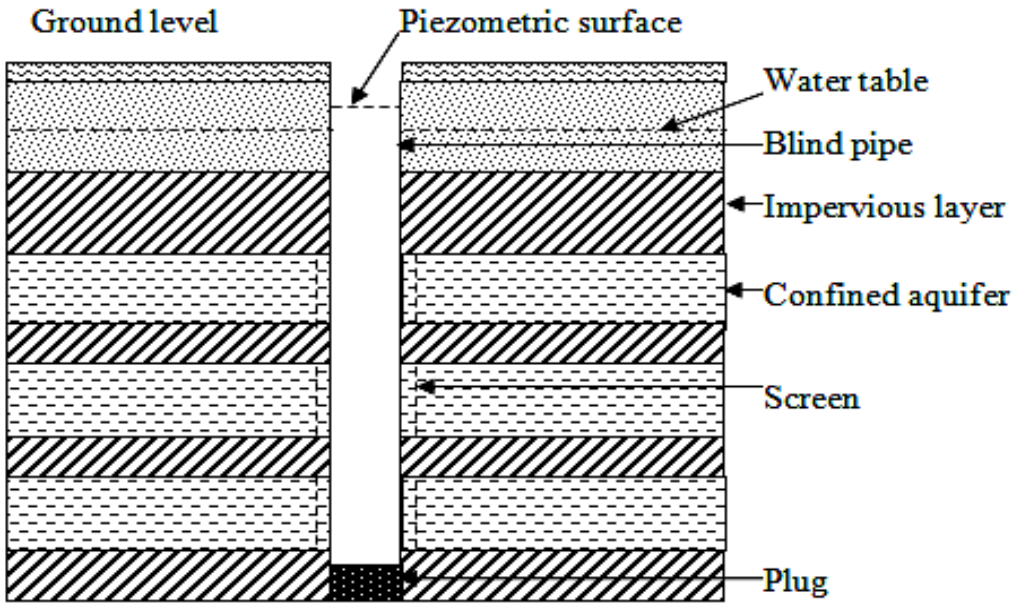

Figure 3.2: Aquifers underlying the study area.

The Figures A1, A2, and A3 in Appendix A show the stratigraphy of the overburden and the bedrock in which the aquifers were located and how deep the wells were. In Appendix A, Figure A1, fractures were met in dark grayish schists, quartzite schists, dark grayish schists and light schists for BH1, BH2, BH3 and BH4 respectively. The fracture positions were indicated in the borehole logs for BH2, BH3 and BH4 but not indicated for BH1 since it was low yielding. In Figure A2 of Appendix A, fractures were encountered in schists, grayish schists, and quartzite schists for BH5, BH7 and BH8 respectively and no fracture position indicated for BH6.

In Figure A3 of Appendix A, fractures were encountered in a weathered quartzite for BH9 and BH10 but not pronounced in BH10 and fracture positions not indicated in BH10 were in quartzite schists. Generally, nine out of ten boreholes have fractures in schists with three of them not having fracture position indicated due to low yield and the other one borehole having fracture in weathered quartzite. The average groundwater temperature was found to be 26.5^{o}C for all the wells.

3.2.2 Aquifer Type Characterization

Aquifer formation types were determined using pumping test data for the respective boreholes in the domain of study. The Microsoft Office 2007 (Excel) semi-log plots of drawdown s against logarithm of time t using pumping test data were used in identifying the aquifer formation types of the domain.

3.2.3 Effective porosity

The borehole logs of 7 out of 10 successful wells were analyzed in order to obtain accurate estimate of the total porosity (n). The total porosity of aquifers in the study area was estimated using the screen voids/fractures to total bedrock thickness containing the fractures. In other words the total porosity was estimated from the ratio of sum of screen vertical lengths (e) installed to total vertical length of bedrock (E). The vertical length of the bedrock was taken from the top of the bedrock to the bottom of the well for consolidated, confined, fractured domain of the study area.

The total porosity was estimated as the ratio of fracture volume to volume of the bedrock containing the fracture. The total porosity is the fraction of effective length of screen installed that was used during groundwater flow multiplied by the ratio of fracture volume to volume of bedrock containing the fracture. This effective fraction used during groundwater flow was taken to be 80% of the total installed screen length. The amount of perforation or voids created in the effective screen section that enable fracture flow was also taken to be 40% of the effective screen section that permits groundwater flow into the well.

The result of the analysis gives secondary porosity also known as effective porosity as 0.32(e/E) estimated for the respective boreholes. It must be noted that the total porosity assuming the fracture size used during groundwater flow is 0.8(e/E) if no

screen is installed. If screen is installed, the effective porosity is calculated using 0.32(e/E) for the study area.

3.2.4 Transmissivity, Hydraulic Conductivity and Storativity

The hydrologic parameters (transmissivity, hydraulic conductivity and storativity) make the description of groundwater in the aquifer possible. The pumping test recovery data were analyzed using [28] recovery method. In this method the residual drawdown s' in the well was plotted against the time ratio (t/t'), where t represents the time elapsed since pumping began and t' is the time elapsed since pumping stopped. The residual drawdown plotted on the y-axis and the time ratio (t/t') plotted on the logarithmic x-axis. A straight line was fitted through the data plot and the slope of the line determined for a one-log cycle to estimate the transmissivity (T) of the aquifer.

The aquifer transmissivity for the wells were estimated from the Theis recovery method [28] as

$$T = \frac{2.303Q}{4\pi\Delta s'} \tag{3.1}$$

where, Q is rate of discharge and $\Delta s'$ is residual drawdown for one log cycle.

The aquifer thickness b was estimated from the well construction borehole logs and water level data for the seven wells reported to be successful by deducting the aquifer top screen level from the bottom level of the well. The only exceptions to this aquifer thickness determination were the three wells reported to be marginal as the screen locations were not indicated on the borehole logs. Knowing the thickness of the aquifer, the hydraulic conductivity (K) was calculated from the relation,

$$K = \frac{T}{b} \tag{3.2}$$

where, b is the thickness of the aquifer.

According to [15], the recovery method [28] is valid for estimating aquifer transmissivity if: (a) the aquifer is confined, unconfined or leaky, (b) $t > 25Sr^2/T$, and (c) $t' > 25Sr^2/T$. The r represents the radius of the wells and the S represents the storage coefficient of the aquifer.

The parameter S is calculated from aquifer tests where drawdown data collected were analyzed for a monitoring well used in an aquifer test. The storativity was estimated using Cooper Jacob method, which is similar to Theis recovery method. In the Cooper Jacob straight line method, drawdown of a monitoring well is plotted arithmetically against the time on logarithmic axis. The slope and the time intercept on the time axis were used to estimate the hydraulic parameters of the aquifer as

$$T = \frac{2.3Q}{4\pi\Delta s} \tag{3.3}$$

and

$$S = \frac{2.25Tt_0}{r^2} \tag{3.4}$$

where, T is transmissivity, S is storativity, Q is pumping rate or yield, Δs is drawdown over one-log cycle, t_0 is intercept on time axis and r is radial distance from pumping well to monitoring well [99]. The storativity estimated was used as a guide in the actual domain storativity estimation through model simulation.

It should be noted that the only available data on the domain of study at the time and complete were used in the analyses. There was only one data on a pumping well and a monitoring well constructed in 2003 that was used in the analysis of the storativity. The coordinates of these wells were not taken as several attempts were made to locate them failed because the wells were abandoned and covered with thick bushes. The location can be estimated as being in a vicinity of mechanized borehole for which there were not enough data to analyze.

The specific storage *Ss* were estimated by dividing storativity by the aquifer thickness. Also, the diffusivity *Ds* of the study domain were also estimated by dividing transmissivity by storativity or by dividing the hydraulic conductivity by the specific storage.

3.3 Groundwater Pattern Assessment

3.3.1 Flow Path

Three-point method in determining groundwater flow path/direction was used. The coordinates of the wells were plotted on a map Figure 3.3 and the static water levels were considered for the three-group set of wells. Three main things needed to determine the groundwater flow path are; (i) static water level (ii) location of the wells and (iii) distances between well pairs that form the set of three [16].

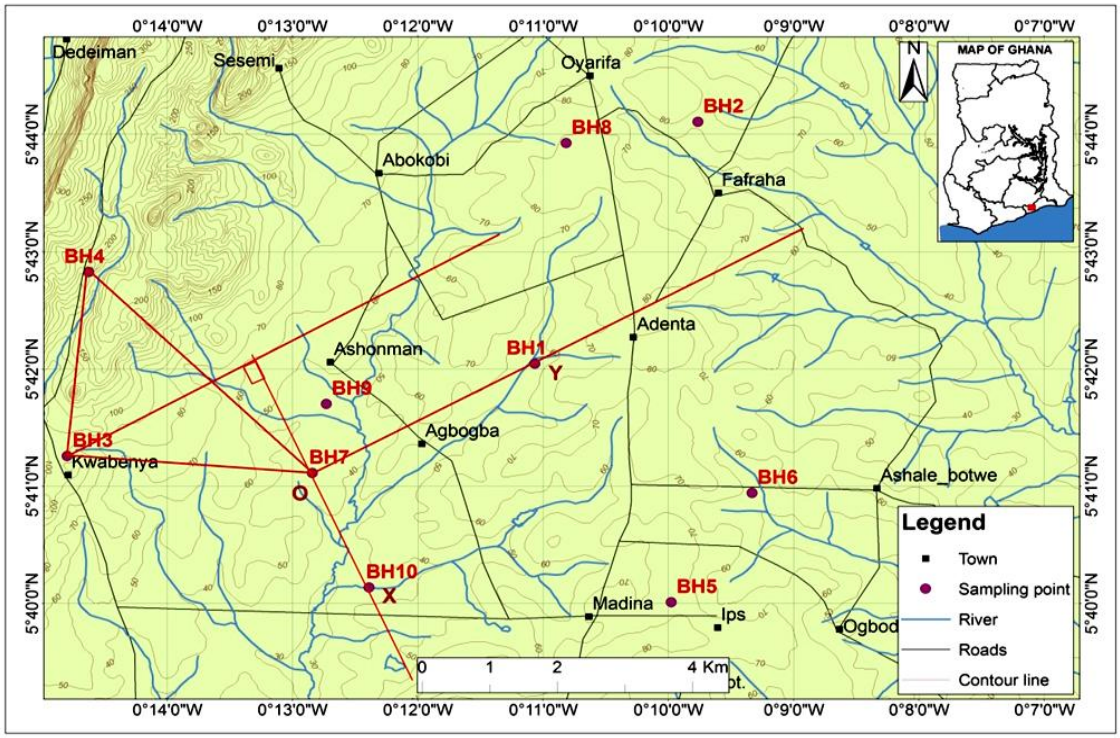

Figure 3.3: The topography of study area showing the sample boreholes.

The static water level of each well was part of the data taken from CWSA. Figure 3.3 shows the location of wells used in the research analysis. The well locations were taken using Garmin 12 Global Positioning System (GPS) at the respective boreholes during the site visits. Static water levels were then standardized using the elevation above mean sea level data taken.

3.3.2 Hydraulic Gradient

The hydraulic gradient determines how fast or slow groundwater flows and contaminant transported based on its value in the study area. This research made use of the three-well graphical method to determine the hydraulic gradient and the flow path/direction [16] of the well field for ten well sets Table 3.1.

Table 3.1 Ten well sets of three used in the analysis

Well set 1	Well set 2	Well set 3	Well set 4	Well set 5	Well set 6	Well set 7	Well set 8	Well set 9	Well set 10
BH4	BH4	BH4	BH3	BH5	BH1	BH1	BH3	BH4	BH4
BH3	BH3	BH3	BH5	BH9	BH7	BH10	BH5	BH1	BH3
BH9	BH7	BH6	BH2	BH8	BH10	BH6	BH9	BH10	BH10

The hydraulic gradients were determined by using procedures in [16]. A sketch was made to scale indicating the wells positions as shown in Figure 3.4, using the following procedure:

1. The three-well sets were connected with lines between each pair of wells
2. Hydraulic head elevation for each well was indicated
3. Map distance between wells with highest and lowest head level of three well set was measured
4. Difference in head elevation of the highest and lowest of three well set was determined

5. Map distances for each unit change in hydraulic head of the highest and lowest of three well set were found by dividing the map distance by the head difference
6. Even increments along the highest and lowest head well pairs were marked
7. Steps 3 to 6 for all ten highest and lowest well pairs were repeated
8. Contour line of equal heads of the medium head level joined with that in-between highest and the lowest head level
9. The gradient of the surface was in the direction of increasing head and perpendicular to the contour line but opposite to the direction of flow.

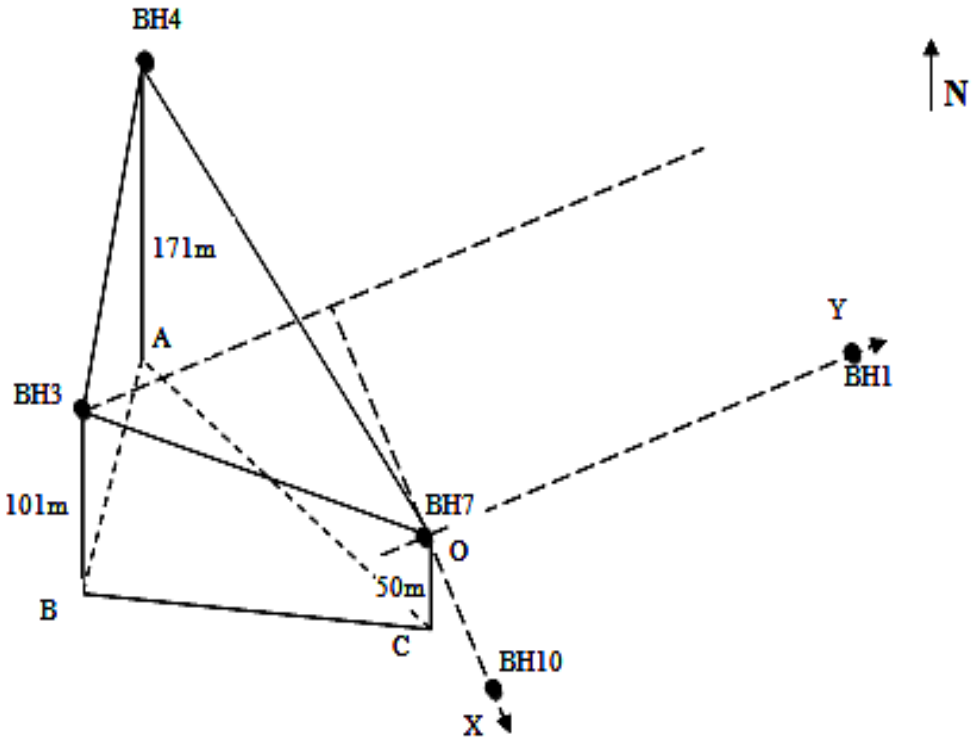

Figure 3.4: Three point problem indicating well positions.

For three wells forming a right triangle, the direction of flow can be mathematically determined [16]. For three wells at the corners of a triangle forming OX and OY at right angles to each other at O, $\frac{dh}{dx}$ (head difference in two wells, divided by separating

distance) represents the gradient of the wells measured from well O to well X and $\frac{dh}{dy}$ represents gradient of wells measured from well O to well Y. The gradient at right angle (perpendicular) to the equipotential lines is given as:

$$\nabla h = \sqrt{(dh/dx)^2 + (dh/dy)^2} \quad (3.5)$$

The angle $\emptyset$ that the direction of the gradient makes with line OX is given as

$$\emptyset = \tan^{-1}\left(\frac{dh/dy}{dh/dx}\right) \quad (3.6)$$

3.3.3 Flow Velocity

The flow velocity referred to as the Darcy velocity measured in (L/T) is estimated by first finding the hydraulic gradient and the hydraulic conductivity of the aquifer. The flow velocity was calculated using Darcy's equation i.e.

$$v_x = -K_x \frac{dh}{dx} \quad (3.7)$$

$$v_y = -K_y \frac{dh}{dy} \quad (3.8)$$

K_x is the average hydraulic conductivity in the x direction and K_y is the average hydraulic conductivity in the y direction measured in (L/T). The pore water velocity in x and y directions are $\bar{v}_x = v_x/n$ and $\bar{v}_y = v_y/n$, where n is the effective porosity. In the same vein the flow rate (L^2/T) is determined as a product of transmissivity and hydraulic gradient. Groundwater flow direction, hydraulic gradients in both x and y coordinate axes and flow rates were estimated for each of the ten well sets presented in Table 3.1.

3.4 Development of Conceptual Framework and Physical Models

A conceptual model is a simplified representation of the key features of the physical system. It forms the basis for the site-specific computer model, but is itself subject to

some simplifying assumptions [100]. Figure 3.5 represents the conceptual model of the physical hydrogeologic system developed.

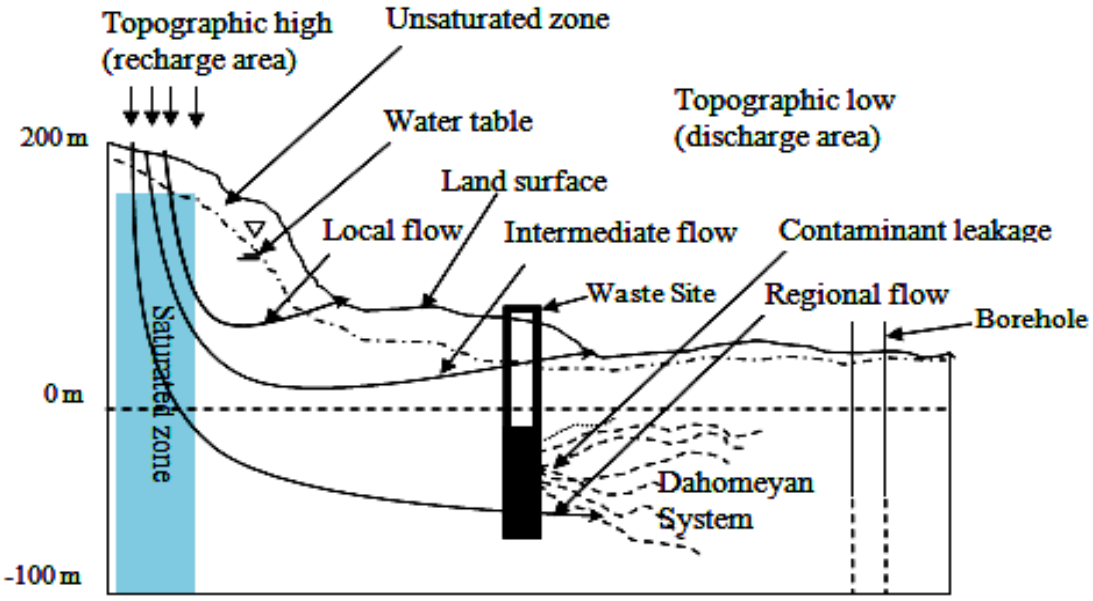

Figure 3.5: Physical domain developed.

The physical domain of the study area shows the topography of the recharge (high level) and the discharge (low level) areas as indicated. The domain below the water table shows the saturated zone. The saturated zone marks the region in the subsurface where water fills all the voids in the porous media. The unsaturated zone is that above the water table. A radioactive waste borehole disposal facility site is indicated as well as a monitoring borehole. Also shown in the diagram are the local flow, the intermediate flow and the regional flow directions. Groundwater flows from high topographic level to low topographic level of the study area [64]. Many researchers including [64] maintained that groundwater flows in three regions – local flow, intermediate flow and regional flow. For local flow, groundwater moves fast and discharges in the immediate valley or low land whiles in the intermediate flow water moves slowly and discharges into a far distant point separated by high land. For

regional flow, groundwater moves very slowly horizontally and discharges in a very far distant low land and mainly in the sea.

3.4.1 Simplifying Assumptions used in Model Formulation

The simplifying assumptions used in obtaining analytical solution were used in reducing a heterogeneous geometry to a simple homogeneous geometry that is easy to solve. These are:

(a) Newtonian fluid (water) is considered

(b) Water is incompressible with constant density and viscosity

(c) Water is miscible and at constant temperature

(d) Aquifer stress-strain is elastic

(e) Aquifer is rigid and non-deformable

(f) Chemical reaction is in equilibrium

(g) Domain is homogeneous and isotropic in permeability

(h) Water/contaminant flow is laminar and Darcy's law is valid

(i) Flow is horizontal and in 2D sufficient for the simulations

(j) Change in thickness of aquifer in -response to changes in head is negligible

(k) Radioactive contaminant transport occurs in saturated zone of confined aquifer

(l) Gaseous release not considered

(m) Contaminant subject to first-order transformation (for conservative contaminant, $\lambda = 0$)

(n) Flow is in x-direction (SSE) only and velocity is constant (uniform flow)

(o) The longitudinal and transverse dispersion coefficients (D_x, D_y) are constants

3.4.2 Application of EPM Model

Models are simplified representation of reality because of the inherent complexity of flow in porous and fractured formations [101]. The application of EPM model to aquifers of the study area using pumping test data from which the hydraulic conductivities of fractured schists were estimated was on a scale of a few hundreds of meters. This preliminary study in modelling horizontal groundwater flow (regional groundwater flow) and radioactive contaminant movement in the study area is based on EPM model that considered the fractured domain as confined saturated porous medium in continuum representative elemental volume (REV)/control volume with properties of the medium assumed to be constant. The physical models developed in Figures 3.6a and 3.6b are geometries for modelling groundwater flow and radioactive contaminant transport respectively.

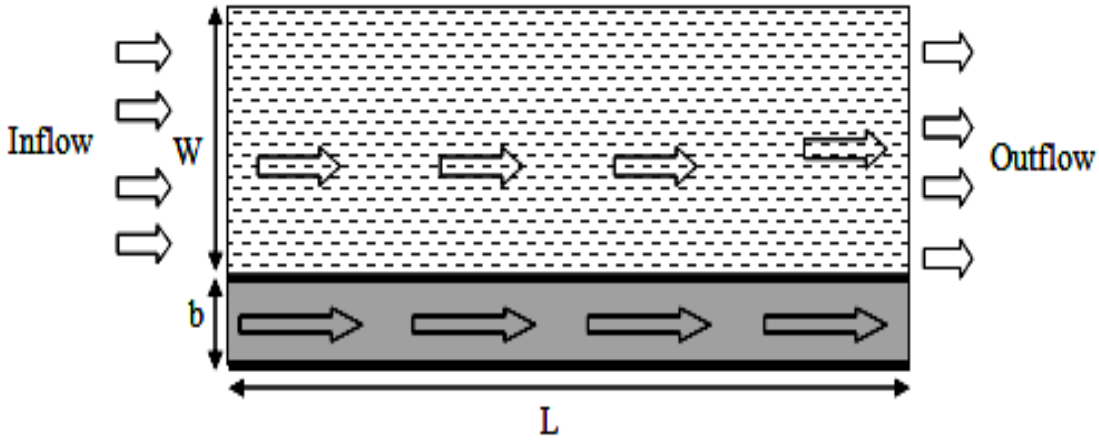

Figure 3.6a: The physical model for groundwater flow.

In Figure 3.6a, W, L, and b represent aquifer width, length, and thickness respectively. Inflow and outflow are flow boundaries and top and bottom of the aquifer model represents aquicludes (no flow boundaries). The thickness of the aquifer model was so small and negligible compared to the width and the length. For a

constant thickness b, that is negligible the model represents an areal model that is 2D in x and y directions. The model was used to model uniform flow in x direction.

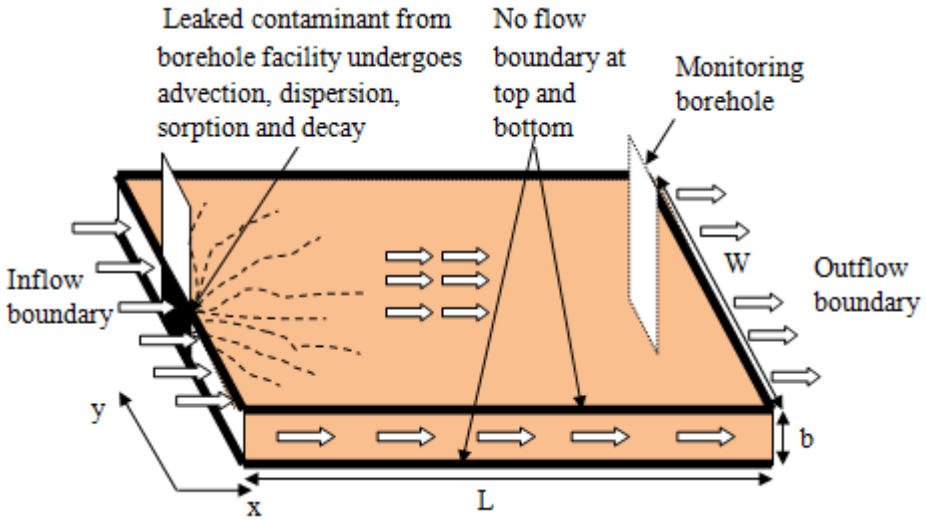

Figure 3.6b: The physical model for radionuclide transport.

In Figure 3.6b, L represents the length of the aquifer, b denotes the thickness of the aquifer bounded at top and bottom with aquicludes (impermeable layers) and W refers to the width of the aquifer and all these quantities (i.e., L, b, and W) were measured in meters. Inflow and outflow boundaries were indicated in addition to the no flow boundaries. As with the flow model, the radioactive contaminant model has the same geometrical representation except that radioactive contaminant source is leaking into the groundwater that undergoes advection, dispersion, sorption, and decay processes in space and time.

3.4.3 Groundwater Flow

Darcy's relation or law is used to predict the rate of flow through geologic porous media. The water flow rate is written as a flux or the volume of water per unit cross-sectional area per unit time. Darcy deduced the apparent water velocity (flux, v_x) in

the x-direction as (3.7). The total hydraulic head is given as the sum of the pressure head (ψ), the elevation head (z) and velocity head. Thus,

$$h = \psi + z + \frac{v^2}{2g} \tag{3.9}$$

where, $\psi = P/\rho g$, P is the pressure of water at elevation z, ρ is the density of water and g the acceleration due to gravity. For laminar flow, velocity is very small and negligible. Taking the derivative of (3.9) ignoring the velocity term gives, $dh = d\psi + dz$. But $dz = 0$, therefore $dh = d\psi$. Groundwater flows in three dimensions and the apparent water velocity vector is given as

$$\boldsymbol{v} = -(K_x \frac{\partial h}{\partial x} + K_y \frac{\partial h}{\partial y} + K_z \frac{\partial h}{\partial z}) \tag{3.10}$$

where, K_x, K_y, and K_z are the hydraulic conductivities in the x, y, and z directions and h, the hydraulic head. The groundwater flow velocity will be determined using Darcy's equation and the result compared with groundwater flow velocity calculated from numerical computational software, ANSYS Fluent 13.0.

3.4.4 Radionuclide Transport

Strontium-90 and Carbon-14 were radionuclides used in this research work. Strontium-90 is a radioactive element that has a half-life of about 28 years, a decay constant of 9.4E-05 and the same distribution coefficient as that of Carbon-14 [102]. The source of radioactive waste in the domain was through leakage of by-products from nuclear reactor placed in the borehole disposal facility. The radiations emitted from the radioactive materials and carried by groundwater are hazardous to human health and knowledge on its distribution in the ground is very important to decision makers.

The canisters of the radioactive waste repository contain activated metal parts that corrode and release radioactive carbon-14. The gas phase of carbon-14 is not considered in this research. However, in a saturated geologic medium, the radioactive carbon-14 is transported by the groundwater in the aquifers through fracture spaces. Carbon-14 has a decay constant of 4.6E-07 and a distribution coefficient of 0.0001 in crystalline rocks [102].

These radioactive contaminants undergo processes as they move from recharge area to discharge area in the subsurface. Advection, diffusion, dispersion, reaction and decay are five main processes that control radioactive contaminant movement by groundwater in crystalline rock formations. These processes are combined in the mathematical model to represent the behaviour of contaminant in the aquifer. Advection is the process by which contaminants are transported by the bulk motion of the flowing groundwater whiles diffusion is the process by which contaminants are transported by random thermal motion of contaminant molecule. The mechanical dispersion (hydraulic dispersion) is a mixing or spreading process caused by small-scale fluctuations in groundwater flow rate along the tortuous flow paths within individual pores. On a much larger scale, mechanical dispersion is caused by the presence of heterogeneities (clay lenses or faults) within the aquifer. Sorption and decay processes also occur in the contaminant transport in the subsurface. Detailed information on contaminant transport can be found in [14, 16, 63, 81, 103].

3.5 Mathematical Formulation of Aquifer Flow Equations

3.5.1 Transient Groundwater Flow Equation

Groundwater flow equations were formulated from the conceptual framework using simplifying assumptions, boundary and initial conditions, governing laws (i.e.,

conservation of mass, momentum, Darcy's law, Fick's law) and constitutive equations. To analyze the flow of water, a unit volume, representative elemental volume (REV) or control volume of saturated porous media has been considered Figure 3.7 whose boundaries are control surfaces.

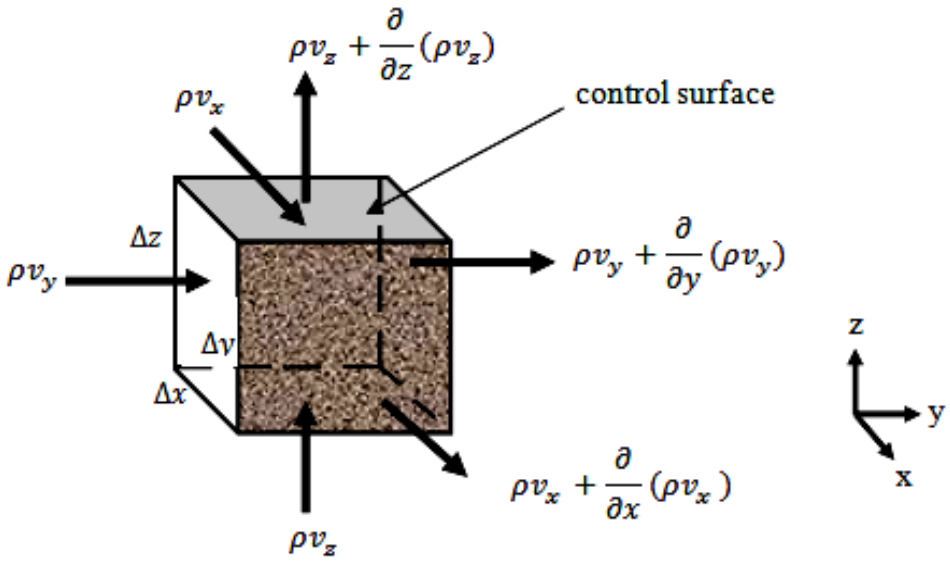

Figure 3.7: Control volume for groundwater flow through porous media.

For transient flow, the law of conservation of mass requires that, net rate at which water enters control volume equal the time rate of change of water mass within the control volume.

Net rate of inflow = inflow - outflow = rate of change in storage (3.11)

$$-\frac{\partial}{\partial x}(\rho v_x) - \frac{\partial}{\partial y}(\rho v_y) - \frac{\partial}{\partial z}(\rho v_z) = \frac{\partial}{\partial t}(\rho n) \quad (3.12)$$

The dimensions of the term $\frac{\partial}{\partial t}(\rho n)$ are M/L^{3}T, which is the time rate of change of water mass per unit control volume. For transient flow in saturated porous media, the rate of water storage in the control volume is related to the rate of change in hydraulic head.

Considering the x-direction, the rate at which groundwater leaves the control volume is given by the Taylor series approximation

$$\rho v_x + \frac{\partial}{\partial x}(\rho v_x)\Delta x + \frac{\partial^2}{2!\partial x^2}(\rho v_x)\Delta x^2 + \frac{\partial^3}{3!\partial x^3}(\rho v_x)\Delta x^3 + \cdots \quad (3.13)$$

For a small REV, the higher order terms of Δ are negligible i.e., Δ^2, Δ^3, but in this case, a unit control volume was used ($\Delta x = \Delta y = \Delta z = 1$). The rate at which groundwater leaves the REV in the x-direction is $\rho v_x + \frac{\partial}{\partial x}(\rho v_x)\Delta x$. Expanding the right-hand side of equation (3.12) gives

$$\frac{\partial}{\partial t}(\rho n) = \frac{\partial}{\partial h}(\rho n)\frac{\partial h}{\partial t} \quad (3.14)$$

and

$$\frac{\partial}{\partial h}(\rho n) = \rho\frac{\partial n}{\partial h} + n\frac{\partial \rho}{\partial h} \quad (3.15)$$

At the right hand side of equation (3.15), the first term represents the mass of water produced by expansion or compression of the porous media and the second term represents the mass of water produced by the expansion and compression of the water. This means that for a saturated porous media, water can only enter the control volume if the porosity increases i.e. $\frac{\partial n}{\partial h} > 0$ or the water density increases, $\frac{\partial \rho}{\partial h} > 0$.

The porous media has two parameters; the porous media compressibility α and fluid compressibilityβ. The compression or expansion of porous media is caused by change in effective stress σ_e .

$$d\sigma_e = -\rho g d\psi \quad (3.16)$$

But, $h = z + \psi$, and $dh = d(\mathrm{z} + \psi)$, $dh = d\mathrm{z} + d\psi$, z = constant, $d\mathrm{z} = 0$. Therefore,

$$d\sigma_e = -\rho g dh \quad (3.17)$$

The compressibility α of a porous media is

$$\alpha = -\frac{d\mathrm{V_w}}{V}\frac{1}{d\sigma_e} = -\frac{dn}{d\sigma_e} \quad (3.18)$$

where, V is the control volume and V_w the water volume. Equations (3.16) and (3.18) yields

$$\frac{dn}{dh} = \alpha\rho g \tag{3.19}$$

The fluid compressibility is defined as

$$\beta = \frac{dV_w}{V_w}\frac{1}{dp} \tag{3.20}$$

where, p is the water pressure. The change in pressure is given as

$$dp = \rho g d\psi = \rho g dh \tag{3.21}$$

with $dV_w/V_w = d\rho/\rho$. Then equation (3.20) becomes

$$\beta = \frac{d\rho}{\rho}\frac{1}{\rho g dh} \tag{3.22}$$

or

$$\frac{d\rho}{dh} = \rho^2 g\beta \tag{3.23}$$

Substituting equations (3.17) and (3.23) into equation (3.12) yields

$$\frac{\partial}{\partial t}(\rho n) = \left(\rho\frac{\partial n}{\partial h} + n\frac{\partial \rho}{\partial h}\right)\frac{\partial h}{\partial t} \tag{3.24}$$

$$= (\rho^2 g\alpha + n\rho^2 g\beta)\frac{\partial h}{\partial t} \tag{3.25}$$

where, S_s defines the specific storage and given as

$$S_s = \rho g(\alpha + n\beta) \tag{3.26}$$

S_s represent the volume of water that a unit volume of aquifer releases from storage for a unit decline in hydraulic head with dimension, L^{-1}.

Putting equation (3.26) into equation (3.25) yields

$$\frac{\partial}{\partial t}(\rho n) = \rho S_s\frac{\partial h}{\partial t} \tag{3.27}$$

Substituting equation (3.27) into (3.11) gives

$$-\frac{\partial}{\partial x}(\rho v_x) - \frac{\partial}{\partial y}(\rho v_y) - \frac{\partial}{\partial z}(\rho v_z) = \rho S_s\frac{\partial h}{\partial t} \tag{3.28}$$

For an incompressible fluid (water) of constant density, ρ, equation (3.28) becomes

$$-\frac{\partial}{\partial x}(v_x) - \frac{\partial}{\partial y}(v_y) - \frac{\partial}{\partial z}(v_z) = S_s \frac{\partial h}{\partial t} \tag{3.29}$$

Applying Darcy's law to equation (3.29) in 2D yields, inhomogeneous, anisotropic, transient, saturated flow equation

$$\frac{\partial}{\partial x}\left(K_x \frac{\partial h}{\partial x}\right) + \frac{\partial}{\partial y}\left(K_y \frac{\partial h}{\partial y}\right) = S_s \frac{\partial h}{\partial t} \tag{3.30}$$

In terms of transmissivity, (3.30) becomes

$$\frac{\partial}{\partial x}\left(T_x \frac{\partial h}{\partial x}\right) + \frac{\partial}{\partial y}\left(T_y \frac{\partial h}{\partial y}\right) = S \frac{\partial h}{\partial t} \tag{3.31}$$

For homogeneous porous media, T_x, and T_y are constants and equation (3.31) reduces to

$$T_x \frac{\partial^2 h}{\partial x^2} + T_y \frac{\partial^2 h}{\partial y^2} = S \frac{\partial h}{\partial t} \tag{3.32}$$

For horizontal, 2-dimensional groundwater flow in a confined aquifer of constant thickness b, equation (3.32) reduces to

$$\frac{T_x}{S} \frac{\partial^2 h}{\partial x^2} + \frac{T_y}{S} \frac{\partial^2 h}{\partial y^2} = \frac{\partial h}{\partial t} \tag{3.33}$$

where, $S = bS_s$, $T = bK$, diffusivity in x direction $Ds_x = T_x/S$, diffusivity in y direction $Ds_y = T_y/S$.

3.5.2 Advective-Dispersive Equation (ADE)

To analyze radioactive contaminant transport in the saturated porous media, a control volume in Figure 3.8 that allows contaminant into it and out of it was used. A non-radioactive contaminant transport equation was formulated after which the decay term was added to reflect the radioactive nature of the contaminant.

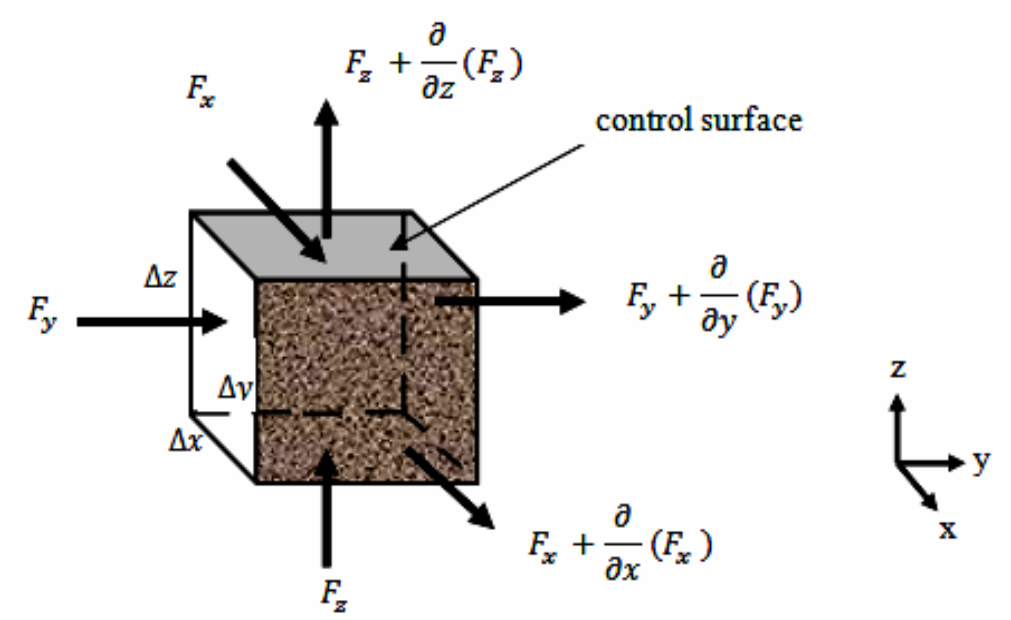

Figure 3.8: Control volume for contaminant transport through porous media.

The law of conservation of mass of contaminant transport in a porous media states

$$rate\ of\ change\ of\ contaminant\ mass = net\ rate\ of\ contaminant\ inflow + net\ rate\ of\ contaminant\ production \quad (3.34)$$

The rate at which contaminant enters the control volume is considered to consist of three components: F_x, F_y and F_z in the x, y and z directions respectively. The dimensions of F_x, F_y, and F_z are M/L^{2}T.

Applying the Taylor Series, in x direction gives,

$$F_x + \frac{\partial}{\partial x}(F_x)\Delta x + \frac{\partial^2}{2!\partial x^2}(F_x)\Delta x^2 + \frac{\partial^3}{3!\partial x^3}(F_x)\Delta x^3 + \cdots$$

The rate at which contaminant leaves the control volume are

$F_x + \frac{\partial}{\partial \mathrm{x}}(F_x)$ in the x direction,

$F_y + \frac{\partial}{\partial \mathrm{y}}(F_y)$ in the y direction, and

$F_z + \frac{\partial}{\partial \mathrm{z}}(F_z)$ in the z direction

The net rate of contaminant inflow is the difference between the inflow and outflow in each direction.

$$\text{Net rate of inflow} = F_x - \left[F_x + \frac{\partial}{\partial \mathrm{x}}(F_x)\right] + F_y - \left[F_y + \frac{\partial}{\partial \mathrm{y}}(F_y)\right] + F_z - \left[F_z + \frac{\partial}{\partial \mathrm{z}}(F_z)\right]$$

$$= \quad -\frac{\partial}{\partial \mathrm{x}}(F_x) - \frac{\partial}{\partial \mathrm{y}}(F_y) - \frac{\partial}{\partial \mathrm{z}}(F_z) \tag{3.35}$$

Contaminant transport in porous media occurs by three processes: advection, diffusion and mechanical dispersion.

The rate of contaminant transport by advection is given by the product of the contaminant concentration C and the components of the apparent groundwater flow rate, v_x, v_y, and v_z. The rate of contaminant transport by advection in the three directions of x, y, and z are

$$F_x]_{Advection} = v_x C$$

$$F_y]_{Advection} = v_y C$$

$$F_z]_{Advection} = v_z C \tag{3.36}$$

Fick's law gives the rate at which contaminants are transported by diffusion. The rate of contaminant transport by diffusion in x, y, and z directions are;

$$F_x]_{Diffusion} = -D^* \frac{\partial C}{\partial x}$$

$$F_y]_{Diffusion} = -D^* \frac{\partial C}{\partial y}$$

$$F_z]_{Diffusion} = -D^* \frac{\partial C}{\partial z} \tag{3.37}$$

where, D^* is the contaminant's apparent diffusion coefficient. The apparent diffusion coefficient for a contaminant in porous media is much smaller than the diffusion coefficient for the same contaminant in aqueous solution D_0. An empirical relationship for D^* is written as

$$D^* = nD_0 \tag{3.38}$$

where, *n* represents the porosity which is a correction factor for a saturated soil (~ 0.5) or crystalline rock (~ 0.1). Apparent diffusion coefficients are strongly temperature dependent but are only weakly dependent on the concentrations of other dissolved species [81]. But the temperature of the study area is constant making diffusion in the domain to be negligibly small and dispersion dominant.

A generalized form of Fick's Law of diffusion gives the rate of radioactive contaminant transport by mechanical dispersion. The rate of contaminant transport by mechanical dispersion in the x, y, and z directions are:

$$\begin{aligned} F_x]_{Mechanical\ Dispersion} &= -D_{xx}\frac{\partial}{\partial x}(nC) - D_{xy}\frac{\partial}{\partial y}(nC) - D_{xz}\frac{\partial}{\partial z}(nC) \\ F_y]_{Mechanical\ Dispersion} &= -D_{yx}\frac{\partial}{\partial x}(nC) - D_{yy}\frac{\partial}{\partial y}(nC) - D_{yz}\frac{\partial}{\partial z}(nC) \\ F_z]_{Mechanical\ Dispersion} &= -D_{zx}\frac{\partial}{\partial x}(nC) - D_{zy}\frac{\partial}{\partial y}(nC) - D_{zz}\frac{\partial}{\partial z}(nC) \end{aligned} \tag{3.39}$$

where, D_{xx}, D_{xy}, etc are the coefficients of mechanical dispersion. These coefficients can be computed from the expression

$$D_{ij} = \eta_{ijkm}\frac{\bar{v}_m\bar{v}_n}{\sqrt{\bar{v}_m^2+\bar{v}_n^2}} \tag{3.40}$$

where, the subscripts i and j refer to the three coordinate directions x, y, and z, $\bar{v}_m$ and $\bar{v}_n$ are the components of the pore water flow rate and the subscripts m and n refer to the direction of the principal components of pore water velocity. Components of the pore water flow rate are computed from

$$\bar{v}_x = \frac{v_x}{n},\ \bar{v}_y = \frac{v_y}{n},\ \bar{v}_z = \frac{v_z}{n} \tag{3.41}$$

where, *n* is the effective porosity of the porous media.

The terms η_{ijkm} are the components of the aquifer's dispersivity. If the aquifer is assumed to be isotropic with respect to dispersion, all component of the aquifer's dispersivity are zero except for

$$\eta_{iiii} = \eta_L, \eta_{iijj} = \eta_T, \eta_{ijij} = \eta_{ijji} = \frac{1}{2}(\eta_L - \eta_T), i \neq j \quad (3.42)$$

where η_L is the longitudinal dispersivity and η_T is the transverse dispersivity of the aquifer. "Longitudinal" refers to a direction along the flow path and "transverse" refers to a direction at right angles to the flow path. The coefficients of mechanical dispersion can be computed from the following expressions:

$$D_{xx} = \left[\eta_L \bar{v}_x^2 + \eta_T(\bar{v}_y^2 + \bar{v}_z^2)\right]/|\bar{v}|$$

$$D_{yy} = \left[\eta_L \bar{v}_y^2 + \eta_T(\bar{v}_z^2 + \bar{v}_x^2)\right]/|\bar{v}|$$

$$D_{zz} = \left[\eta_L \bar{v}_z^2 + \eta_T(\bar{v}_x^2 + \bar{v}_y^2)\right]/|\bar{v}|$$

$$D_{xy} = D_{yx} = \left[(\eta_L - \eta_T)\bar{v}_x \bar{v}_y\right]/|\bar{v}|$$

$$D_{xz} = D_{zx} = [(\eta_L - \eta_T)\bar{v}_x \bar{v}_z]/|\bar{v}|$$

$$D_{yz} = D_{zy} = \left[(\eta_L - \eta_T)\bar{v}_y \bar{v}_z\right]/|\bar{v}| \quad (3.43)$$

where, $|\bar{v}| = \sqrt{\bar{v}_x^2 + \bar{v}_y^2 + \bar{v}_z^2}$.

In 2-dimensions, equation (3.43) becomes

$$D_{xx} = \left[\eta_L \bar{v}_x^2 + \eta_T \bar{v}_y^2\right]/|\bar{v}|$$

$$D_{yy} = \left[\eta_L \bar{v}_y^2 + \eta_T \bar{v}_x^2\right]/|\bar{v}|$$

$$D_{xy} = D_{yx} = \left[(\eta_L - \eta_T)\bar{v}_x \bar{v}_y\right]/|\bar{v}| \quad (3.44)$$

where, $|\bar{v}| = \sqrt{\bar{v}_x^2 + \bar{v}_y^2}$.

In 1-dimension, equation (3.43) becomes

$$D_{xx} = D_x = \eta_L \bar{v}_x \quad (3.45)$$

Considering a uniform flow in x-direction, $(v_x \neq 0, v_y = 0, v_z = 0)$ in a three dimensional aquifer, equation (3.27) becomes

$$F_x]_{Mechanical\ Dispersion} = -D_x \frac{\partial}{\partial x}(nC)$$

$$F_y]_{Mechanical\ Dispersion} = -D_y \frac{\partial}{\partial y}(nC)$$

$$F_z]_{Mechanical\ Dispersion} = -D_z \frac{\partial}{\partial z}(nC) \quad (3.46)$$

where, $D_x = \eta_L \bar{v}_x$, $D_y = D_z = \eta_T \bar{v}_x$. .

Neglecting diffusion term and putting advection term equation (3.36) and dispersion term equation (3.46) into equation (3.35) gives a 3D ADE;

Net rate of contaminant inflow

$$= -\frac{\partial}{\partial x}\left[v_x C - D_x \frac{\partial}{\partial x}(nC)\right] - \frac{\partial}{\partial y}\left[-D_y \frac{\partial}{\partial y}(nC)\right] - \frac{\partial}{\partial z}\left[-D_z \frac{\partial}{\partial z}(nC)\right]$$

$$= -\frac{\partial}{\partial x}(v_x C) + D_x \frac{\partial^2}{\partial x^2}(nC) + D_y \frac{\partial^2}{\partial y^2}(nC) + D_z \frac{\partial^2}{\partial z^2}(nC) \quad (3.47)$$

3.5.3 Advective-Dispersive Equation with Decay Term (ADDE)

Several processes can act as sources or sinks for contaminant within the control volume including sorption/desorption, chemical reactions, and radioactive decay [81]. For transport involving sorption/desorption reaction,

$$A \rightleftharpoons \bar{A}$$

between a dissolved species A and a sorbed species $\bar{A}$. The net rate of reaction r gives

$$r = n\frac{\partial C}{\partial t} = -\rho_b \frac{\partial \bar{C}}{\partial t} \quad (3.48)$$

where, n and ρ_b are the porosity and bulk density of the porous media respectively, C is the concentration of the dissolved species A (mass of contaminant/volume of groundwater), and $\bar{C}$ is the concentration of the sorbed species $\bar{A}$ (mass of contaminant/ mass of saturated porous media). Equation (3.48) becomes

$$r = -k_f C + k_r \bar{C} \tag{3.49}$$

where, k_f is the rate constant for forward reaction ($A \longrightarrow \bar{A}$) and k_r is the rate constant for reverse reaction ($A \longleftarrow \bar{A}$). A rate law of this mathematical form for example may be used if the sorption process can be described by a first-order, reversible reaction or by combination of linear diffusion and a linear equilibrium isotherm. Assuming the rate of reaction is zero (i.e. the reaction is in equilibrium), equation (3.49) can be solved for the concentration of the sorbed species $\bar{A}$.

$$\bar{C} = \frac{k_f}{k_r} C = K_d C \tag{3.50}$$

where, K_d is the equilibrium distribution coefficient (L^3/M). The net rate of radioactive contaminant production due to a sorption/desorption reaction between a radioactive contaminant and the porous media within the control volume can be obtained by combining equations (3.48) and (3.50) and introducing the porosity of the porous media n.

$$\left.\frac{\partial(nC)}{\partial t}\right]_{Sorption} = -\rho_b K_d \frac{\partial C}{\partial t} \tag{3.51}$$

As the contaminant undergoes radioactive decay the net rate of radioactive contaminant production by this mechanism can be written

$$\left.\frac{\partial(nC)}{\partial t}\right]_{Decay} = -\lambda(nC + \rho_b K_d C) \tag{3.52}$$

where, λ is decay constant for the contaminant. The integral of equation (3.52) yields

$$(nC + \rho_b K_d C)_t = (nC + \rho_b K_d C)_{t_0} e^{-\lambda t} \tag{3.53}$$

where, the left-hand side is the mass of radioactive contaminant (dissolved and sorbed) in the control volume at some future time t and the first term on the right-hand side is the initial mass of radioactive contaminant in the control volume. Equation

(3.52) applies to processes that display exponential decay. The half-life $T_{1/2}$ for such a process is defined by

$$\frac{(nC+\rho_b K_d C)_t}{(nC+\rho_b K_d C)_{t_0}} = \frac{1}{2} \qquad \text{at } t = T_{1/2} \tag{3.54}$$

which gives

$$e^{-\lambda t} = \frac{1}{2} \qquad \text{or} \qquad \lambda = \frac{\ln 2}{T_{1/2}} = \frac{0.693}{T_{1/2}} \tag{3.55}$$

Putting equations (3.47), (3.51) and (3.52) into (3.34) and the rate of change of solute mass in the control volume as $\frac{\partial(nC)}{\partial t}$, the Advection-Dispersion-Decay Equation (ADDE) for uniform flow in a saturated porous media is

$$\frac{\partial(nC)}{\partial t} = -\frac{\partial}{\partial x}(v_x C) + D_x \frac{\partial^2}{\partial x^2}(nC) + D_y \frac{\partial^2}{\partial y^2}(nC) + D_z \frac{\partial^2}{\partial z^2}(nC)$$

$$-\frac{\partial}{\partial t}(\rho_b K_d C) - \lambda(nC + \rho_b K_d C) \tag{3.56}$$

$$\frac{\partial C}{\partial t} = -\frac{\partial}{\partial x}\left(\frac{v_x C}{n}\right) + D_x \frac{\partial^2 C}{\partial x^2} + D_y \frac{\partial^2 C}{\partial y^2} + D_z \frac{\partial^2 C}{\partial z^2} - \frac{\partial}{\partial t}\left(\frac{\rho_b K_d C}{n}\right) - \lambda\left(C + \frac{\rho_b K_d C}{n}\right) \tag{3.57}$$

Similar equations can be written for uniform groundwater flow in the y or z directions. The retardation factor R, a dimensionless parameter that shows the retarding effect of adsorption on contaminant transport can be written as

$$R = 1 + \frac{\rho_b K_d}{n} \tag{3.58}$$

and equation (3.45) becomes

$$R\frac{\partial C}{\partial t} = -\frac{\partial}{\partial x}\left(\frac{v_x C}{n}\right) + D_x \frac{\partial^2 C}{\partial x^2} + D_y \frac{\partial^2 C}{\partial y^2} + D_z \frac{\partial^2 C}{\partial z^2} - \lambda RC \tag{3.59}$$

If the groundwater flow is not uniform ($v_x \neq 0, v_y \neq 0, v_z \neq 0$), the rate of radioactive contaminant transport by mechanical dispersion is given by equation (3.39). The net rate of radioactive contaminant inflow into the control volume becomes

$$= -\frac{\partial}{\partial x}(v_x C) - \frac{\partial}{\partial y}(v_y C) - \frac{\partial}{\partial z}(v_z C)$$

$$+D_{xx}\frac{\partial^2(nC)}{\partial x^2} + D_{xy}\frac{\partial^2(nC)}{\partial x \partial y} + D_{xz}\frac{\partial^2(nC)}{\partial x \partial z}$$

$$+D_{yx}\frac{\partial^2(nC)}{\partial y \partial x} + D_{yy}\frac{\partial^2(nC)}{\partial y^2} + D_{yz}\frac{\partial^2(nC)}{\partial y \partial z}$$

$$+D_{zx}\frac{\partial^2(nC)}{\partial z \partial x} + D_{zy}\frac{\partial^2(nC)}{\partial z \partial y} + D_{zz}\frac{\partial^2(nC)}{\partial z^2} \quad (3.60)$$

Substituting equations (3.51), (3.52) and (3.60) into (3.34), the rate of change of mass in the control volume, $\frac{\partial(nC)}{\partial t}$, gives the radioactive contaminant transport equation for non-uniform flow

$$\frac{\partial(nC)}{\partial t} = D_{xx}\frac{\partial^2(nC)}{\partial x^2} + D_{xy}\frac{\partial^2(nC)}{\partial x \partial y} + D_{xz}\frac{\partial^2(nC)}{\partial x \partial z}$$

$$+D_{yx}\frac{\partial^2(nC)}{\partial y \partial x} + D_{yy}\frac{\partial^2(nC)}{\partial y^2} + D_{yz}\frac{\partial^2(nC)}{\partial y \partial z}$$

$$+D_{zx}\frac{\partial^2(nC)}{\partial z \partial x} + D_{zy}\frac{\partial^2(nC)}{\partial z \partial y} + D_{zz}\frac{\partial^2(nC)}{\partial z^2}$$

$$-\frac{\partial}{\partial x}(v_x C) - \frac{\partial}{\partial y}(v_y C) - \frac{\partial}{\partial z}(v_z C)$$

$$-\frac{\partial}{\partial t}(\rho_b K_d C) - \lambda(nC + \rho_b K_d C) \quad (3.61)$$

3.6 Radioactive Contaminant Equations (ADDEs)

Equation (3.59) was reduced to 2D and 1D radioactive transport equations that can be solved to give the profile of radioactive concentration distribution in space and time for uniform flow in x direction.

$$R\frac{\partial C}{\partial t} = D_x\frac{\partial^2 C}{\partial x^2} + D_y\frac{\partial^2 C}{\partial y^2} - \frac{v_x}{n}\frac{\partial C}{\partial x} - \lambda RC \quad \text{(2-Dimensional ADDE)} \quad (3.62)$$

$$R\frac{\partial C}{\partial t} = D_x\frac{\partial^2 C}{\partial x^2} - v\frac{\partial C}{\partial x} - \lambda RC \quad \text{(1-Dimensional ADDE)} \quad (3.63)$$

3.7 Analytical and Numerical Solution for 1D ADDE

3.7.1 Laplace Transform Solution

1D Laplace transform analytical solution for ADDE was formulated using the model geometry in Figure 3.9.

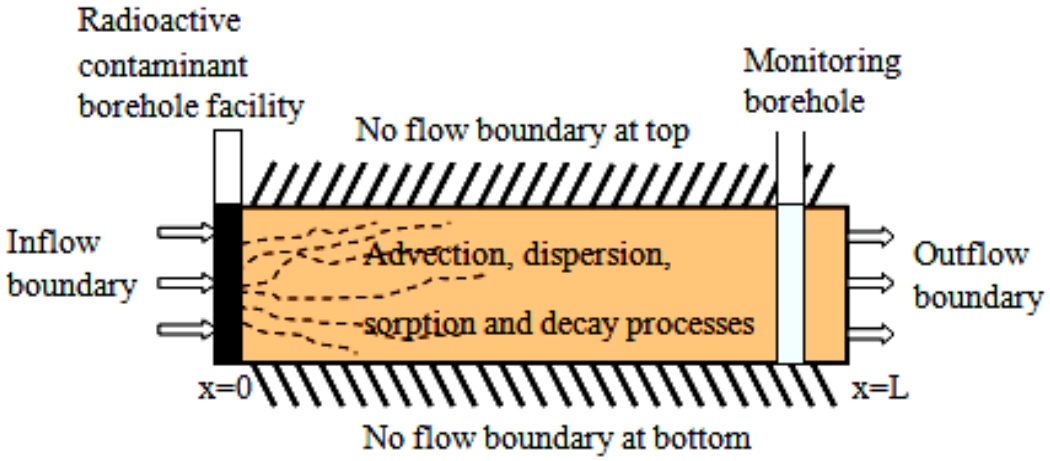

Figure 3.9: Model geometry for 1D radionuclide transport.

Boundary Conditions

$$C(0,t) = C_0,\ for\ x = 0,\ t > 0 \tag{3.64}$$

$$C(L,t) = 0,\ for\ x = L = \infty,\ t > 0 \tag{3.65}$$

Initial Condition

$$C(x,0) = 0,\ for\ 0 \le x \le L = \infty,\ t = 0 \tag{3.66}$$

Taking Laplace Transform of the BC, IC and the terms in equation (3.63) yields

$$\mathcal{L}\{C(0,t)\} = \mathcal{L}\{C_0\} \quad \Longrightarrow \bar{C}(0,s) = \frac{C_0}{s} \tag{3.67}$$

$$\mathcal{L}\{C(L,t)\} = \mathcal{L}\{0\} \quad \Longrightarrow \bar{C}(L,s) = 0,\ L \to \infty \tag{3.68}$$

$$\mathcal{L}\{C(x,0)\} = \mathcal{L}\{0\} \quad \Longrightarrow C(x,0) = 0 \tag{3.69}$$

$$\mathcal{L}\left\{R\frac{\partial C}{\partial t}\right\} = R\mathcal{L}\left\{\frac{\partial C}{\partial t}\right\} = R[s\bar{c} - C(x,0)] = Rs\bar{c} \tag{3.70}$$

$$\mathcal{L}\left\{D_x\frac{\partial^2 C}{\partial x^2}\right\} = D_x\mathcal{L}\left\{\frac{\partial^2 C}{\partial x^2}\right\} = D_x\frac{\partial^2}{\partial x^2}\int_0^\infty C(x,t)e^{-st}dt = D_x\frac{\partial^2 \bar{c}}{\partial x^2} \tag{3.71}$$

$$\mathcal{L}\left\{v\frac{\partial C}{\partial x}\right\} = v\mathcal{L}\left\{\frac{\partial C}{\partial x}\right\} = v\frac{\partial}{\partial x}\int_0^\infty C(x,t)e^{-st}dt = v\frac{\partial \bar{C}}{\partial x} \tag{3.72}$$

$$\mathcal{L}\{\lambda RC\} = \lambda R\mathcal{L}\{C\} = \lambda R\int_0^\infty C(x,t)e^{-st}dt = \lambda R\bar{C} \tag{3.73}$$

Putting the Laplace Transform of the respective terms into equation (3.63), yields

$$Rs\bar{c} = D_x\frac{\partial^2\bar{c}}{\partial x^2} - v\frac{\partial \bar{c}}{\partial x} - \lambda R\bar{C} \tag{3.74}$$

Rearranging equation (3.74) gives

$$D_x\frac{\partial^2\bar{c}}{\partial x^2} - v\frac{\partial \bar{C}}{\partial x} - (\lambda R + Rs)\bar{c} = 0 \tag{3.75}$$

The characteristic/auxiliary equation for (3.75) is

$$m^2 - \frac{v}{D_x}m - \frac{R}{D_x}(\lambda + s) \tag{3.76}$$

The solution of the characteristic equation (3.76) is given as

$$m_{1,2} = \frac{-b\pm\sqrt{(b^2-4ac)}}{2a} \tag{3.77}$$

where, $a = 1,\ b = -\frac{v}{D_x}$, and $c = -\frac{R}{D_x}(\lambda + s)$. Substituting the respective terms into equation (3.77) yields

$$m_{1,2} = \frac{v}{2D_x} \pm \sqrt{\frac{R}{D_x}\left[\left(\frac{v^2}{4RD_x} + \lambda\right) + s\right]} \tag{3.78}$$

where, $m_1 = \frac{v}{2D_x} + \sqrt{\frac{R}{D_x}\left[\left(\frac{v^2}{4RD_x} + \lambda\right) + s\right]}$ and $m_2 = \frac{v}{2D_x} - \sqrt{\frac{R}{D_x}\left[\left(\frac{v^2}{4RD_x} + \lambda\right) + s\right]}$

At this stage, the coefficient of dispersion D_x shall be used without the subscript x. The solution of equation (3.75) is of the form

$$\bar{C}(x,s) = Ae^{m_1x} + Be^{m_2x} \tag{3.79}$$

Therefore, applying the outflow boundary condition to equation (3.79) yields

$$\bar{C}(L,s) = \bar{C}(\infty,s) = Ae^{m_1\infty} + Be^{m_2\infty} = 0 \qquad \Longrightarrow A = 0$$

Putting the value of $A = 0$ into equation (3.79) yields

$$\bar{C}(x,s) = Be^{m_2x} \tag{3.80}$$

Applying the inflow boundary condition, the value of B can be found. Thus,

$$\bar{C}(0,s) = Be^{m_2(0)} = {}^{C_0}/_{s} \Longrightarrow B = {}^{C_0}/_{s}$$

Substituting the value of B into equation (3.80) yields

$$\bar{C}(x,s) = \frac{C_0}{s}\left[\exp\left\{\frac{v}{2D} - \sqrt{\frac{R}{D}\left[\left(\frac{v^2}{4RD} + \lambda\right) + s\right]}\right\}x\right] \tag{3.81}$$

Let $\beta = \frac{v^2}{4RD_x} + \lambda$, $G = \beta + s \Longrightarrow s = G - \beta$, therefore, equation reduces to

$$\bar{C}(x,s) = \frac{C_0}{s}\left[\exp\left\{\frac{v}{2D} - \sqrt{\frac{R}{D}[\beta + s]}\right\}x\right] \tag{3.82}$$

$$\bar{C}(x,s) = exp\left\{\frac{vx}{2D}\right\}\left[\frac{C_0}{G-\beta}exp\left\{-x\sqrt{\frac{R}{D}G}\right\}\right] \tag{3.83}$$

From the 1st Shift Theorem, [83]

$$\mathcal{L}^{-1}[F(s+a)] = \mathcal{L}^{-1}[e^{-at}F(s)] = e^{-at}\mathcal{L}^{-1}[F(s)] \tag{3.84}$$

where, $a = \beta$

Therefore, taking Inverse Laplace Transform of equation (3.83) yields

$$\mathcal{L}^{-1}\{\bar{C}(x,s)\} = \mathcal{L}^{-1}\left\{exp\left\{\frac{vx}{2D}\right\}\left[\frac{C_0}{G-\beta}exp\left\{-x\sqrt{\frac{R}{D}G}\right\}\right]\right\} \tag{3.85}$$

From equation (3.85), it follows that

$$C(x,t) = C_0.exp\left\{\frac{vx}{2D}\right\}.exp\{-\beta t\}.\mathcal{L}^{-1}\left[\frac{1}{s-\beta}\right].exp\left\{-x\left(\sqrt{\frac{R}{D}}\right)\sqrt{s}\right\} \tag{3.86}$$

However, it was shown that [104]

$$\mathcal{L}^{-1}\left[\frac{1}{s-\beta}\right].exp\left\{-x\left(\sqrt{\frac{R}{D}}\right)\sqrt{s}\right\} =$$

$$0.5exp\{\beta t\}.\left\{\begin{array}{l} exp\left\{-\frac{vx}{2D}\right\}erfc\left[\frac{x}{2}\sqrt{\frac{R}{Dt}} - \sqrt{\beta t}\right] \\ + exp\left\{\frac{vx}{D}\right\}.erfc\left[\frac{x}{2}\sqrt{\frac{R}{Dt}} + \sqrt{\beta t}\right] \end{array}\right\} \tag{3.87}$$

Substituting equation (3.87) into equation (3.86) yields the Laplace Transform solution for model 1D ADDE as

$$C(x,t) =$$

$$\frac{C_0}{2}.exp\left\{\frac{vx}{2D}\right\}.exp\{-\beta t\}.exp\{\beta t\}.\begin{Bmatrix} exp\left\{-\frac{vx}{2D}\right\}erfc\left[\frac{x}{2}\sqrt{\frac{R}{Dt}}-\sqrt{\beta t}\right] \\ +\ exp\left\{\frac{vx}{D}\right\}.erfc\left[\frac{x}{2}\sqrt{\frac{R}{Dt}}+\sqrt{\beta t}\right] \end{Bmatrix} \quad (3.88)$$

Substituting for β in Equation (3.88) yields

$$C(x,t) = \frac{C_0}{2}\left\{erfc\left[\frac{xR-vt\sqrt{1+\frac{4RD\lambda}{v^2}}}{\sqrt{4RDt}}\right] + exp\left\{\frac{vx}{D}\right\}.erfc\left[\frac{xR+vt\sqrt{1+\frac{4RD\lambda}{v^2}}}{\sqrt{4RDt}}\right]\right\} \quad (3.89)$$

3.7.2 Finite Difference Discretization of 1D-ADDE

Finite Difference discretization was used to calculate the unknown field variable i.e., contaminant concentration at the nodes. The finite difference grid for determining the contaminant concentration was formed in Figure (3.10).

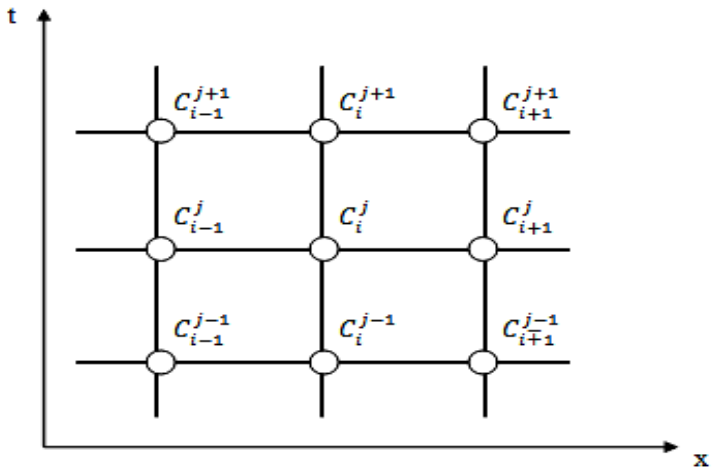

Figure 3.10: Finite difference grid

At the middle of the grid, component of contaminant concentration is denoted $C_{i,j}$ at (i,j). Moving forward in the x-direction at point $(i+1,j)$ the contaminant concentration $C_{i+1,j}$ about the point $C_{i,j}$ can be expressed in Taylor Series as

$$C_{i+1,j} = C_{i,j} + \frac{\partial C}{\partial x}\Big|_{i,j} \Delta x + \frac{1}{2!}\frac{\partial^2 C}{\partial x^2}\Big|_{i,j} (\Delta x)^2 + \frac{1}{3!}\frac{\partial^3 C}{\partial x^3}\Big|_{i,j} (\Delta x)^3 + \cdots \quad (3.90)$$

The Taylor Series for $C_{i+1,j}$ is exact for all the terms and converges as $\Delta x \to 0$. Moving in the reverse x-direction at $(i-1, j)$ the contaminant concentration $C_{i-1,j}$ about the point $C_{i,j}$ is given by the Taylor Series as

$$C_{i-1,j} = C_{i,j} + \frac{\partial C}{\partial x}\Big|_{i,j} (-\Delta x) + \frac{1}{2!}\frac{\partial^2 C}{\partial x^2}\Big|_{i,j} (\Delta x)^2 + \frac{1}{3!}\frac{\partial^3 C}{\partial x^3}\Big|_{i,j} (-\Delta x)^3 + \cdots \quad (3.91)$$

From equation (3.90), the first derivative term of contaminant concentration is given as

$$\frac{\partial C}{\partial x}\Big|_{i,j} = \frac{C_{i+1,j} - C_{i,j}}{\Delta x} - \frac{1}{2!}\frac{\partial^2 C}{\partial x^2}\Big|_{i,j} \Delta x - \frac{1}{3!}\frac{\partial^3 C}{\partial x^3}\Big|_{i,j} (\Delta x)^2 + \cdots \quad (3.92)$$

The Finite Difference formula for the derivative at LHS of equation (3.92) is given by the first term at the RHS where the other terms represent truncation error of first order, $O(\Delta x)$. A simplified form of equation (3.92) known as Forward Difference can be written as

$$\frac{\partial C}{\partial x}\Big|_{i,j} = \frac{C_{i+1,j} - C_{i,j}}{\Delta x} + O(\Delta x) \quad (3.93)$$

Deductively, the Backward Difference and the Central Difference formulae of the first derivative of the contaminant concentration are given respectively as:

$$\frac{\partial C}{\partial x}\Big|_{i,j} = \frac{C_{i,j} - C_{i-1,j}}{\Delta x} + O(\Delta x) \quad (3.94)$$

$$\frac{\partial C}{\partial x}\Big|_{i,j} = \frac{C_{i+1,j} - C_{i-1,j}}{2\Delta x} + O(\Delta x)^2 \quad (3.95)$$

Clearly, the Backward Difference formula also has first order truncation error whiles the Central Difference formula has second order truncation error.

The addition of both the LHS and the RHS of equations (3.90) and (3.91) result in a Finite Difference formula for second derivative of contaminant concentration with second order accuracy as;

$$C_{i+1,j} + C_{i-1,j} = 2C_{i,j} + \frac{\partial^2 C}{\partial x^2}\Big|_{i,j} (\Delta x)^2 + \frac{1}{12}\frac{\partial^4 C}{\partial x^4}\Big|_{i,j} (\Delta x)^4 + \cdots \quad (3.96)$$

Equation (3.96) simplifies to

$$\frac{\partial^2 C}{\partial x^2}\Big|_{i,j} = \frac{C_{i+1,j} - 2C_{i,j} + C_{i-1,j}}{(\Delta x)^2} + O(\Delta x)^2 \quad (3.97)$$

Applying the Finite Difference formula to the terms in 1D radioactive contaminant transport equation (3.63), yield

$$R\frac{\partial C}{\partial t} = R\frac{C_i^{j+1} - C_i^j}{\Delta t} \quad (3.98)$$

$$D\frac{\partial^2 C}{\partial x^2} = D\frac{C_{i+1}^{j+1} - 2C_i^{j+1} + C_{i-1}^{j+1}}{(\Delta x)^2} \quad (3.99)$$

$$v\frac{\partial C}{\partial x} = v\frac{C_{i+1}^{j+1} - C_{i-1}^{j+1}}{2\Delta x} \quad (3.100)$$

$$\lambda RC = \lambda RC_i^{j+1} \quad (3.101)$$

The Finite Difference equation of the 1D ADDE is

$$R\frac{C_i^{j+1} - C_i^j}{\Delta t} = D\frac{C_{i+1}^{j+1} - 2C_i^{j+1} + C_{i-1}^{j+1}}{(\Delta x)^2} - v\frac{C_{i+1}^{j+1} - C_{i-1}^{j+1}}{2\Delta x} - \lambda RC_i^{j+1} \quad (3.102)$$

Equation (3.102) reduces to

$$C_i^{j+1} - C_i^j =$$

$$\frac{D\Delta t}{R(\Delta x)^2}\left[C_{i+1}^{j+1} - 2C_i^{j+1} + C_{i-1}^{j+1}\right] - \frac{v\Delta t}{2R\Delta x}\left[C_{i+1}^{j+1} - C_{i-1}^{j+1}\right] - \lambda\Delta t C_i^{j+1} \quad (3.103)$$

Let $p = \frac{D\Delta t}{R(\Delta x)^2}$, $q = \frac{v\Delta t}{2R\Delta x}$ and $r = \lambda\Delta t$

Therefore, substituting p, q, and r, the Finite Difference equation becomes

$$-(p+q)C_{i-1}^{j+1} + (1 + 2p + r)C_i^{j+1} + (q-p)C_{i+1}^{j+1} = C_i^j \quad (3.104)$$

For $i = 1$, and applying the beginning/inflow boundary condition equation (3.64) C_0^{j+1} was known. Thus, equation (3.104) becomes

$$(1 + 2p + r)C_1^{j+1} + (q-p)C_2^{j+1} = C_1^j + (p+q)C_0^{j+1} \quad (3.105)$$

For $i = n - 1$, equation (3.104) becomes

$$-(p+q)C_{n-2}^{j+1}+(1+2p+r)C_{n-1}^{j+1}+(q-p)C_{n}^{j+1}=C_{n-1}^{j} \tag{3.106}$$

For $i=n$, equation (3.104) becomes

$$-(p+q)C_{n-1}^{j+1}+(1+2p+r)C_{n}^{j+1}=C_{n}^{j}+(q-p)C_{n+1}^{j+1} \tag{3.107}$$

Applying the end/outflow boundary condition (3.65) where, $C_{n+1}^{j+1}=0$, thus equation (3.107) reduces to

$$-(p+q)C_{n-1}^{j+1}+(1+2p+r)C_{n}^{j+1}=C_{n}^{j} \tag{3.108}$$

Let $a=p+q$, $b=1+2p+r$, and $c=q-p$. Thus, the simultaneous equations formed can be expressed in a tridiagonal matrix form as $\boldsymbol{M}B=G$, where $\boldsymbol{M}$ is the tridiagonal matrix, B is the solution/current concentration and G is the previous concentration iterated for $t=1{:}n$. Therefore, the vector B is given as, $B=\boldsymbol{M}\backslash G$.

$$\begin{bmatrix} b & c & 0 & 0 & & & & \\ -a & b & c & 0 & \cdots & & & \\ 0 & -a & b & c & & & & \\ & & & \ddots & & & & \\ & \vdots & & & & \vdots & & \\ & & & & -a & b & c & 0 \\ & \cdots & & & 0 & -a & b & c \\ & & & & 0 & 0 & -a & b \end{bmatrix}\begin{bmatrix} C_1^{j+1} \\ C_2^{j+1} \\ C_3^{j+1} \\ \vdots \\ C_{n-2}^{j+1} \\ C_{n-1}^{j+1} \\ C_n^{j+1} \end{bmatrix}=\begin{bmatrix} C_1^{j}+(p+q)C_0^{j+1} \\ C_2^{j} \\ C_3^{j} \\ \vdots \\ C_{n-2}^{j} \\ C_{n-1}^{j} \\ C_n^{j} \end{bmatrix} \tag{3.109}$$

The flow chart algorithm for the implementation of the tridiagonal matrix is shown in Figure 3.11.

3.8 Flow Chart Algorithm for 1D ADDE Numerical Model

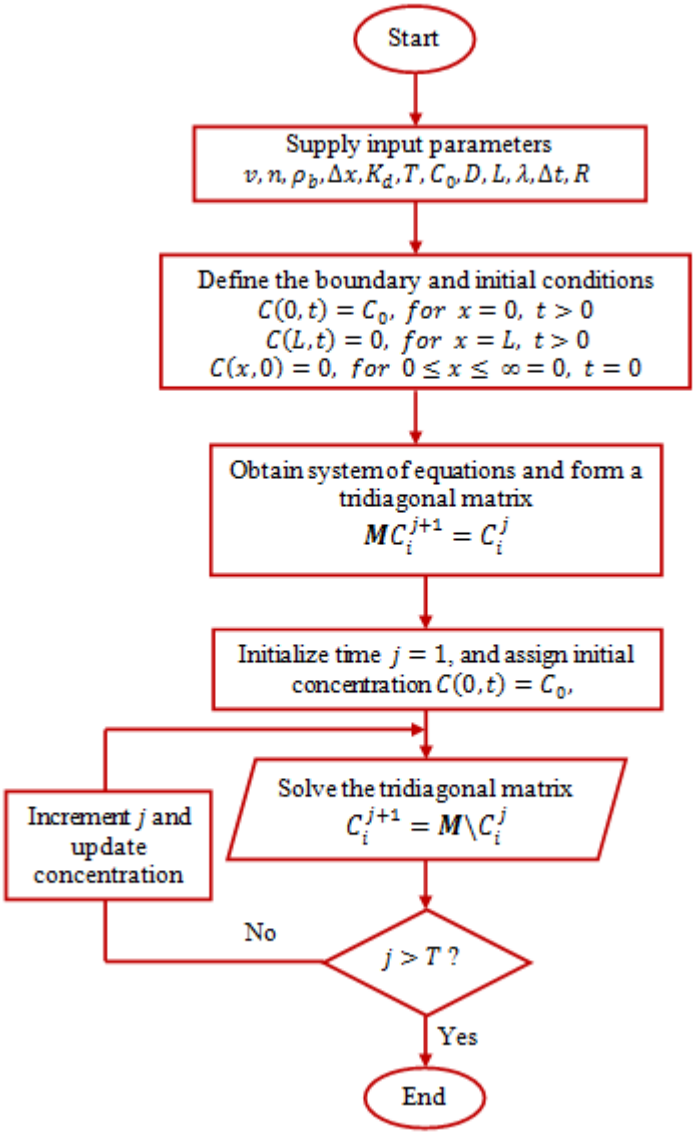

Figure 3.11: Flow chart algorithm for 1D ADDE MatLab simulation.

3.9 Analytical Solution for 2D ADDE

The 2D contaminant transport model equation (3.62) in the form of partial differential equation, boundary and initial conditions has been simplified as

$$\frac{\partial C}{\partial t} = D_x^d \frac{\partial^2 C}{\partial x^2} + D_y^d \frac{\partial^2 C}{\partial y^2} - \bar{v}_x^d \frac{\partial C}{\partial x} - \lambda C \tag{3.110}$$

where, D_x^d is retarded coefficient of dispersion in x-direction, D_y^d is retarded coefficient of dispersion in y-direction, $\bar{v}_x^d$ is retarded pore water velocity, C is

radioactive contaminant concentration, and λ is the decay constant. Equation (3.110) has been solved analytically by [103] and the solution given as

$$C(x,y,t) =$$

$$C_0 \sum_{n=0}^{\infty} L_n P_n \cos(\eta y) \left\{ exp\left[\frac{x(\bar{v}_x^d - B)}{2D_x^d}\right] erfc\left[\frac{x - Bt}{2\sqrt{D_x^d t}}\right] + exp\left[\frac{x(\bar{v}_x^d + B)}{2D_x^d}\right] erfc\left[\frac{x + Bt}{2\sqrt{D_x^d t}}\right] \right\}$$

where, n is an integer, η, B, L_n and P_n are arbitrary constants that vary with n, x, y are position variables and t is time variable and $\pi = 3.142$.

$$L_n = \begin{cases} \frac{1}{2}, & n = 0 \\ 1, & n > 0 \end{cases}$$

$$P_n = \begin{cases} \frac{Y_2 - Y_1}{W}, & n = 0 \\ \frac{[\sin(\eta Y_2) - \sin(\eta Y_1)]}{n\pi}, & n > 0 \end{cases}$$

$$\eta = \frac{n\pi}{W}, \quad n = 0, 1, 2, 3 \ldots$$

$$B = \sqrt{\bar{v}_x^{d\,2} + 4D_x^d(\eta^2 D_y^d + \lambda)} \qquad (3.111)$$

Boundary conditions:

$C = C_0, x = 0$ and $Y_1 < y < Y_2$ $\qquad t > 0$

$C = 0, x = 0$ and $y < Y_1$ or $y > Y_2$ $\qquad t > 0$

$C, \frac{\partial C}{\partial y} = 0, y = 0$

$C, \frac{\partial C}{\partial y} = 0, y = W$

$C, \frac{\partial C}{\partial x} = 0, x = \infty$

where, v_x is apparent flow velocity in x-direction, $\bar{v}_x$ is pore water flow velocity, Y_1 is y-coordinate of lower limit of contaminant source at x = 0, Y_2 is y-coordinate of upper limit of contaminant source at x = 0, and W is aquifer width.

Initial condition:

$C = 0, 0 < x < \infty$ and $0 < y < W$ at $t = 0$

3.10 ANSYS Fluent 13.0 Software Implementation and Application

To simulate the behaviour of groundwater flow in the study area, an industry standard ANSYS CFD package, a comprehensive product for modelling fluid flow and other related physical phenomena was used [86]. A 2D groundwater flow model in equation (3.33) with uniform flow in x-direction was implemented and executed using ANSYS Fluent 13.0 software installed on HP Compaq 6830s Notebook Laptop, with Windows 7 Ultimate 32 bits SP1 Operating System, Intel Core Duo CPU P8400 @ 2.26 GHz (2 CPUs), 3.0 GB RAM, ATI Mobility Radeon HD3430. ANSYS Fluent software as part of the ANSYS CFD package contains the broad physical modelling capabilities required to predict the impact of all fluid behaviour with confidence.

3.10.1 Geometry Design and Meshing

ANSYS Fluent 13.0 computer software was used to simulate the groundwater flow governing equation to get the, static pressure distribution, flow and contour pattern and flow rate. A 2D geometry was developed in this study using ANSYS Workbench and meshed into triangular elements using the ANSYS Design Modeller Figure 3.12.

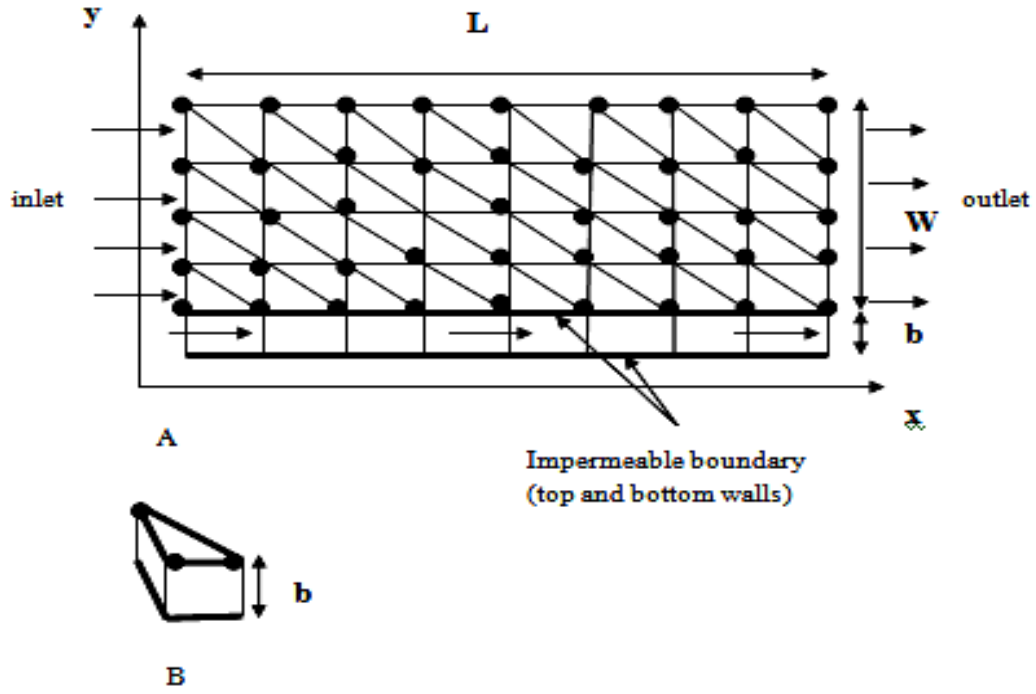

Figure 3.12: Domain mesh (A) and elemental control volume (B).

The aquifer thickness b of 5 m used was very small and negligible compared to the length L of 500 m and width W of 50 m of the geometry. The finite volume discretization is equivalent to finite element discretization for triangular element as flow thickness is very small and negligible compared to the length of the domain. The material properties were supplied and the model was run.

3.10.2 ANSYS Fluent 13.0 Input Data for Flow Simulation

Table 3.2: Input data for 2D groundwater flow simulation

Description	**Value**	**Unit**
Geometry		
Length of geometry	500	m
Width of geometry	50	m
Thickness of geometry	5	m
Mesh		
Number of nodes	25551	
Number of triangular element	50000	

Material Properties		
Water density	998.2	kg/m^3
Viscosity	0.001003	
Schists bulk density	2400	kg/m^3
Temperature	300	K
Diffusivity range	0.1 - 10	m^2/s
Effective Porosity	0.11	
Initial velocity	5E-8	m/s
Solution Controls		
Pressure Under Relaxation Factor	0.3	
Monitors-Residuals		
Continuity	1e-03	
x-velocity	1e-03	
y-velocity	1e-03	

3.10.3 ANSYS Fluent Solver Technology and Accuracy

ANSYS Fluent's pressure-based solver was used to solve for pressure and momentum sequentially for transient, incompressible, and laminar flows in this simulation. Velocity interpolation for advective flow used was second-order upwind that converges slowly. The pressure velocity coupling applied in this simulation was PISO – Pressure Implicit with Splitting of Operators for unsteady flow problems and for meshes comprising higher than average skewness. Appropriate residual monitors were set and the iterative solution initialized with a realistic flow rate for faster solution convergence.

3.10.4 ANSYS Fluent 13.0 Solution Algorithm

Figure 3.13 shows the ANSYS Fluent flowchart algorithm procedure followed in the groundwater flow simulation. ANSYS Workbench was used to model 2D physical geometry of the domain and the geometry meshed using design modeller with the

boundaries labelled. ANSYS Fluent solver was set up by selecting appropriate model type, material properties, solver type, solution monitors and the solution initialized. The solution was calculated by setting the time step and appropriate iteration for the simulation set.

The process was repeated as certain parameters were adjusted, solution initialised and calculation done until convergence was reached. The simulation results were analysed and post-processed to get the pressure contour, the velocity magnitude and some quantitative statistical values that describe the flow pattern and visualization.

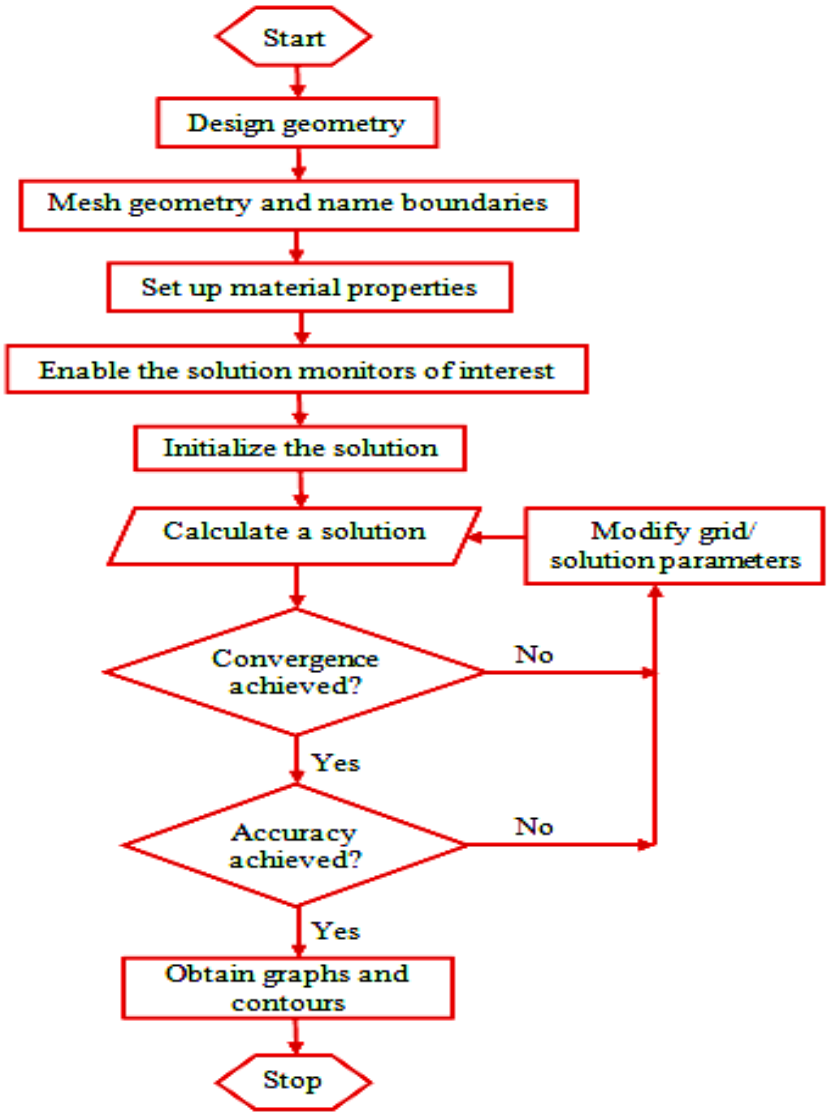

Figure 3.13: Flowchart algorithm for groundwater flow simulation.

3.11 MatLab Simulation of Analytical and Numerical Solution of 1D ADDE

The 1D analytical and numerical solutions of ADDE were coded and the programs were implemented and run on MatLab R2013a software installed and executed on an HP Notebook of the same features as used in the ANSYS Fluent implementation.

3.11.1 Input Data for MatLab Simulation of 1D ADDE

The model inputs for a radioactive contaminant that leaked from the disposal facility into the aquifer as a result of corrosion assuming 1 kg/m^3 of initial concentration are:

Table 3.3: Geometry and parameters for 1D ADDE simulation

Property	**Value**
Aquifer length (x)	500 m
Groundwater pore flow rate $\bar{v}_x$	0.0269 m/day
Aquifer porosity (effective porosity)	0.11
Source concentration C_0	1 kg/m^3
Longitudinal dispersivity ($\eta_L = 0.1 * length$) [105]	50 m
Coefficient of longitudinal dispersion ($D_x = \eta_L \bar{v}_x$)	1.3473 m^2/day

Table 3.4: Radioactive contaminants input data

Radioactive Element	**Decay Constant**	**Distribution Coefficient**
Carbon-14	4.6E-7	0.0001
Strontium-90	9.4E-5	0.0001

3.11.2 Input Data for MatLab Simulation of 2D Analytical ADDE

The 2D analytical solution equation (3.111) was coded in MatLab R2013a and simulated to show the distribution of radioactive contaminants in space and time. The

model inputs for radioactive contaminant that leaked from the disposal facility into the aquifer as a result of corrosion assuming 1 kg/m^3 of initial concentration of each radioactive contaminant are given in addition to radioactive contaminant properties used in the 1D model:

Table 3.5: Geometry and parameters for 2D ADDE simulation

Property	**Value**
Aquifer length (x)	500 m
Aquifer width (y)	500 m
Groundwater pore flow rate $\bar{v}_x$	0.0269 m/day
Aquifer porosity (effective porosity)	0.11
Source concentration C_0	1 kg/m^3
Longitudinal dispersivity ($\eta_L = 0.1 * length$) [105]	50 m
Transverse dispersivity ($\eta_T = 0.1 * \eta_L$)	5 m
Coefficient of longitudinal dispersion ($D_x = \eta_L \bar{v}_x$)	1.3473 m^2/day
Coefficient of transverse dispersion ($D_y = \eta_T \bar{v}_x$)	0.1374 m^2/day

3.12 Calibration, Verification and Validation

Calibration was done on diffusivity through trial and error on the flow model. A range of diffusivity values were tested for a good input velocity. The groundwater flow model was verified by comparing flow velocity from field method (exact solution) and that from ANSYS Fluent (approximate solution). The groundwater flow velocity calculated from ANSYS Fluent 13.0 software was validated by comparing the velocity calculated with the groundwater flow velocity estimated from field methods and the results compared well.

1D analytical and numerical codes were simulated and the results compared for verification and validation. The 2D analytical code was simulated but was not verified and validated due to complexities in the 2D numerical coding and time insufficiency.

3.13 Numerical Error, Convergence and Stability

The numerical errors encountered in the numerical model development were truncation errors and round-off errors. In the mathematical formulation, truncation errors occurred as Taylor's series was used in the finite difference scheme where first-order of Δx was considered resulting in a truncation error of order $O(\Delta x)^2$. Round-off errors were encountered in arithmetic computation using the computer. The grid size of the model geometry for the computer numerical solution was varied and it was observed that numerical solution approaches exact (field) solution as the mesh/grid size become smaller which made ANSYS Fluent discretization scheme to be consistent. To avoid numerical oscillation, appropriate value of Δt was chosen and under relaxation value of 0.3 was used, which made the solution to be stable.

CHAPTER FOUR

RESULTS AND DISCUSSIONS

This chapter presents the results and discussions of the research work. The results were discussed to reflect their impact on the domain of study and on the wider environment as a whole.

RESULTS

4.1 Aquifer System

The results on aquifer system were categorised into aquifer model types, hydrologic chart, and hydraulic properties.

4.1.1 Aquifer Formation Types

Appendix A, show the extracts of the lithology of the ten wells used in this research from the borehole logs. Nine wells were mainly in schist and one located in weathered quartzite. Figure 4.1 shows a summary graph of graphs in **Appendix B** plotted on response of borehole to pumping using borehole data.

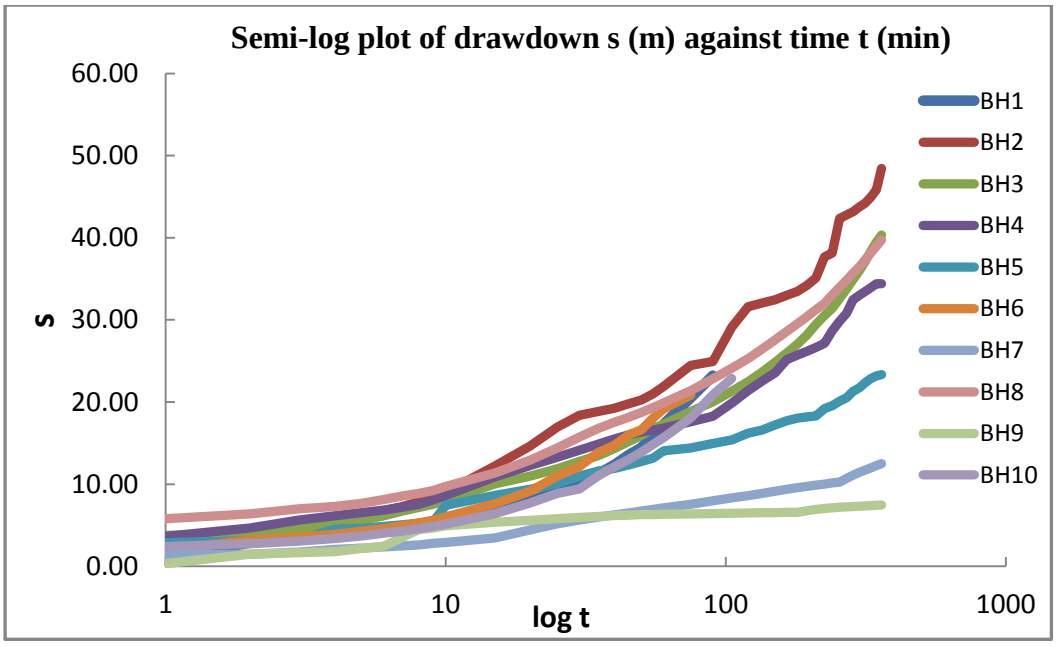

Figure 4.1: Semi-log plot of drawdown against time for sample boreholes.

These graphs are characteristic semi-log graphs that determined the type of aquifer the ten boreholes were drilled in. The drawdown-time graphs show boreholes that were drilled in consolidated, confined and fractured aquifers of the study area.

Graphs of BH1, BH3, BH6, BH8 and BH10 show smooth curves. These graphs suggest that at early times, the flow towards the well is completely through the fractures which are heavily blocked. Throughout pumping, the flow comes almost entirely from fractured storage as the contributions from micro fractures are highly negligible. The low yields encountered in BH1, BH6 and BH10 were because of fractures that may have been blocked by clayey materials hence the domain is a heterogeneous fractured aquifer system.

The BH2, BH4, BH5 and BH7 graphs also exhibited the same trend but wavy in nature. These graphs show wells whose fracture were not blocked and the fracture density increases from BH2, BH4, BH5, and BH7. Therefore groundwater flow also increases in that order. At early pumping times, the flow is entirely from fractured storage. The flow is then supplied minimally intermittently from micro fractures of matrix block mainly from the storage in the fracture until late time of pumping. These are pumped wells whose fractures were not blocked and the aquifer system can be described as purely fractured with varying degrees.

The graph of BH9 represents a well in confined fractured/weathered quartzite aquifer having double porosity. Two systems shown in this aquifer are (i) fractures of high permeability and low storage and (ii) the matrix blocks of low permeability and high storage capacity. At early pumping time all the flow comes from storage in the fractures. The medium pumping time shows a transition area where the matrix blocks feed their water at increasing rate to the fractures with a partly stabilized drawdown.

At late pumping times, water comes from storage in both fractures and matrix blocks and this fracture domain exhibit a dual porosity aquifer system.

4.1.2 Porosity Estimation

Table 4.1 shows the boreholes with respective coordinates, elevations, aquifer screen thickness, thickness of the bedrock and estimated secondary porosities.

Table 4.1 Borehole locations and parameters in the study area

Borehole Ref. No.	GPS Lattitude	GPS Longitude	Elevation above mean sea level (m)	Aquifer Screen Thickness e/voids (m)	Thickness of the hard-rock E (m)	Secondary porosity (0.32e/E)
BH1	05°42’2.6”	0°11’3.9”	66	-	64	-
BH2	05°44’6.4”	0°9’45.8”	74	13	47	0.09
BH3	05°41’15.3”	0°14’48.0”	112	15	48	0.10
BH4	05°42’49.5”	0°14’37.6”	176	12	22	0.17
BH5	05°40’0.6”	0°9’58.6”	92	9	32	0.09
BH6	05°40’56.5”	0°9’19.9”	66	-	78	-
BH7	05°41’6.7”	0°12’50.5”	53	12	28	0.14
BH8	05°43’55.5”	0°10’49”	92	15	48	0.10
BH9	05°41’42”	0°12’43.9”	53	12	50	0.08
BH10	05°40’8.1”	0°12’23.4”	58	-	78	-

The total porosity estimated ranges between 0.19 – 0.44 with mean total porosity of 0.27 and secondary/effective porosity ranging between 0.08 – 0.17 with a mean 0.11 for the study area.

4.1.3 Hydrogeologic Chart of Elevation versus Borehole

Figure 4.2 shows groundwater level before and after pumping. The borehole elevation, depth, static water level (SWL), aquifer top, and dynamic water level (DWL) relative to mean sea level were plotted against borehole reference arranged

from west to east in the study area for convenience. **Appendix C** show the data used in plotting the hydrogeologic chart of the study area.

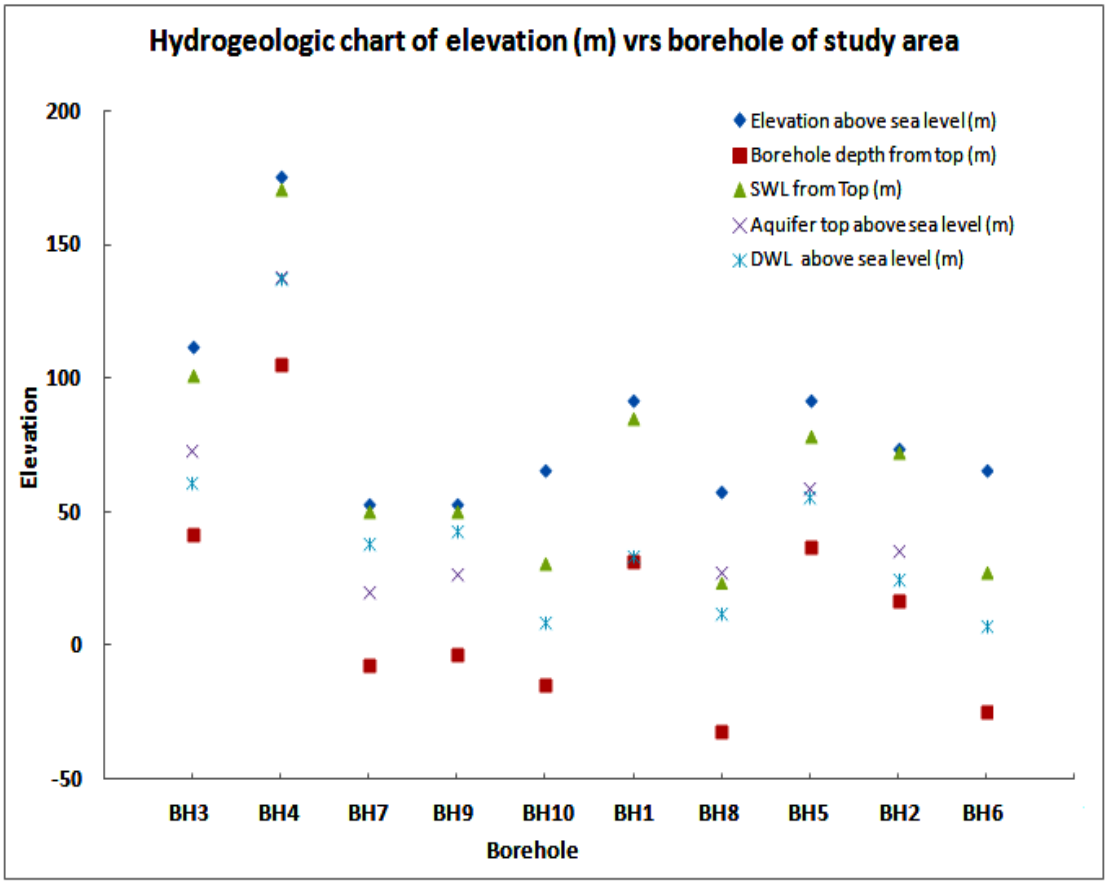

Figure 4.2: Hydrogeologic chart of elevation versus borehole of study area.

Generally, hydrogeologic domains are complex and difficult to visualize. However, an attempt was made to visualize the Dahomeyan System with respect to aquifer response to disturbance. The first legend in Figure 4.2 shows the elevation of the topography with individual points indicating the borehole location at respective elevation relative to mean sea level. The second legend shows the depth of the wells in the geological stratum at that location. The third legend refers to the static water level (SWL) in the subsurface. It is the water level with respect to the mean sea level before pumping began. The top of the aquifer with respect to the mean sea level is represented by the fourth legend. The aquifer top sections of BH1, BH6 and BH10

were not determined, because the fractures met were not yielding much and their positions were not recorded during the pumping test. The dynamic water level (DWL) is represented by the fifth legend. It refers to the water level during pumping. It must be noted that the pumping rates are not the same for all the boreholes and the duration of pumping was the same for only seven boreholes described as being successful (i.e. six hours). Also, the DWL for most of the boreholes show that there were well losses as a result of constant pumping which renders some of the wells inefficient.

4.1.4 Aquifers Hydraulic Parameters

The semi-log graphs in Figures 4.3(a-j) show the residual drawdown s' versus time ratio (t/t') plotted for recovery test data of borehole used in the research where, t is the time since pumping began and t' is the time since pumping stopped. These graphs were used in estimating the transmissivities using [28] method Equation (3.1) for the individual boreholes. The aquifer thickness b was obtained through analyses of borehole logs data and the hydraulic conductivity calculated using Equation (3.2).

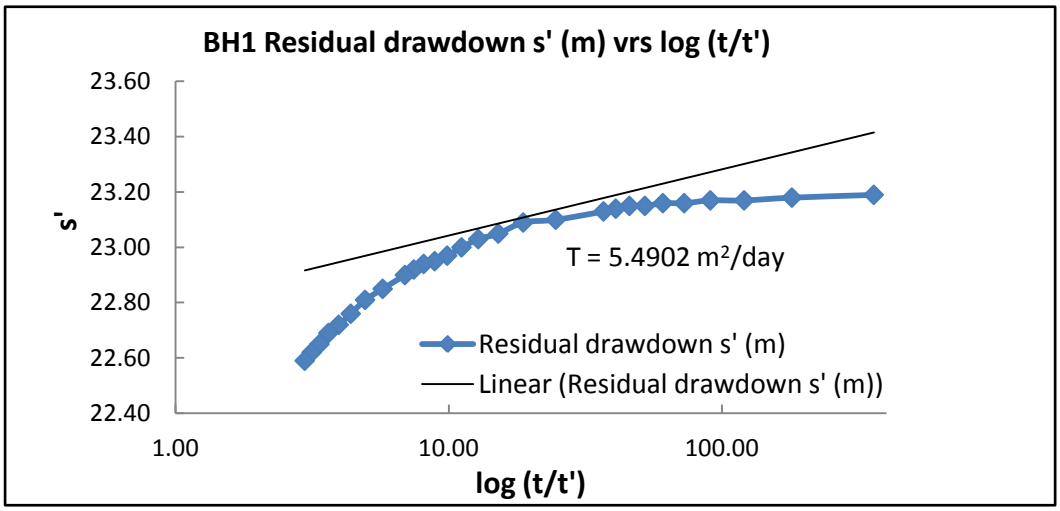

Figure 4.3a: Semi-log graph of residual drawdown versus time ratio of BH1.

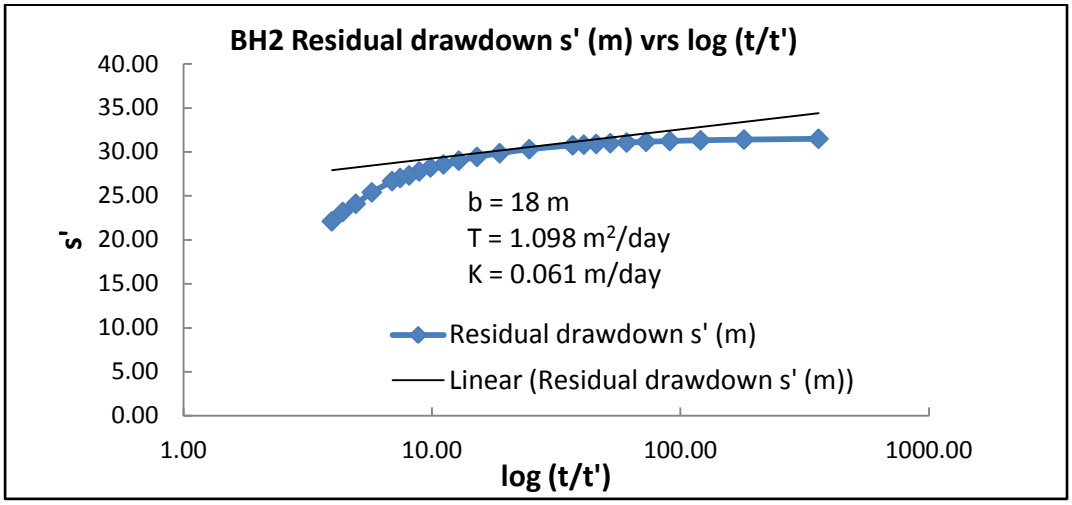

Figure 4.3b: Semi-log graph of residual drawdown versus time ratio of BH2.

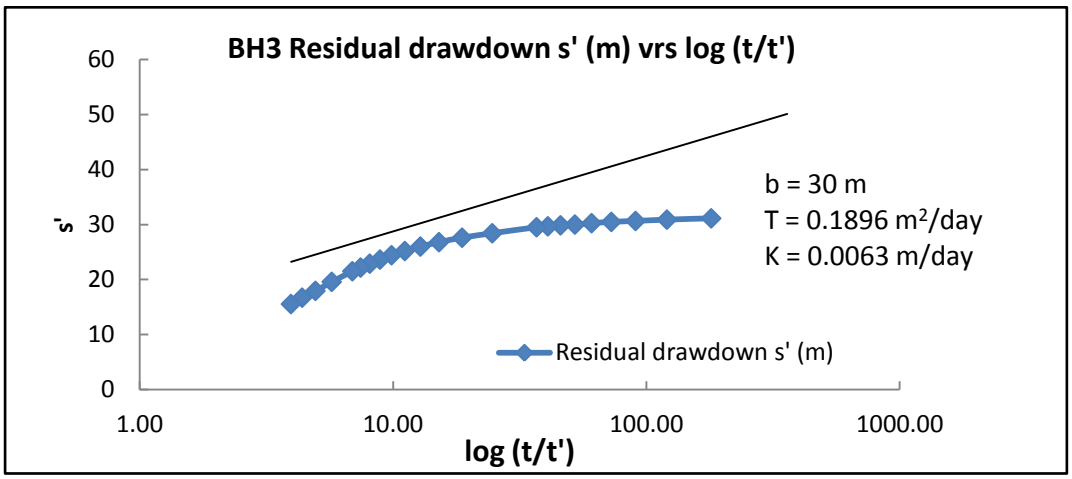

Figure 4.3c: Semi-log graph of residual drawdown versus time of BH3.

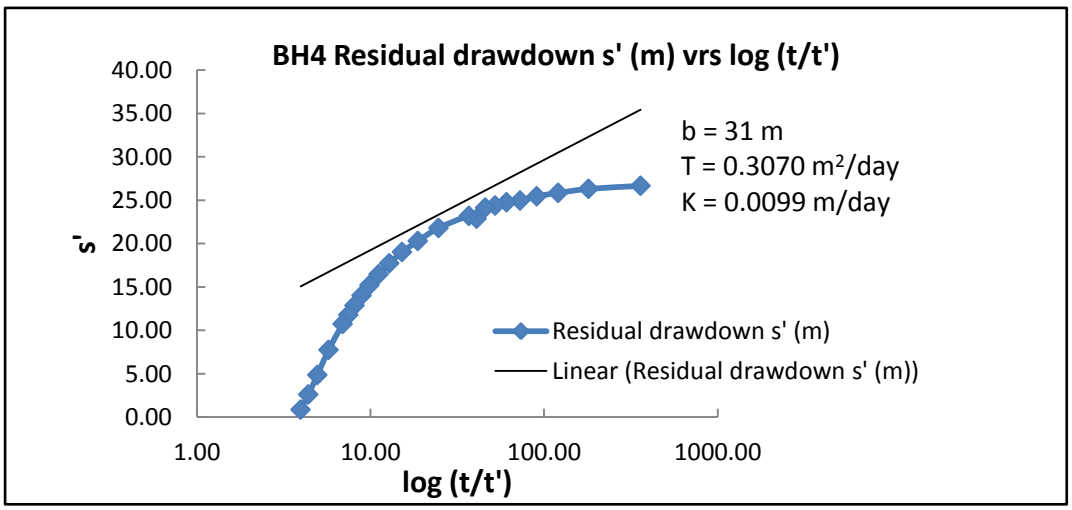

Figure 4.3d: Semi-log graph of residual drawdown versus time ratio of BH4.

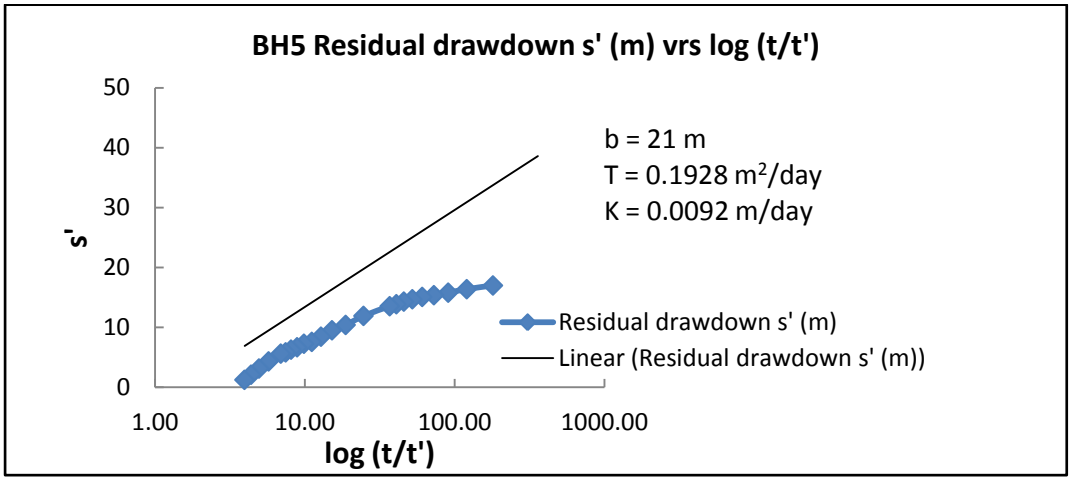

Figure 4.3e: Semi-log graph of residual drawdown versus time ratio of BH5.

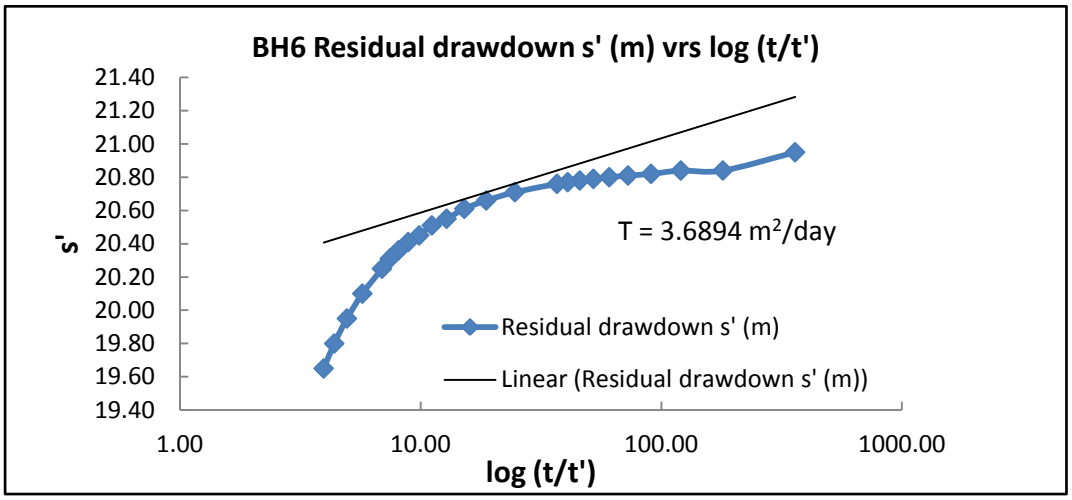

Figure 4.3f: Semi-log graph of residual drawdown versus time ratio of BH6.

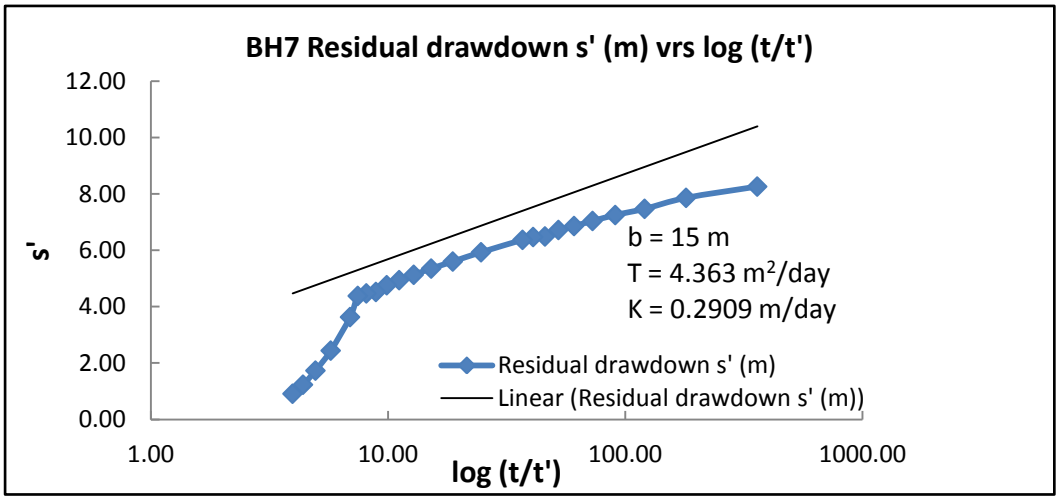

Figure 4.3g: Semi-log graph of residual drawdown versus time ratio of BH7.

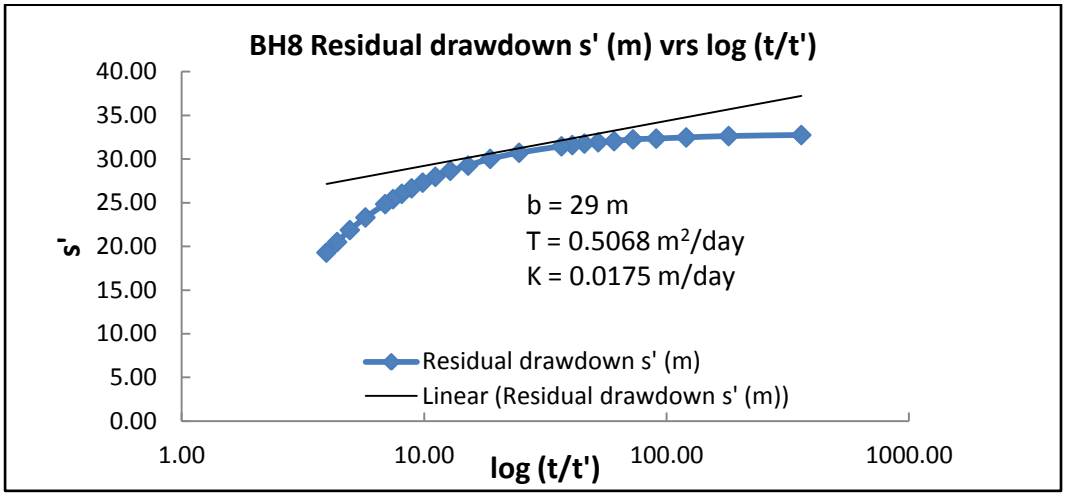

Figure 4.3h: Semi-log graph of residual drawdown versus time ratio of BH8.

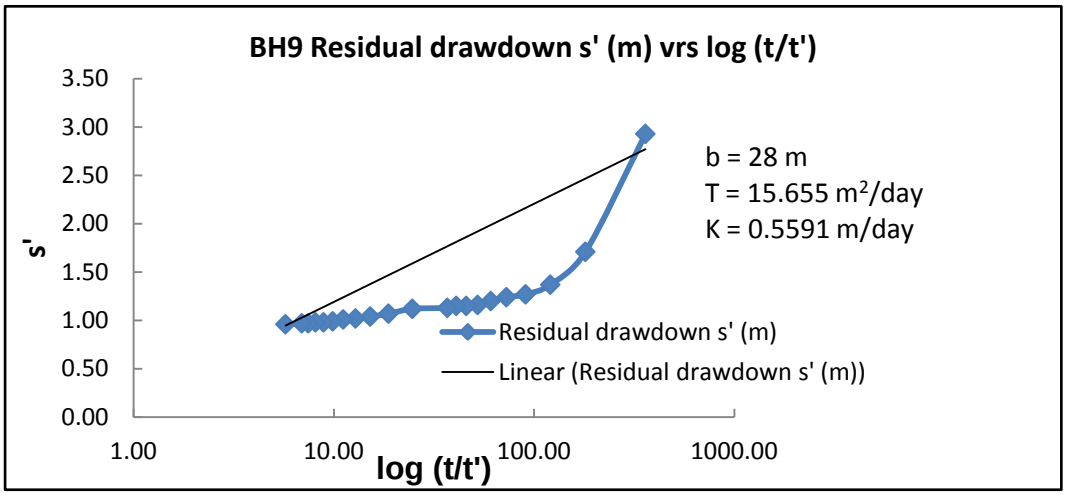

Figure 4.3i: Semi-log graph of residual drawdown versus time ratio of BH9.

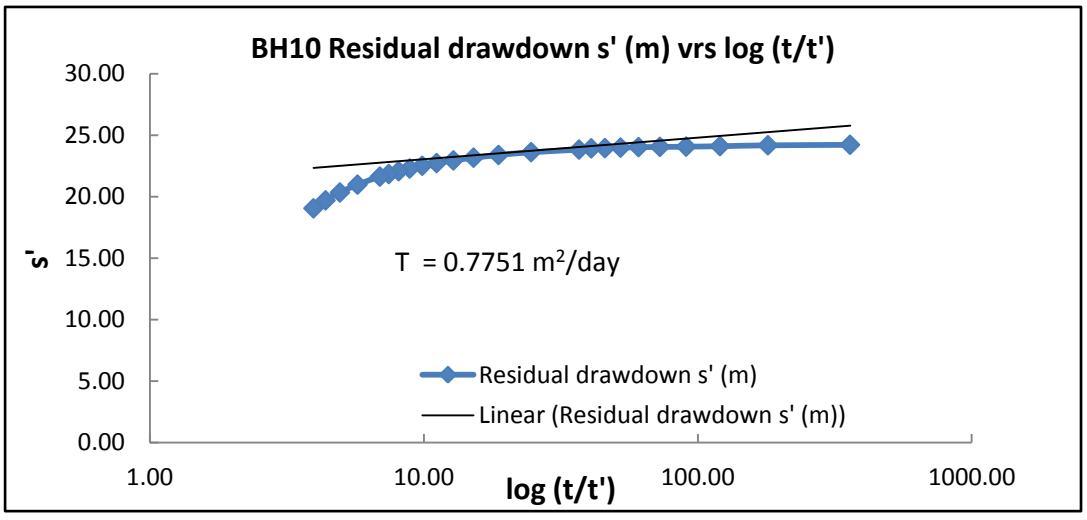

Figure 4.3j: Semi-log graph of residual drawdown versus time ratio of BH10.

The hydraulic parameters estimated from the borehole data were summarized and presented in the Table 4.2.

Table 4.2 Aquifers hydraulic properties

Well Ref.	b (m)	Q (l/min)	$\Delta s'$ (m)	T (m^2/day)	K (m/day)
BH1	-	5	0.24	5.4902	-
BH2	18	10	2.40	1.0980	0.0610
BH3	30	10	13.90	0.1896	0.0063
BH4	31	12	10.30	0.3070	0.0099
BH5	21	12	16.40	0.1928	0.0092
BH6	-	7	0.50	3.6894	-
BH7	15	50	3.00	4.3921	0.2928
BH8	29	10	5.20	0.5068	0.0175
BH9	28	60	1.01	15.655	0.5591
BH10	-	5	1.70	0.7751	-

In Table 4.2, b is the aquifer thickness, Q is the aquifer yield, $\Delta s'$ is change in residual drawdown for one log cycle, T is the transmissivity, and K is the hydraulic conductivity. The yields of boreholes range between 5 – 60 L/min with the majority ranging between 10 – 12 L/min.

4.1.5 Flow Rate and Flow Direction

Tables 4.4 and 4.5 show the hydraulic properties, flow rates and flow directions determined for the ten well sets used. Analyses of groundwater flow in the study area revealed two dimensional hydraulic properties, flow rates and flow directions. Hydraulic parameters determined for the study area is located in **Appendix D.**

Table 4.3 Hydraulic properties, gradient, flow rate and flow direction on x-axis

Well Sets	Hydraulic gradient in x direction	Average T in x direction	Average K in x direction	Apparent flow rate ν_x (m^2/day)	Apparent velocity υ_x (m/day)	Flow direction
1	0.0308	7.922	0.283	0.244	0.0087	144°N
2	0.0253	2.291	0.150	0.058	0.0038	153°N
3	0.0260	1.940	-	0.050	-	166°N
4	0.0031	0.645	0.035	0.002	0.0001	80°N
5	0.0071	8.081	0.288	0.057	0.0020	353°N
6	0.0139	2.584	-	0.036	-	201°N
7	0.0102	2.232	-	0.023	-	160°N
8	0.0229	7.924	0.008	0.181	0.0002	20°N
9	0.0221	3.133	-	0.069	-	155°N
10	0.0230	0.482	-	0.011	-	168°N

Table 4.4 Hydraulic properties, gradient, flow rate and flow direction on y-axis

Well Sets	Hydraulic gradient in y direction	Average T in y direction	Average K in y direction	Apparent flow rate ν_y (m^2/day)	Apparent velocity υ_y (m/day)	Flow direction
1	0.0141	0.348	0.012	0.005	0.0002	54°N
2	0.0036	0.644	0.034	0.002	0.0001	63°N
3	0.0057	2.840	-	0.016	-	76°N
4	0.0071	8.081	0.288	0.057	0.0020	-10°N
5	0.0157	10.573	-	0.166	-	263°N
6	(0.0065)	2.292	0.151	(0.015)	(0.0010)	111°N
7	0.0005	2.232	-	0.001	-	70°N
8	0.0048	2.292	0.151	0.011	0.0007	-70°N
9	0.0088	2.837	-	0.025	-	65°N
10	0.0125	0.348	0.283	0.099	0.0035	78°N

4.2 Groundwater Flow Patterns and Contours

ANSYS Fluent 13.0 software was used to numerically simulate uniform groundwater flow model (3.33) in the x-direction. Residual criteria of 0.001 for monitoring continuity, x-velocity and y-velocity were set and the simulation performed for 10 s. The simulation results are presented in Figure 4.4 to 4.6.

4.2.1 Static Pressure against Position

Figure 4.4 shows the static pressure distribution in the modelled domain. The graph shows how static pressure varies with position along the flow direction.

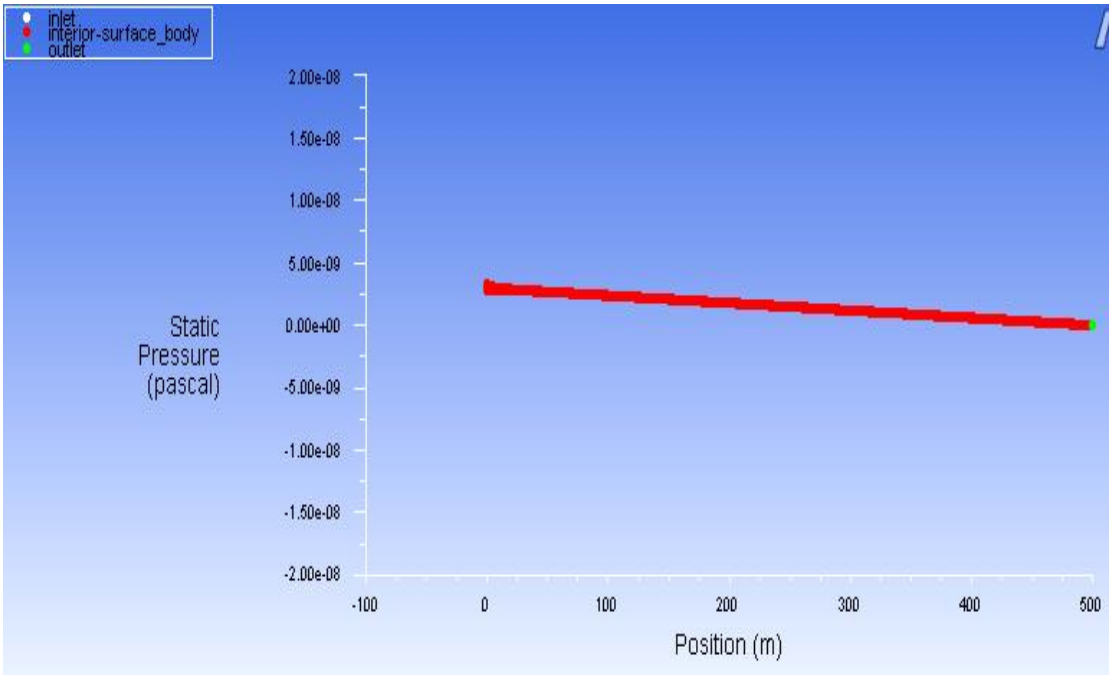

Figure 4.4: Static pressure distributions along flow domain.

4.2.2 Velocity Magnitude Distribution

In Figure 4.5 the graph shows the flow pattern as groundwater flows from recharge area (inflow) to a discharge area (outflow) of the 2D flow model geometry. The parabolic pattern indicates the nature of advection in a uniform flow longitudinally.

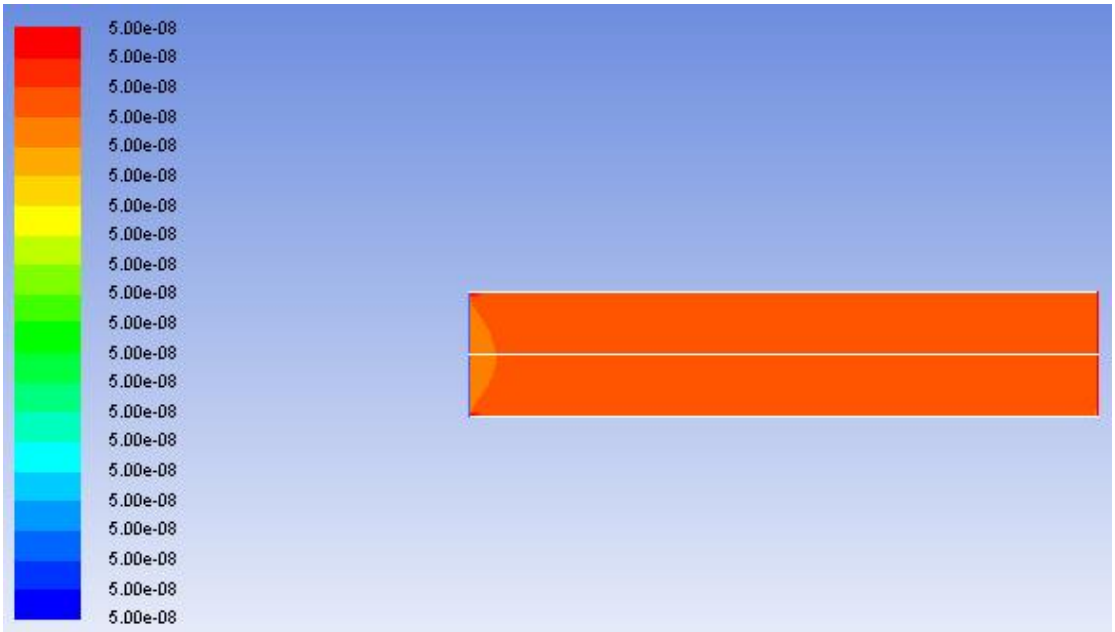

Figure 4.5: Pattern of flow velocity distribution

Initial input velocity of 5.00E-8 m/s was used in the diffusive groundwater flow simulation and the output flow velocity magnitude in direction of flow ranges between 4.99E-08 to 5.00E-08 m/s.

4.2.3 Pressure Contour

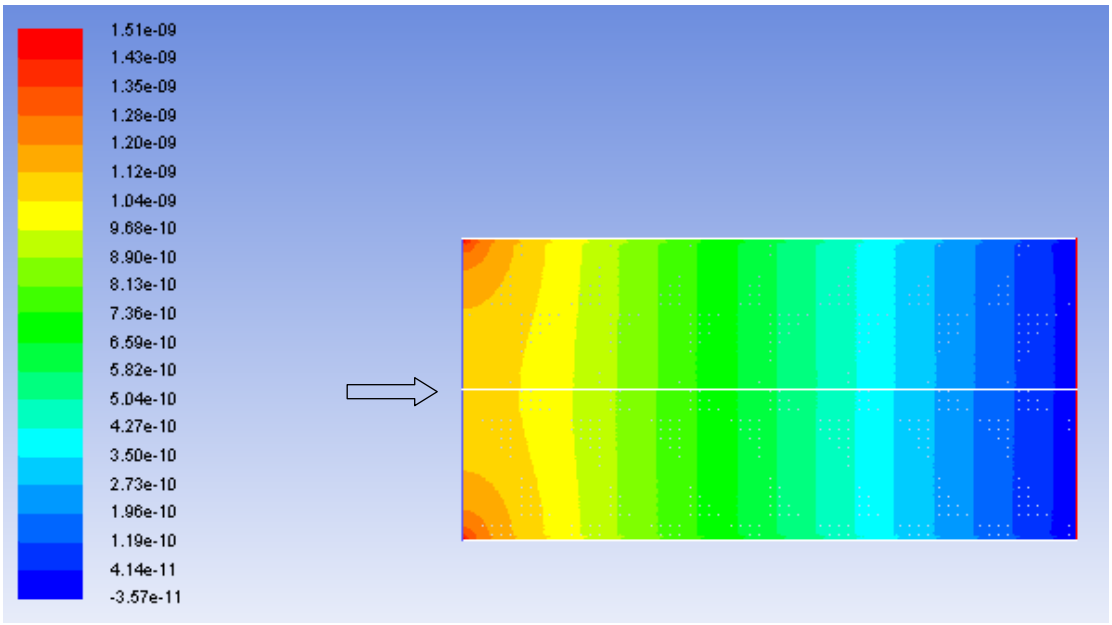

Figure 4.6: Pressure contour in the direction of flow.

Figure 4.6 shows a pressure contour of groundwater flow in saturated confined model geometry of the Dahomeyan System. For uniform flow in the flow direction, the Dahomeyan System resisted flow longitudinally than transversally initially.

4.2.4 Statistical Quantities that Describe the Groundwater Flow

The Reynolds number (Re) from the simulation of the model geometry was approximately 0.035. The Courant number (Cu) from the simulation range between 8.6E-8 to 1.5E-7 and was less than one ($Cu < 1$). The net mass flow rate was also found to be -9.74E-11 kg/s. The small value of the net mass flow rate is indicative of the fact that the solution has converged. Grid independence was achieved as the grid spacing was increased from step size of 1 m to a step size of 5 m and confirms stability of the solution. Diffusivity values were varied during the simulation from 10 – 0.1 m^2/s and storativity values calculated range between 2.2E-6 to 1.8E-4 with an average of 3.74E-5.

4.3 Contaminants Distribution and Concentration

4.3.1 MatLab Simulation Result of 1D ADDE

The results of simulating 1D ADDE for C-14 and Sr-90 in space and time for 20 and 50 years using MatLab R2013a were presented in Figures 4.7 – 4.14.

4.3.2 Carbon-14 and Strontium-90 spread in space for 20 years

Figure 4.7 shows Carbon-14 distribution for 20 years in the flow direction from the source. The analytical and numerical graphs overlap which implies that at time far less than the half life and of very low decay constant of Carbon-14 the numerical error did not increase.

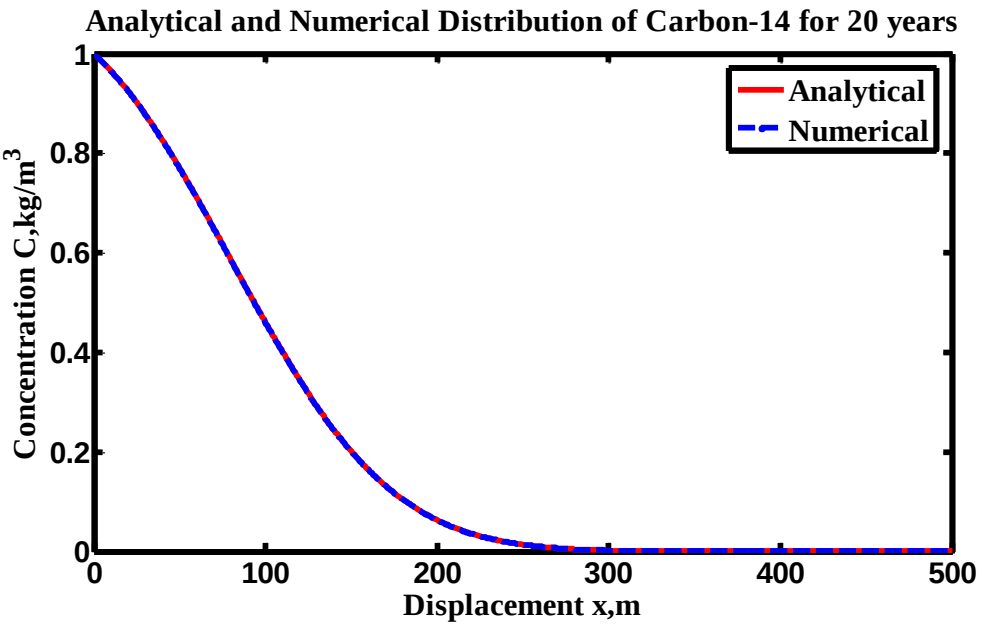

Figure 4.7: Spatial variation of Carbon-14 for 20 years.

The Figure 4.8 shows Strontium-90 distribution for 20 years in the flow direction from the source. The numerical showed deviation from the analytical graph in varying degrees for duration of 20 years. This implies that at a time close to half life with moderately higher decay constant than Carbon-14 the numerical error increased and the numerical graph lagged the analytical graph.

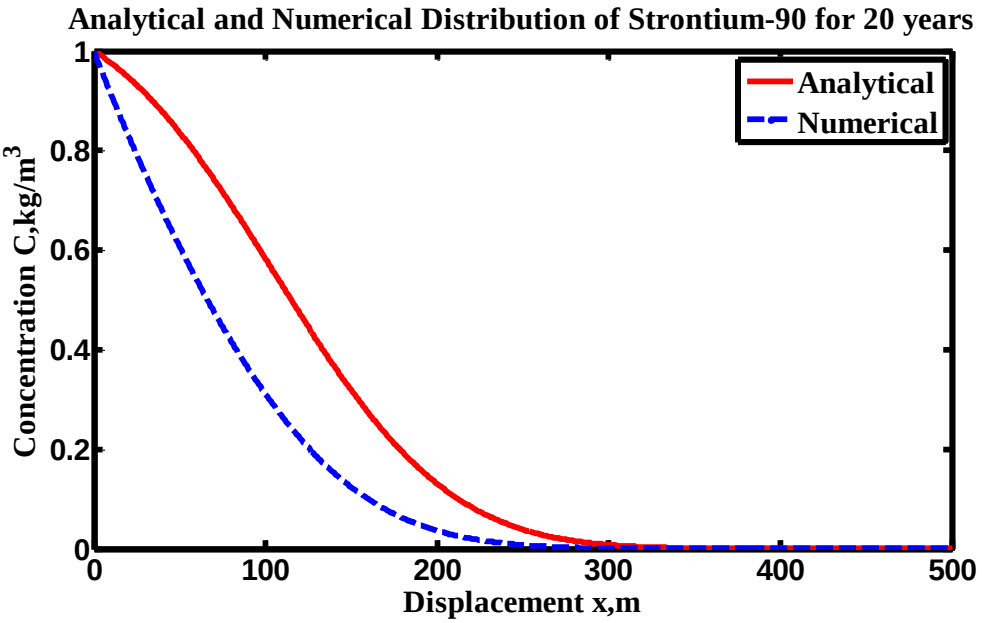

Figure 4.8: Spatial variation of Strontium-90 for 20 years.

4.3.3 Carbon-14 and Strontium-90 spread monitoring for 20 years

Figure 4.9 shows the monitoring of Carbon-14 monitoring for 20 years in a well at 100 m in the flow direction from the source. The analytical and numerical graphs overlap which implies that at time far less than the half life of Carbon-14 with a low decay constant the numerical error did not increase.

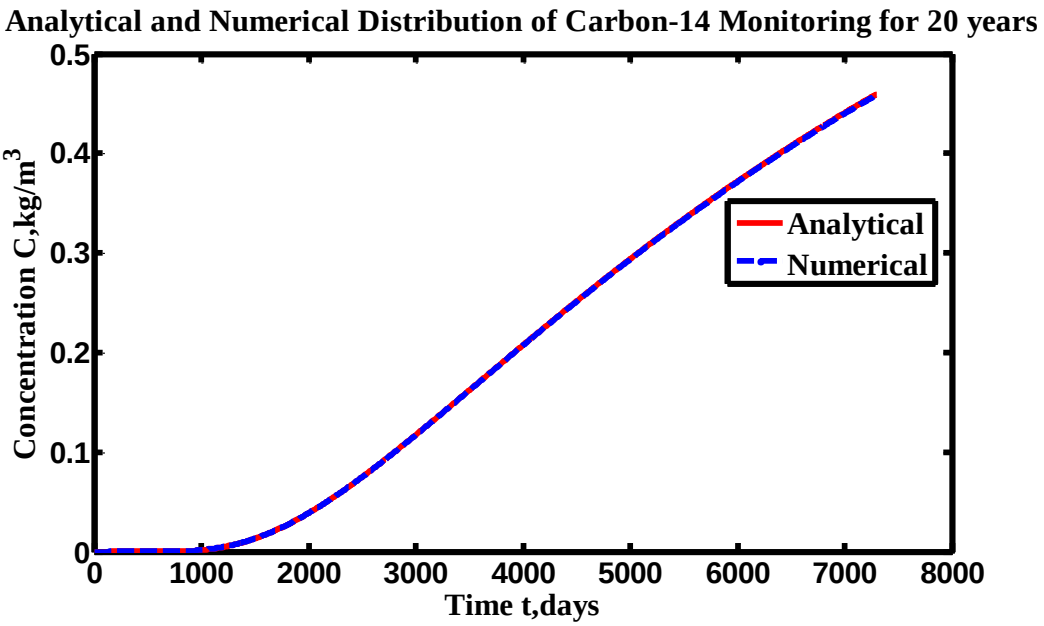

Figure 4.9: Temporal variation of Carbon-14 monitoring for 20 years.

Figure 4.10 shows the monitoring of Strontium-90 for 20 years in a well at 100 m in the flow direction from the source. The numerical graph deviates from the analytical graph. The deviation increases gradually due to increase in computational error with time for Strontium-90 with a higher decay constant than Carbon-14.

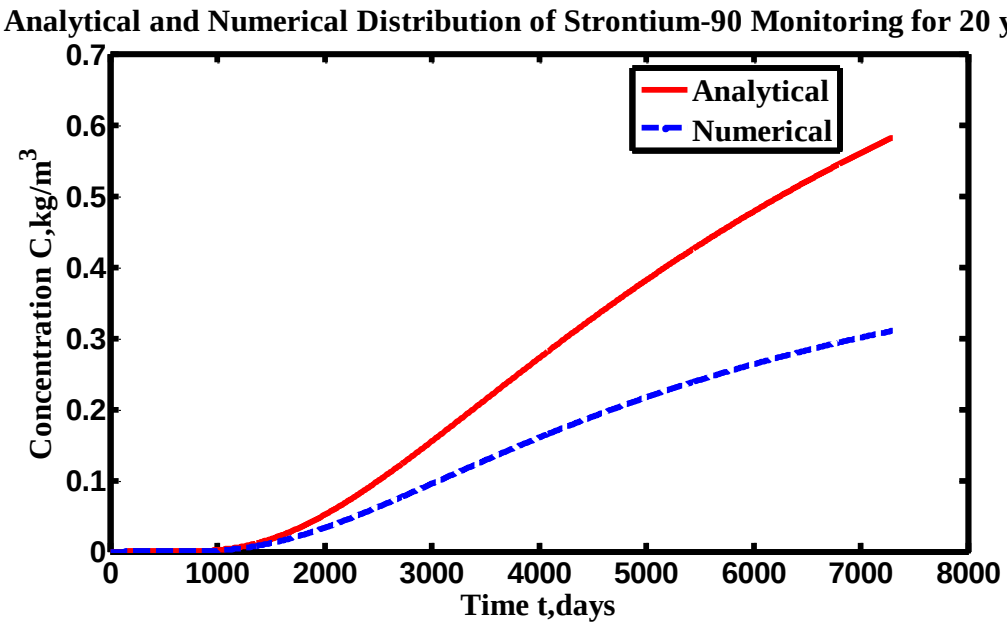

Figure 4.10: Temporal variation of Strontium-90 monitoring for 20 years.

4.3.4 Carbon-14 and Strontium-90 spread for 50 years

Figure 4.11 shows Carbon-14 distribution for 50 years in the flow direction from the source. The analytical and numerical graphs overlap which implies that at time far less than the half life and of very low decay constant of Carbon-14 the numerical error did not increase.

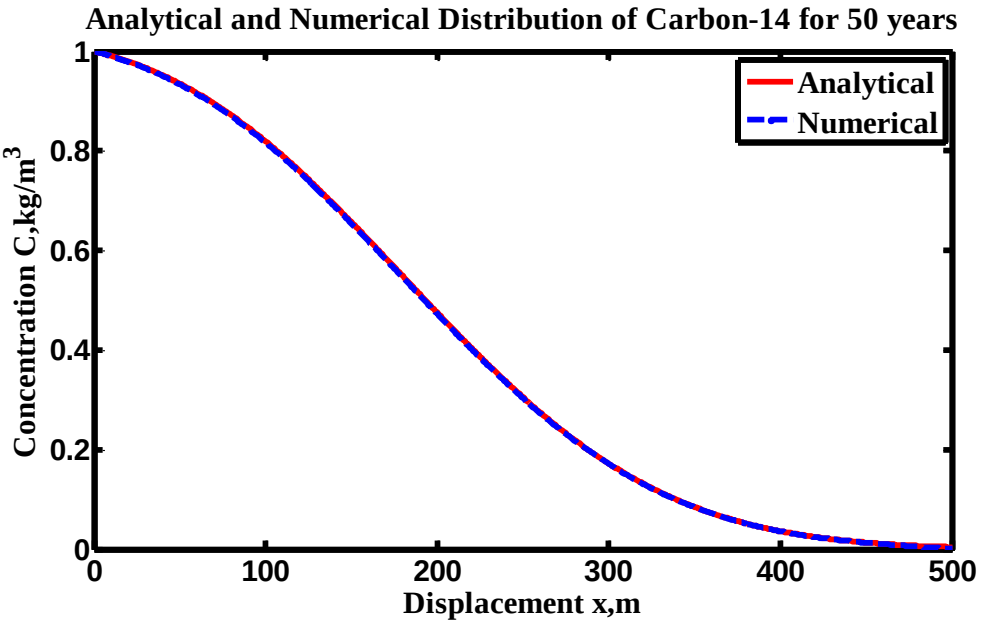

Figure 4.11: Spatial variation of Carbon-14 for 50 years.

The Figure 4.12 shows Strontium-90 distribution for 50 years in the flow direction from the source. The numerical showed deviation from the analytical graph in varying degrees for duration of 50 years. This implies that at a time close to 2 half lives of Strontium-90 with moderately higher decay constant than Carbon-14 the numerical error increased and the numerical graph lagged the analytical graph.

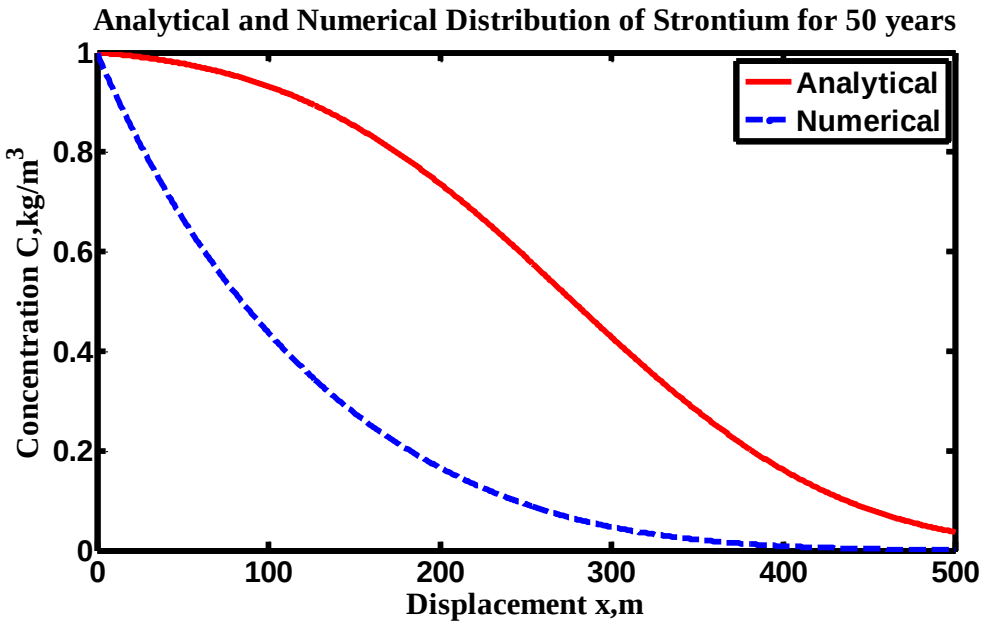

Figure 4.12: Spatial variation of Strontium-90 for 50 years.

4.3.5 Carbon-14 and Strontium-90 spread monitoring for 50 years

Figure 4.13 shows the monitoring of Carbon-14 monitoring for 50 years in a well at 100 m in the flow direction from the source. The analytical and numerical graphs overlap which implies that at time far less than the half life of Carbon-14 with a low decay constant the numerical error did not increase.

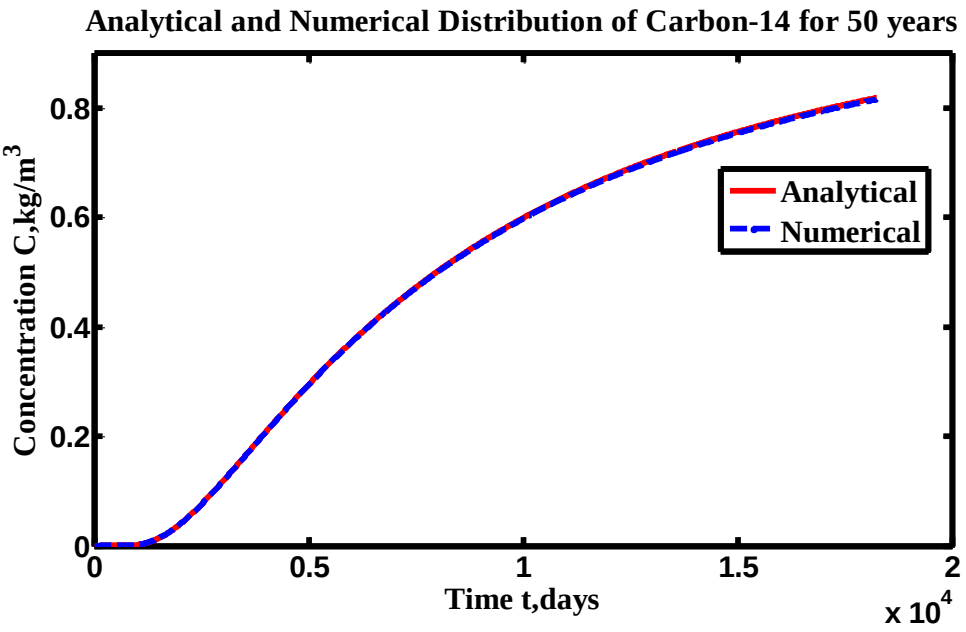

Figure 4.13: Temporal variation of Carbon-14 monitoring for 50 years.

Figure 4.14 shows the monitoring of Strontium-90 for 50 years in a well at 100 m in the flow direction from the source. The numerical graph deviates from the analytical graph with time. The deviation increases gradually due to increase in computational error with time for Strontium-90 with a higher decay constant than Carbon-14.

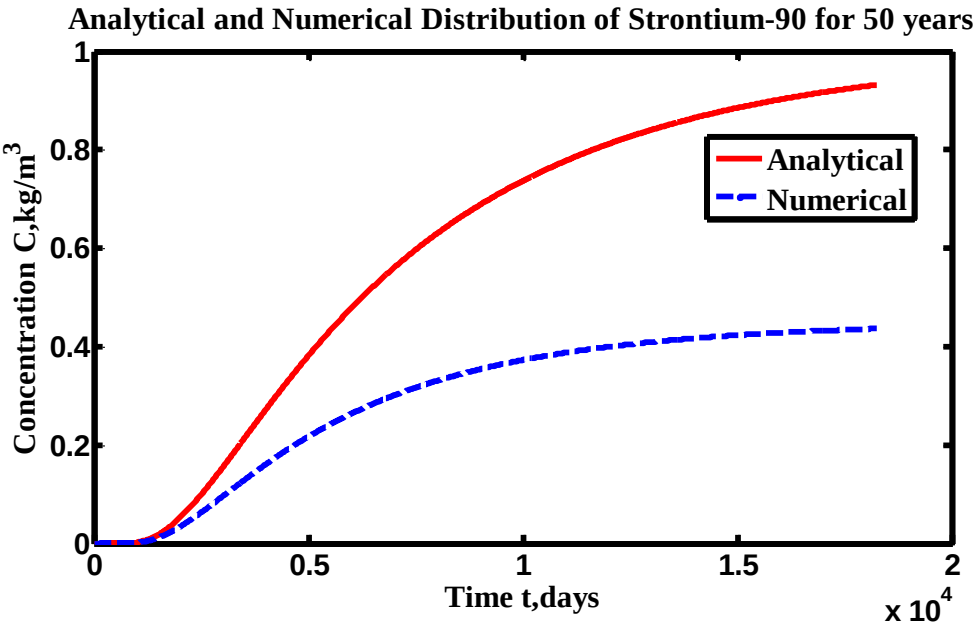

Figure 4.14: Temporal variation of Strontium-90 monitoring for 50 years.

4.3.6 MatLab Simulation of 2D ADDE

A 2D contaminant transport solution by [101] for saturated confined aquifer was coded and simulated using MatLab R2013a. The results of the simulations for radioactive Carbon-14 and Strontium-90 transport in the saturated confined aquifers of the Dahomeyan System of the Accra Plains for 30 and 100 years were given were presented in Figures 4.15 – 4.26.

4.3.7 Carbon-14 Simulation

Figure 4.15 is a surface graph that shows the distribution of Carbon-14 in the aquifer for 30 years as it was distributed longitudinally in the flow direction and transversally. For a uniform flow, the radionuclide undergoes advection, dispersion and decay longitudinally and transversally, the radionuclide undergoes dispersion and decay.

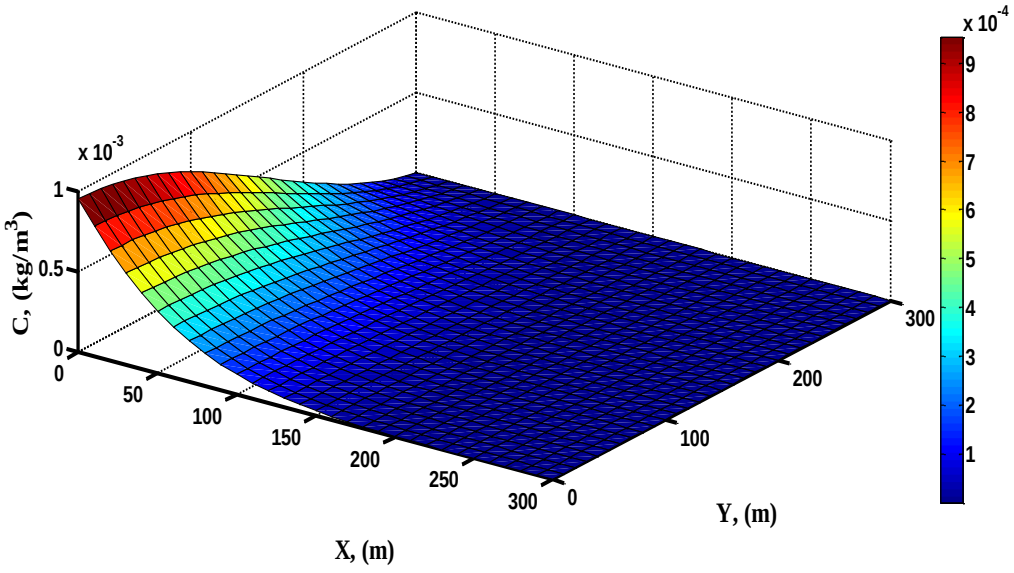

Figure 4.15: Carbon-14 spread in groundwater for 30 years.

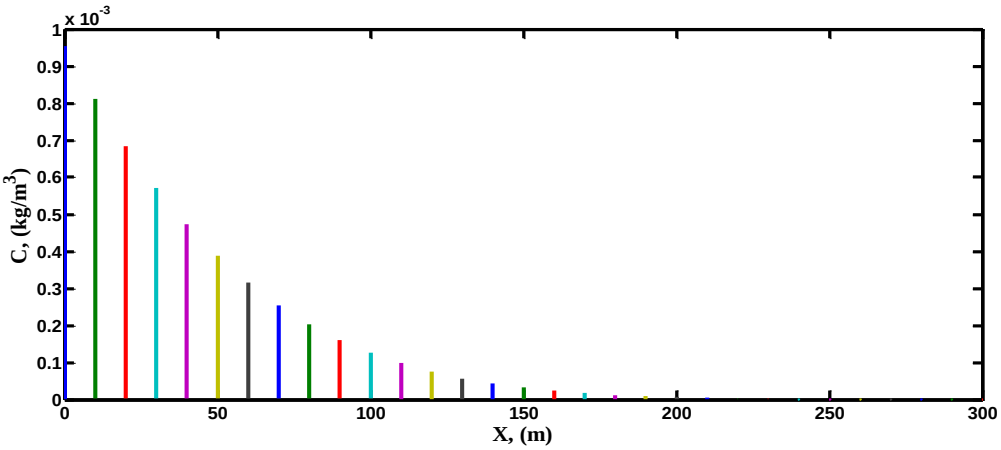

Figure 4.16: Carbon-14 spread in groundwater for 30 years in x direction.

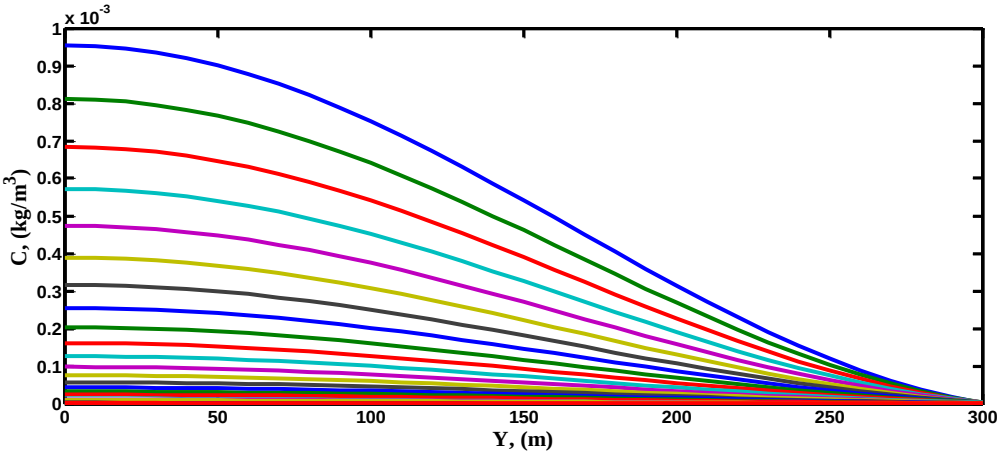

Figure 4.17: Carbon-14 spread in groundwater for 30 years in y direction.

The result showed that in 30 years carbon-14 contaminant covered a distance of about 170 m in the flow direction (longitudinally) Figure 4.16 and covered a distance of about 300 m transversally Figure 4.17.

Figure 4.18 is a surface graph that shows the distribution of Carbon-14 in the aquifer for 100 years as it was distributed longitudinally in the flow direction and transversally. The result showed that in 100 years carbon-14 contaminant reaches a distance of about 250 m in the flow direction (longitudinally) Figure 4.19 and covered a distance a little over 300 m transversally Figure 4.20.

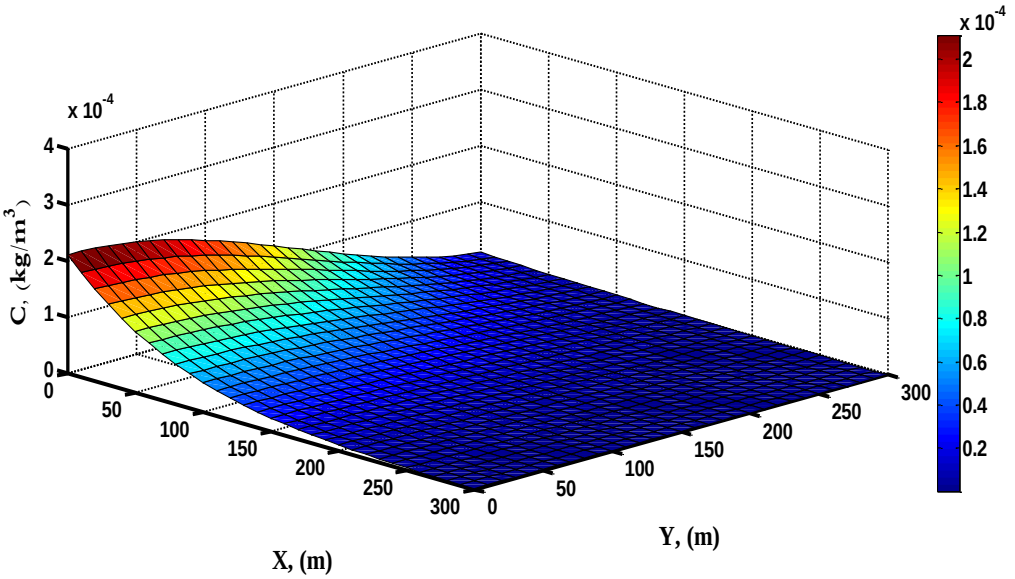

Figure 4.18: Carbon-14 spread in groundwater for 100 years.

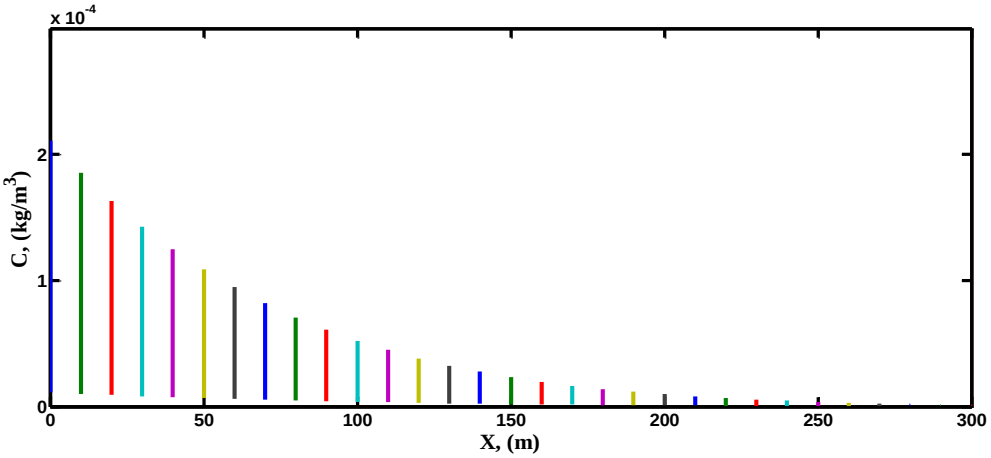

Figure 4.19: Carbon-14 spread in groundwater for 100 years in x direction.

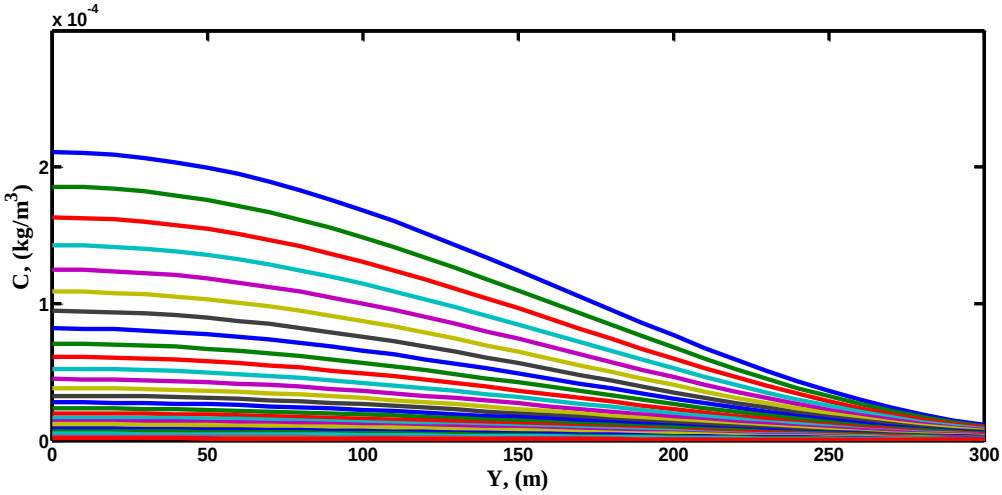

Figure 4.20: Carbon-14 spread in groundwater for 100 years in y direction.

4.3.8 Strontium-90 Simulation

Figure 4.21 is a surface graph of Strontium-90 spread in the Dahomeyan System for 30 years. Strontium-90 undergoes advection, dispersion and decay, longitudinally and covered a distance of about 160 m in the flow direction (Figure 4.22) and undergoes dispersion and decay transversally and covered a distance of about 300 m (Figure 4.23).

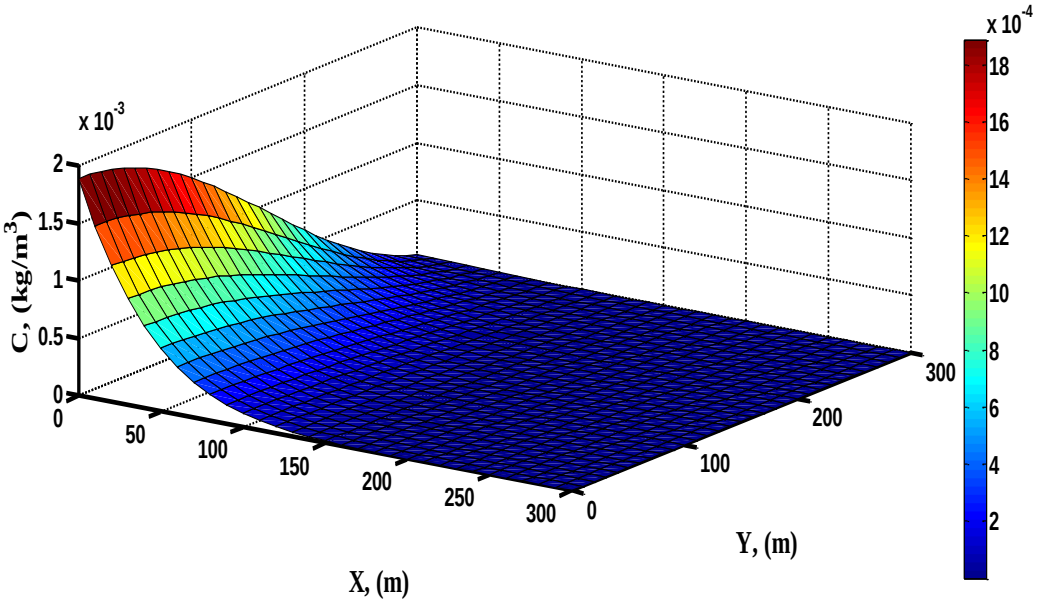

Figure 4.21: Strontium-90 spread in groundwater for 30 years.

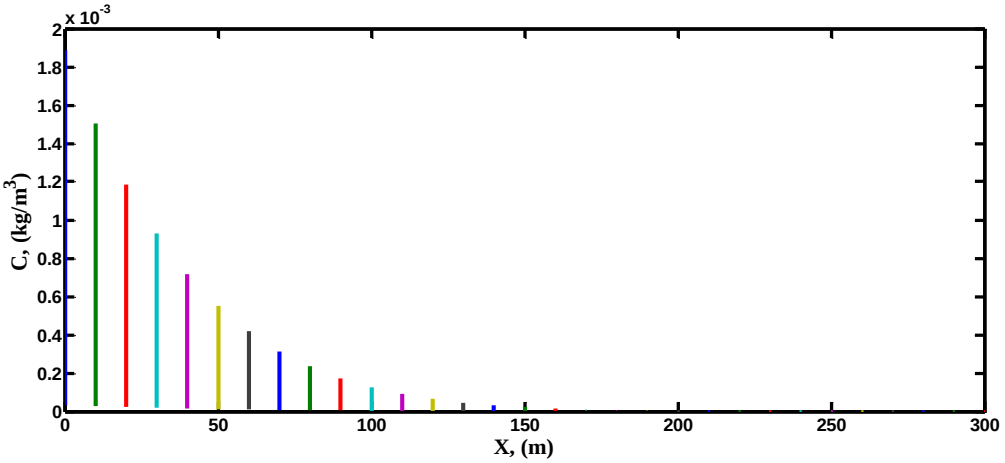

Figure 4.22: Strontium-90 spread in groundwater for 30 years in x direction.

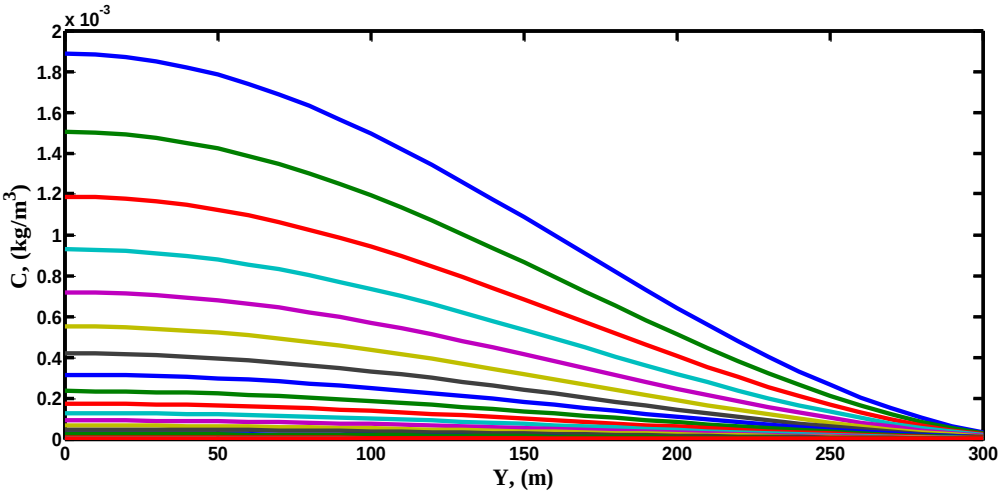

Figure 4.23: Strontium-90 spread in groundwater for 30 years in y direction.

Figure 4.24 is a surface graph of Strontium-90 spread in the aquifer as it was advected in x direction, and dispersed and decayed in both x and y directions. The result showed that in 100 years Strontium-90 contaminant reaches a distance of about 260 m in the flow direction (longitudinally) Figure 4.25 and covered a distance of a little over 300 m transversally Figure 4.26.

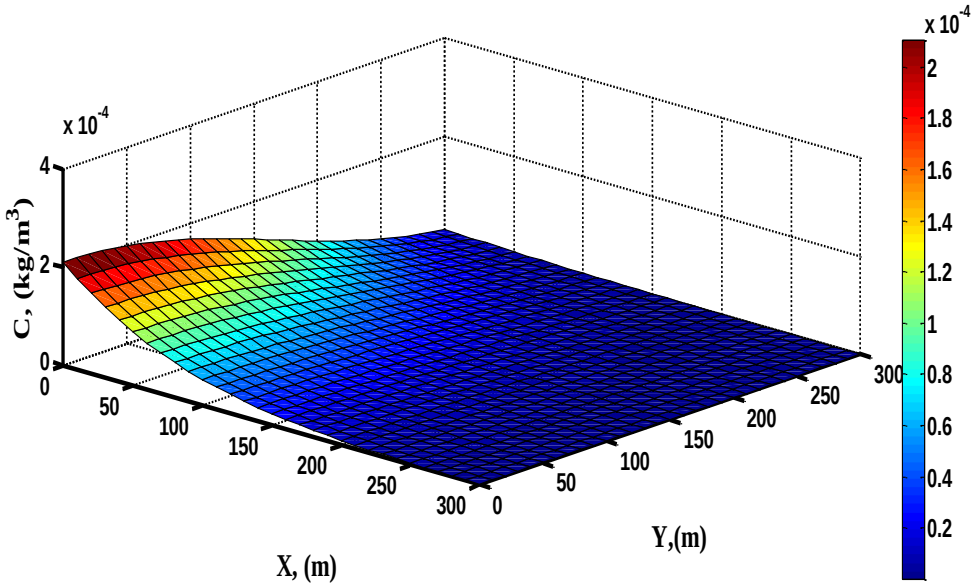

Figure 4.24: Strontium-90 spread in groundwater for 100 years.

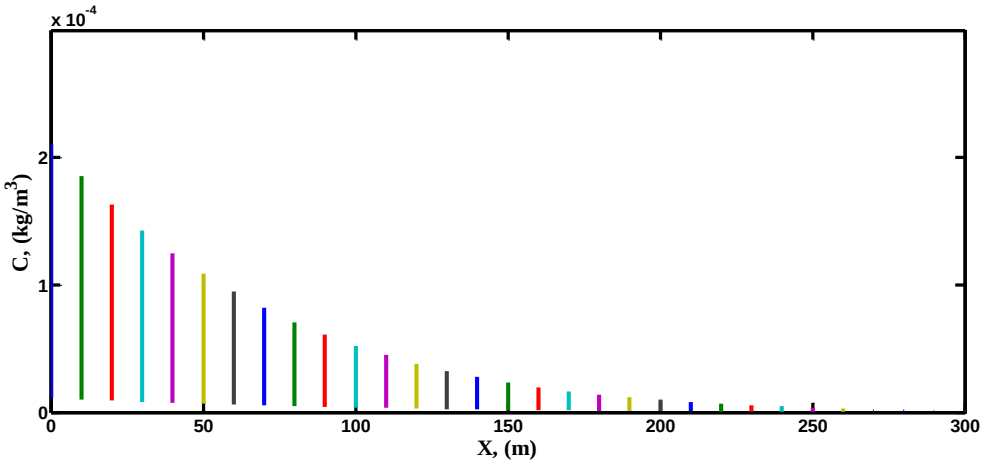

Figure 4.25: Strontium-90 spread in groundwater for 100 years in x direction.

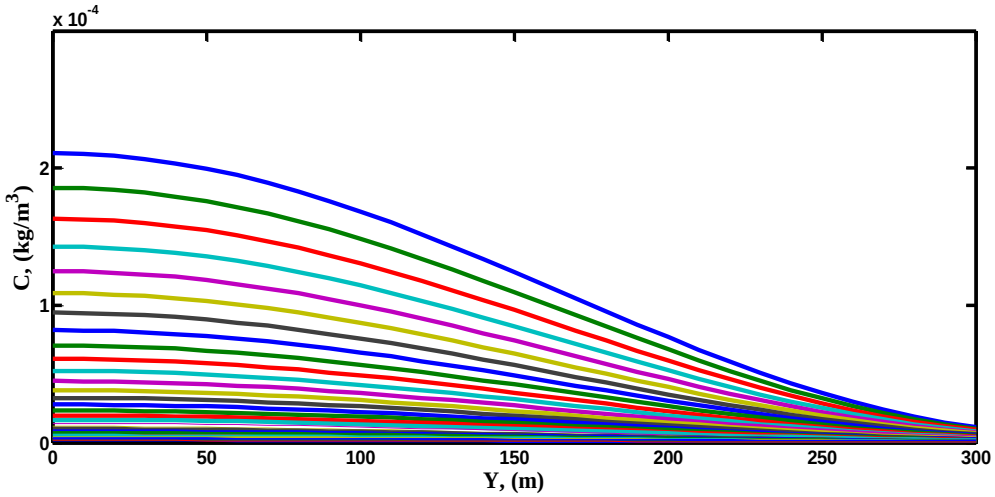

Figure 4.26: Strontium-90 spread in groundwater for 100 years in y direction.

DISCUSSIONS

The main goal of this research was to model and simulate groundwater flow and radioactive contaminant transport in the confined saturated zone of hard rock, fractured aquifer of the Dahomeyan System to understand the behaviour of groundwater flow and radioactive contaminant transport. The discussion presented is based on the objectives of the research.

Three aquifer formation types were observed from the MS Excel 2007 semi-log plots of drawdown versus time. These are fractured heterogeneous, purely fractured

homogeneous and double porosity aquifer formations. These aquifer formation types agree with that used by [47].

1. Aquifer Parameter Estimation

The porosity and effective porosities of the fractured aquifer system were estimated by analysing the borehole logs of the wells used in this research. The total porosity estimated for the study area ranges from 0.19 – 0.44 with a mean of 0.27 and the secondary/effective porosity in Table 4.1 ranging from 0.08 – 0.17 with a mean of 0.11. The ranges of total porosity and effective porosity estimated compared well with that estimated by [106] for schists and the averages of the total and the effective porosities showed some slight variations. The total porosity they estimated ranges between 0.04 – 0.49 with a mean of 0.38 and an effective porosity ranging between 0.22 – 0.33 with a mean of 0.26. The effective porosity also agreed with that of igneous and metamorphic fractured rocks [81] in **Appendix E.** The effective porosity estimated was used in modelling of groundwater flow and contaminant transport in the Dahomeyan System. The effective porosity is very small and which reflected in the slow movement of groundwater and radioactive contaminant in the study area. It must be noted that total porosity is not constant for fractured rocks and site specific values should be estimated to represent the total porosity of the domain.

The hydraulic properties determined in the Dahomeyan System include, transmissivity T, hydraulic conductivity K, and storativity S. In Table 4.2, the transmissivity estimated using borehole data and Theis recovery method for the study area ranges from 0.18 – 15.66 m^2/day with a mean of 4.70 m^2/day. The hydraulic conductivity estimated ranged from 0.0063 – 0.5591 m/day with an average value of 0.1119 m/day. The storativity estimated for a borehole which has a monitoring well

using the Cooper Jacob method was 0.0058 which is high due to high transmissivity of the fracture zone was used as a guide.

Further analyses of the hydraulic properties, flow rates and flow directions were presented in Tables 4.3 and 4.4. In Table 4.3, the transmissivity in the x-direction ranges between 0.482 – 8.081 m^2/day with a mean of 3.723 m^2/day. The hydraulic conductivity ranges between 0.008 – 0.288 m/day with a mean of 0.153 m/day in the x-direction. The hydraulic gradients range between 0.003 – 0.031 with a mean of 0.018 in the x-direction. The flow rate ranges between 0.002 – 0.245 m^2/day with a mean of 0.073 m^2/day. The major direction of flow lies between 144^{o}N – 168^{o}N (i.e. in the south-southeast direction). The apparent groundwater velocity in x direction ranges between 0.0001 – 0.0087 m/day with a mean of 0.0030 m/day and a mean pore water velocity in x-direction of 0.0269 m/day.

In Table 4.4, the hydraulic gradients determined transverse (y-direction) to flow direction ranges between 0.0005 – 0.0157 with a mean of 0.007 in magnitude. The transmissivity transversal to the y direction ranges between 0.348 – 10.573 m^2/day with a mean of 4.006 m^2/day. The hydraulic conductivity in the y-direction ranges between 0.012 – 0.288 m/day with a mean of 0.153 m/day. The flow rate in the y-direction ranges from 0.001 – 0.166 m^2/day with a mean of 0.37 m^2/day. The apparent flow velocity in the y-direction ranges between 0.0001 – 0.0020 m/day with a mean of 0.0006 m/day. The y-directions indicated in Table 4.4 were horizontal directions determined 90^o in the positive sense relative to the x-axis.

The analyses revealed that groundwater flows were in 2 dimensions and the hydraulic conductivities estimated showed the domain to be heterogeneous and isotropic. Three well set of ten were considered in the estimation of hydraulic gradient, and the flow

direction. The flow rates were determined using Darcy's law. The small values reported revealed that groundwater flow in the Dahomeyan System were slow and laminar and in the South Southeast (SSE) direction.

As can be seen in the study area, groundwater does not have a constant gradient and it is highly uncommon to find a constant hydraulic gradient and this situation has been noted by [16]. The transmissivity obtained in the Dahomeyan System ranges from 0.18 - 15.66 m^2/day. The difference in transmissivity in x direction 3.723 m^2/day and that in the y direction 4.006 m^2/day may be due to more fractures aligning themselves along the y-axis than were in the x-axis. Transmissivity values for the Basement Complex ranged from 0.40 - 27.0 m^2/day and are characteristic of basement aquifers [107]. However, transmissivity obtained in this research work compared well with that obtained from the Basement Complex as indicated by [94].

The hydraulic conductivities also ranged from 0.05 - 3.39 m/day, with an arithmetic mean of 0.50 m/day, and were also generally low for sedimentary formation [108]. The results of [108] compared well with the results of hydraulic conductivity in the Dahomeyan System which are mainly schists in this research work. The average permeability of the Dahomeyan System was also estimated to be 1.6E-13 m^2. This permeability value is very small indicating groundwater flow in the Dahomeyan System to be very slow. The average apparent flow velocities in flow direction and in transverse directions are 0.003 m/day and 0.001 m/day respectively. The mean pore water velocity in the x-direction (flow direction) is 0.0296 m/day an equivalent of 3.4E-8 m/s. Groundwater flow therefore was dominant in domains where there were more fractures than where fractures are relatively low or blocked.

2. Contour and Pattern

Figure 4.4 shows the static pressure distribution along the flow path with respect to position. The relationship between static pressure and total hydraulic head is $p = \rho g h$, where, p is the static water pressure, ρ is water density and h is the hydraulic head/water level. The graph indicates a small gradient as expected in the flow direction. This means that in the neighbourhood of a well the change in static pressure is negligible small hence the drop in hydraulic head is also negligibly small. The small change in hydraulic head will not cause much change in flow velocity. Therefore, in the neighbourhood of a well (i.e. 500 m) the change in velocity is negligible in the domain considered.

The pattern of velocity magnitude distribution was displayed in Figure 4.5. The groundwater flow was advection dominated for uniform flow in the longitudinal direction. The pattern revealed that groundwater flow more longitudinally that transversally. The initial velocity used in the simulation was 5E-8 m/s. Figure 4.6 show the pressure contour of groundwater flow in the Dahomeyan System. The pattern shows that groundwater flow in the Dahomeyan System initially was dominant transversally than longitudinally. Due to the nature of the study domain, groundwater flow was resisted heavily in the longitudinal direction and this behaviour is good for the domain in resisting radionuclide movement in the Dahomeyan System.

The Reynolds number from ANSYS Fluent simulation was approximately 0.035, Courant number ranges between 8.6E-8 – 1.5E-7. The Reynolds number Re < 1 and Courant number Cu < 1 confirms that groundwater flow in the Dahomeyan System was very slow and laminar. The small value of the net mass flow rate -9.74E-11 kg/s is indicative of the fact that the solution converged. Diffusivity values were varied

during the simulation from 10 – 0.1 m^2/s and storativity values calculated range between 2.2E-6 to 1.8E-4 with an average of 3.74E-5. The

3. Contaminant Spread and Distribution

The 1D ADDE was solved analytically by Laplace Transform and numerically by Finite Difference Method. Both the analytical and numerical solutions enable solution verification and enhance confidence in the results; validation was done [109]. Codes were written for both the analytic and numerical solutions and simulation implemented using MatLab 2013a software installed on HP notebook 6830s with Windows 7 Operating System for Carbon-14 and Strontium-90 in space and time. Analytical and numerical graphs were plotted together for Carbon-14 and Strontium-90 respectively for time durations of 20 years and 100 years in a space of 500 m and radionuclide concentrations monitored 100 m form the source in the flow direction for 20 and 100 years respectively.

Considering Carbon-14, 1 kg/m^3 initial concentration was assumed and in 20 years Carbon-14 spread up to about 270 m in the direction of flow in the domain. Both the analytical and numerical graphs plotted overlapped indicating that for a time far less than the half-life of the radionuclide the numerical solution equals the analytical solution as the numerical error is not enhanced by the time. In the case of Strontium-90, 1 kg/m^3 was used and in 20 years Strontium-90 spread was up to about 300 m. Both analytical and numerical graphs were plotted, and the numerical graph lagged behind the analytical graph. The numerical graph showed that for a time close to the half-life of Strontium-90, the numerical error was enhanced causing numerical graph to lag behind the analytical graph.

The temporal distribution of Carbon-14 was monitored in a well 100 m in the direction of flow for 20 years. Both the analytical and the numerical graphs were plotted and were found to overlap. It was clear from the temporal graph of Carbon-14 that about 0.45 kg/m^3 of Carbon-14 were observed to have been recorded in a well 100 m in the flow direction for duration of 20 years. The temporal distribution of Strontium-90 was monitored from a well 100 m in the direction of flow for 20 years. For 1 kg/m^3 that leaked, it was observed that both the numerical solution deviated from the analytical solution and the deviation was enhanced by the large time duration of 20 years that was close to the half-life of Strontium-90. Again the Strontium-90 concentration observed in the well for numerical solution was about 0.3 kg/m^3 which is half of what the analytical solution was observed to have recorded.

Two dimensional ADDE was modelled for homogeneous flow with anisotropic dispersion of radionuclide. The radionuclide transport equation involved advection, hydraulic dispersion, sorption and decay processes. However due to the complex nature of 2D algebraic numerical and analytical solutions and insufficient time availability, the analytical solution obtained by [103] for a similar 2D ADDE was coded and simulated using MatLab R2013a. The radionuclide transport simulation showed the pattern of Carbon-14 and Strontium-90 distribution in the Dahomeyan System. The simulations of Carbon-14 and Strontium-90 for the durations of 30 years and 100 years showed different degrees of distributions. Though the radionuclide advected, dispersed and decayed in the longitudinal direction, it covered a lesser distance than the extent to which it dispersed and decayed in the transversal direction which may be attributed to the nature of hard rock in the Dahomeyan System.

Analyses of the surface graphs for Carbon-14 and Strontium-90 radionuclide transport showed dispersion dominant movement transversally over advection dominant movement longitudinally. The Peclet number determined for the 2D ADDE using MatLab simulation ranges between 0.2 - 6 along longitudinal direction covering a distance of 300 m. For uniform flow in the longitudinal direction the radionuclide undergo advection, dispersion and decay whiles transversally the radionuclide undergo dispersion and decay. The Peclet number shows that initially in the flow simulation dispersion was dominant transversally as advection was about 0.2 and increases along flow direction. The MatLab R2013a code is located in **Appendix F.**

The results provide useful information on contaminant spread in the Dahomeyan System and shall contribute to locating a radioactive waste repository in the Accra Plains to properly and safely isolate radioactive waste from the environment. However, the limitation of this research was that the many methods available in estimating transmissivity and storativity were not exhaustively explored but rather Theis and Cooper Jacob methods were used in estimating the transmissivity for pumping well and storativity using a monitoring well respectively. The numerical simulation software available ANSYS Fluent 13.0 posed some challenges in terms of its features and performance capabilities and was not used to model the radionuclide transport. Notwithstanding the limitations, the study has been useful and may predict the behaviour of groundwater flow and how the radioactive contaminant spreads in Dahomeyan System in space and time.

The problems encountered in solving numerical equations include instability, convergence, and numerical oscillation. Instability results when the difference between the exact solution and the numerical solution becomes extremely large in a

few times steps. The instability was avoided by selecting an under relaxation factor ω, greater or equal to zero. Groundwater numerical models calculate solution of large sets of simultaneous algebraic equations using complex matrix solution techniques (solvers). The solution techniques most often are iterative where the solution is through successive approximation until a good solution is obtained (model converged on the solution) [110].

Numerical oscillations occur in solving numerical equations when large values of Δt is considered. This occurs when computed values of radioactive contaminant concentration fluctuate about the true (analytical) solution. Numerical oscillation can be avoided by computing the capacitance and conductance matrix for the smallest element in the mesh, obtain minimum value of α for the element and compute Δt and α from $\Delta t = \alpha/(1-\omega)$ and $\omega > 1$. Thus instability will not occur if $\omega \geq 1/2$ and numerical oscillation will not occur if $\Delta t = \alpha/(1-\omega)$ where e.g., $\alpha = 0.3$ [81].

For accuracy and stability two dimensionless numbers Peclet number and Courant number were used to characterize ground water flow and contaminant transport. Peclet number determines the predominant type of solute transport (i.e. advection divided by dispersion) in relation to coarseness of the finite element grid [111]. Peclet number is given as $Pe = \boldsymbol{v}\Delta x/D$, where $\boldsymbol{v}$ is the pore water velocity, Δx is the characteristic length of the finite element and D is the dispersion coefficient. Courant number $Cu = v\Delta t/\Delta x$ must be less or equal to one when the time step Δt for the grid is small for the flow. The v represents Darcy velocity and Δx is the space step [72].

4. Possible repository site

During ANSYS Fluent 13.0 calibration, the storativity for Dahomeyan System was found to range from 2.2E-6 – 1.8E-4 for a diffusivity range of 10.0 – 0.1 m^2/s. The

storativity values from this research show a more confined domain than the storativity given for confined aquifer in the range of 5.0E-05 to 5.0E-03 [15]. The storativity results also compare well with Igneous and Metamorphic rocks in **Appendix E** [81]. Transmissivity, diffusivity, and storativity values are critical determinants for how fast or slow groundwater and radioactive contaminant can flow in the Dahomeyan System. The potential areas to locate radioactive waste facility are areas where the storativity is smallest since areas of higher storativity indicate semi-confined aquifers [112]. The numerical computer solution of flow velocity was verified and validated by comparing with that from the field method (exact solution). The results of the simulation show that groundwater flow in Dahomeyan System was very slow and in order of 10E-8 m/s on average.

The numerical simulation software used ANSYS Fluent 13.0 posed some challenges in terms of its features and performance capabilities and was not used to model the radioactive contaminant transport. Another limitation of this research was that the many methods available in estimating transmissivity and storativity were not exhaustively explored but rather Theis and Cooper Jacob methods were used in estimating the transmissivity for pumping well and storativity using a monitoring well respectively. Notwithstanding the limitations, the study has been useful and can predict the behaviour of groundwater flow and radioactive contaminant concentration and how the radioactive contaminant spreads in the study area.

CHAPTER FIVE

CONCLUSIONS AND RECOMMENDATIONS

This chapter presents the conclusions and recommendations of the research. The chapter also highlights the implications of the results, makes recommendations for practice and offers suggestions for further research.

5.1 Conclusions

Based on the findings from the study conducted in the Dahomeyan System, the following conclusions were drawn:

- The secondary/effective porosity of the rocks in the study area estimated based on researchers analysis was 0.11 that was used in modelling radioactive contaminant transport.
- The transmissivity and hydraulic conductivity estimated using field methods were 3.74E-5 m^2/s and 1.58E-6 m/s of the study area.
- The major direction of groundwater flow was found to be in the south-southeast direction was used as flow direction for radioactive contaminant transport in the domain.
- The hydraulic gradient 0.18, and flow velocity 3.43E-8 m/s determined in direction of flow made the groundwater flow to be laminar
- 2D transient groundwater flow equation in addition to 2D and 1D transient ADDEs were formulated and were used to model groundwater flow and radioactive contaminant transport in the domain.
- Laplace transform solution of 1D ADDE analytical solution was developed to show radioactive contaminant concentration distribution in confined saturated domain of the Dahomeyan System in space and time

- Implicit finite difference solution for 1D ADDE was developed to give the numerical solution of radioactive contaminant concentration distribution in confined saturated domain of the Dahomeyan System in space and time
- The results for groundwater flow simulation using ANSYS Fluent 13.0 showed that flow was laminar with Re = 0.035 and courant number Cu < 1.5E-7, mass flow rate = -9.2E-11 kg/s. The flow pattern showed that groundwater flow in the longitudinal direction was highly resisted by the nature of the domain and initially the flow was dominant in the transversal directions due to preferential flow paths.
- The average storativity value 3.74E-5 of the rocks calculated showed the Dahomeyan System is confined and suitable for locating radioactive waste repository.
- The 1D analytical and numerical distribution of the radioactive contaminant C-14 and Sr-90 in space showed that both radioactive contaminants spread to a distance of approximately 300 m in 20 years of leakage and approximately 500 m in 50 years of leakage. Both C-14 and Sr-90 have the same distribution in the Dahomeyan System as [102] indicated.
- The 1D analytical and numerical distribution of the radioactive contaminant C-14 and S-90 as monitored in a well 100 m along the flow direction for a period of 20 years show that approximately 0.8 kg/m^3 of 1 kg/m^3 of C-14 was observed to have appeared in the well and for 50 years analytical result showed that approximately 0.9 kg/m^3 of 1 kg/m^3 of Sr-14 was observed and numerical result showed that approximately 0.4 k/m^3 of 1 k/m^3 of Sr-14 was observed.

The effective porosity, hydraulic parameters (i.e., T, K, S), flow velocity and the hydraulic gradient were found to be small which reflected on the slow spread or

movement of radioactive contaminants in the study area. The nature of the crystalline rocks and their resistance to flow coupled with the flow velocity determined qualify the crystalline rocks of the study area for that matter the Accra Plains as suitable domain for radioactive waste repository.

Based on the transmissivity values calculated for the domain, the smaller the storativity of order 10^{-6} the more confined the domain is and the bigger their values the more semi-confined the domain is of the order 10^{-4}. Therefore, Dahomeyan System is confined and the vicinity of boreholes BH5, BH8, and BH10 are suitable for locating radioactive waste repository since they are more confined.

5.2 Recommendations

The following recommendations are for consideration by the appropriate institutions in Ghana:

- Radioactive waste disposal authorities in Ghana should consider effective porosity value of less than 0.1, transmissivity value of order 10^{-6} m^2/s or less and storativity value of order 10^{-6} or less as a contribution to locating radioactive waste site.
- Groundwater flow and radioactive contaminant transport in the Dahomeyan System should be simulated using apparent flow velocity of order 10^{-8} m/s or less.
- Groundwater research institutions should consider storativity value as contribution in determining whether groundwater zones are confined and/or unconfined. Confined domains should have storativity values of order less than 10^{-4} where storativity values of order greater 10^{-4} exhibit unconfined domains.
- The 1D ADDE developed may be used in estimating the spread of radioactive contaminant concentration in space and time in the domain.

5.3 Suggestions for Further Research

The following are suggested for further research:

1. Methods should be developed to improve procedures outlined for estimating total porosity and effective porosity of Dahomeyan System in this research work.
2. Further research is necessary that make use of different methods in estimating the hydraulic conductivities and compare their values with that of Theis and Cooper-Jacob method for accuracy.
3. The field storativity calculated do not compare well with that calculated using ANSYS Fluent 13.0. The field storativity calculated showed an unconfined domain where storativity calculated from ANSYS Fluent showed confined domain. Monitoring boreholes need to be drilled in the Dahomeyan System and data taken to verify the storativity estimated for the Dahomeyan System.
4. Detailed geochemistry on the aquifer system in relation to contaminants dispersion should be investigated in the Dahomeyan System.

REFERENCES

[1] Glover E. T. and Fletcher, J. J. (2000). *National waste management infrastructure for the safe management of radioactive waste in Ghana*. WM'00 Conference, Tucson, AZ

[2] Salmi, M. H. (1985). Studies of groundwater flow conditions in crystalline bedrock in southern Finland and its significance to the final disposal of nuclear waste. *Geological Survey of Finland:* Nuclear Waste Disposal Research, Report 42.

[3] Rao, K. R. (2001). Radioactive Waste: The Problem and its Management. *Current Science*, 81, 1534

[4] Muff, R. and Efa, E. (2006). *Explanatory Notes for the Geological Map for Urban Planning of Greater Accra Metropolitan Area*. Ghana-Germany Technical Cooperation Project: Environmental and Engineering Geology for Urban Planning in the Accra-Tema Area.

[5] Glover, E. T., Akiti, T. T. and Osae, S. (2012). Major ion chemistry and identification of hydrogeochemical processes of groundwater in the Accra Plains. *Elixir Geosciences 50*: 10279-10288

[6] Diodato, D. M. (1994). *A compendium of Fracture Flow Models*. US Department of Defence, United States Army, Europe, Hohenfels, Germany.

[7] Teiku, W. A., Njandjock, P. N., Bisso, D., Atangana, Q. Y. and Nlomgan, J-P. S. (2012). Hydrogeophysical Parameters Estimation for Aquifer Characterization in Hard Rock Environment: A Case Study from Yaounde, Cameroon. *Journal of Water Resource and Protection, Scientific Research,* 4: 944-953

[8] Akiti, T. T. (1987). *Environmental isotope study of groundwater in crystalline rocks of the Accra Plains, Ghana*. Proceedings of the 4th Working Meeting, Isotopes in Nature, Leipzig, September 1986.

[9] Kortatsi, B. K. and Jorgensen, N. O. (2001). The origin of high salinity waters in the Accra Plains groundwaters. *First International Conference on Saltwater Intrusion and Coastal Aquifers* – Monitoring, modelling, and management. Morocco.

[10] Dawood, A. M. A., Akiti, T. T. and Glover, E. T. (2012). Seismic Refraction Investigation at a Radioactive Waste Disposal Site. *Geosciences, 2*(2):7-13

[11] Efa, E., Martin, N. and Muff, R. (2006). *Explanation notes for the hydrological map for urban planning of Greater Accra Metropolitan Area*.

Ghana-Germany Technical Cooperation Project: Environmental and Engineering Geology for Urban Planning in the Accra-Tema Area, Ghana.

[12] Muff, R. and Quaye, J. (2006). *Explanatory notes for the Constraint Map for Waste Disposal Sites of Greater Accra Metropolitan Area with Some Considerations on Waste Management and Engineering Waste Disposal Sites*. Ghana-Germany Technical Cooperation Project: Environmental and Engineering Geology for Urban Planning in the Accra-Tema Area, Ghana.

[13] Zhou, Y. and Li W. (2011). A review of regional groundwater flow modelling. *Geoscience Frontiers*, 2(20): 205-214

[14] Bear, J. and Cheng, A. H. D. (2010). *Modelling groundwater flow and contaminant transport, Vol. 23*. Springer, New York.

[15] Kruseman G. P. and de Ridder N. A. (2000). Analysis and Evaluation of Pumping Test Data, (2nd ed.). International Institute of Land Reclamation, Netherlands.

[16] Fetter, C. W. (2001). Applied hydrogeology (4th ed.) Prentice Hall, Inc., New Jersey.

[17] Yeboah, S. A. and Ameyaw, Y. (2012). Analysis of groundwater quality for three selected communities in the Ga East Municipality Assembly (GEMA) in the Greater Accra Region of Ghana. *International Journal of Science and Nature*, Vol. 3(4):853-856

[18] Kankam-Yeboah, K., Darko, P. K., Nishigaki, M. (2005). Sustainable Groundwater Exploitation under Natural Conditions in Southern Ghana. *Journal of the Faculty of Environmental Science and Technology, Okayama University, 10*(1): 83-88

[19] Gyau-Boakye, P. and Dapaah-Siakwan, S. (2000). Groundwater as source of rural water supply in Ghana. *Journal of Applied Science and Technology (JAST), 5(*1 & 2): 77-86

[20] Ackah, M., Agyemang, O., Anim, A. K., Osei, J., Bentil, N. O., Kpattah, L., Gyamfi, E. T. and Hanson, J. E. K. (2011). *Assessment of groundwater quality for drinking and irrigation: The case study of Teiman-Oyarifa Community, Ga East Municipality, Ghana*. Proceedings of IAEES *1*(3-4): 186-194

[21] Glover, E. T., Akiti, T. T. and Osae, O. (2013). Environmental Stable Isotope Studies of Groundwater in the in the Accra Plains. *Elixir Pollution*. *55*: 12813-12819

[22] Davis, J. A. and Kent, D. B. (1990). Mineral-water interface geochemistry. *Rev. Mineral*. *23*: 177–260

[23] Essel, P., Amisigo, B. and Akiti, T. T. (2011). Solute transport model for radioisotopes in layered soil. *Elixir Pollution*, 41: 6041-6044

[24] Yeboah, S., Akiti, T. T. and Fletcher, J. T. (2014). Numerical modelling of radionuclide migration through a borehole disposal site. *SpringerPlus* 3, 155.

[25] Schmelling, S. G. and Ross, R. R. (ND). Superfund Ground Water Issue. *Contaminant transport in fractured media: Models for decision makers.* United States Environmental Protection Agency. EPA/540/4-89/-004.

[26] Driscoll, F. G. (1989). *Groundwater and wells*. (2nd ed.). St. Paul, Minnesota: Johnson Filtration System Inc.

[27] Johnson, T. (2005). Specific capacity – a measure of a well performance, well problems, and aquifer transmissivity: *Technical Bulletin*, *1*(2).

[28] Theis, C.V. (1935). The relationship between lowering of the piezometric surface and the rate and duration of discharge of a well using ground-water storage, *Trans. American Geophysical Union*, *16*(2): 519-524

[29] Williams, J. A. and Soroos, R. L. (1973). Evaluation of Methods of Pumping Test Analyses for Application to Hawaiian Aquifers. Technical Report No. 70

[30] Cooper, H. H. and Jacob, C. E. (1946). A generalized graphical method for evaluating formation constants and summarising well-field history. *Transactions, American Geophysical Union*. 27, 526-534

[31] Driscoll, T. and Dickey S. K. (2012). *Tierra Del Sol Solar farm*, California.

[32] Freeze, R. A. and Cherry, J. A. (1979). *Groundwater*. Prentice Hall, Inc., New Jersey.

[33] Doll, P. and Fiedler, K. (2008). Global-scale modelling of groundwater recharge.

[34] Nyende, J., Van, T. G., and Vermeulen, D. (2013). Conceptual and numerical model development for groundwater resources management in a regolith-fractured-basement aquifer system. *Earth Science and Climate Change*, 4:5.

[35] Gaspà, M. (2004). *Use of hydrochemical, microbiological and physical monitoring to determine contamination mechanisms of spring water discharging from a deeply weathered regolith aquifer, Kampala-Uganda*. University of Neuchâtel, Switzerland.

[36] Abdelaziz, R. and Merkel, B. J. (2012). Analytical and numerical modelling in a fractured gneiss aquifer. *Journal of Water Resource and Protection*, 4: 657-662

[37] De Smedt, F. (2009). *Groundwater Hydrology*. Course Notes, Department of Hydrology and Hydraulic Engineering, Free University, Brussel, Belgium.

[38] Driscoll, F. G. (1986). *Groundwater and wells*. Johnson Division, St. Paul, Minnesota, USA.

[39] (http://il.water.usgs.gov/pubs/ofr01-50_chapter4_3.pdf).

[40] Aggarwal, P. K., Froehlich, K. and Kulkarni, K. M. (ND). Environmental isotopes in groundwater studies. *Groundwater*, Vol. 2.

[41] Clark, I. D. and Fritz, P., (1997). *Environmental isotopes in hydrogeology. International standard*. CRC Boca Raton, Lewis, Florida, USA.

[42] Lucas, L. L. and Utewenger, M. P. (2000). Comprehensive Review and Critical Evaluation of the Half-Life of Tritium. *Journal of Research of the National Institute of Standards and Technology*, *105*(4): 541-549

[43] Freeze, A. B. (1971). Three-Dimensional, Transient, Saturated-Unsaturated Flow in Groundwater Basin. *Water Resources Research*, *7*(2):

[44] Fletcher, J. J. (2000). *Radioactive waste arising in Ghana*. Proceeding of Seminar on Understanding and Implementation of the Regulations on Radioactive Waste Management in Ghana, Accra, October 9-11, 2000.

[45] Darko and Fletcher (1998). National waste management infrastructure in Ghana. Journal of Radiological Protection, 18(4): 293-9

[46] Singhal, B. B. S. and Gupta, R. P. (2010). *Applied Hydrogeology of Fractured Rocks* (2nd ed.). Springer, Netherlands.

[47] Streltsova, T. D. (1977). Storage properties of fracture formations. In: Dilamarter, R. R. and Csallany, S. C. (Eds), *Hydtrologic problems in karst regions* (pp. 188-192). Bowling Green, KY: Western Kentucky University, USA.

[48] National Research Council (1996). US committee on fracture characterization and fluid flow. Rock Fractures and fluid flow: Contemporary understanding and applications, pp 29-35. National Academy Press, Washington DC.

[49] Novaskowski, K., Milloy, C., Gleeson, T., Praamsma, T., Levison, J., and Hall, K. (2007). *Groundwater recharge in a gneissic terrain having minimal*

drift cover. In: Ottawa 2007 Joint CGS/IAH-CNC Groundwater Conference, Ottawa, Ontario, October 21-24, 2007

[50] Bear, J. (1993). Modelling flow and contaminant transport in fractured rocks, in Flow and Contaminant Transport. In Bear, J., Tsang, C. F. and G. De Marsily (Ed). *Fractured Rock*, Academic Press, NY.

[51] Lee, C. and Farmer, I. (1993). *Fluid flow in discontinuous rocks*. Chapman and Hall, NY.

[52] Wilson, C. R. and Witherspoon, P. A. (1985). Steady state flow in rigid network of fractures, *Water Resource Research*, *10*(2): 328-335

[53] Bodin, J., Porel, G. and Delay, F. (2003c). Simulation of solute transport in discrete fracture networks using the time domain random walk method. *Earth Planet. Sci. Lett., 6566*:1-8

[54] Barrenblatt, G. I., Zheltov, I. P. and Kochina, I. N. (1960). Basic concepts in the theory of seepage of homogeneous liquids in fissured rocks. *J. Appl. Mech., 24*: 852-864.

[55] Boulton N. S. and Streltsova T. D. (1977). Unsteady flow to a pumped well in a fissured water-bearing formation. *Journal of Hydrology*, *35*: 257–269

[56] Long, J., Remer, J., Wilson, C. and Witherspoon, P. (1982). Porous media equivalents for networks of discontinuous fractures. *Water Resource Research*, *18*(3):645–658

[56] Eaton, T. T. (2006). On the importance of geological heterogeneity for the flow simulation. *Elsevier Sedimentary Geology*, *184*:187-201

[57] Shapiro, A. M. (1987). Advances in Transport Phenomena in porous media. *NATO ASI Series*, *128*:405-471

[58] Berkowitz, B., Bear, J. and Braester, C. (1988). Continuum models for contaminant transport in fractured porous formations. *Water Resour. Res., 30(6):*1765-1773

[59] Schwartz, F. W. and Smith, L. (1988). A continuum approach for modelling mass transport in fractured media. *Water Resources Research* 24. doi: 10.1029/88WR00014

[60] Neuman, S. P. (1990). Universal scaling of hydraulic conductivities and dispersivities in geologic media. *Water Resour. Res., 26(8):*1749-1758.

[61] Streltsova, T. D. (1988). Well testing in heterogeneous formations. pp. 431, John Wiley, NY.

[62] Germain and Frind, (1989). Modelling of contaminant migration in fracture networks. Effects of matrix diffusion. Proceedings of the International Symposium on Contaminant Transport in Groundwater, Stuttgart, Federal Republic of Germany: 267-274

[63] Wang, H. F. and Anderson M. P. (1995). Introduction to groundwater modeling. Finite Difference and Finite Element Methods. Academic Press Inc., San Diego, California, USA.

[64] Toth, J. (1962). A Theory of Groundwater Motion in Small Drainage Basins in Central Alberta, Canada. *Journal of geophysical Research*, 69: 4375-4387

[65] Toth, J. (1963). A Theoretical Analysis of Groundwater Flow in Small Drainage Basins. *Journal of Geophysical Research*, 68:4795-4812

[66] Engelen, G. B. and Kloosterman, F. H. (1996). *Hydrological system analysis: methods and application.* In: Water Science and Technology Library, Vol. 20. Kluwer Academic Publishers, p. 149

[67] Toth, J. (1971). Groundwater discharge: a common generation of diverse geological and morphological phenomena. *Bulletin of the International Association of Scientific Hydrology XVI*, 9-24.

[68] Toth, J. (1972). *Properties and manifestations of regional groundwater movement*. In: Proceeding of 24th International Geological Congress, Montreal, Section 11, (pp. 153-163)

[70] Freeze, R. A. and Witherspoon, P. A. (1966). Theoretical analysis of regional groundwater flow: 1. Analytical and numerical solutions to the mathematical model. *Water Resources Research*, *2*(4): 641-656

[71] Freeze, R. A. and Witherspoon, P. A. (1967). Theoretical analysis of regional groundwater flow: 2. Effect of water table configuration and subsurface permeability variation. *Water Resources Research*, *3*(2), 623e634

[72] Holzbecher, E. and Sorek, S. (2005). Numerical models of groundwater flow and transport. *Encyclopaedia of Hydrological Sciences*, 155: 1401-1414

[73] Silar, J. and Silar, J. (1995). *Using environmental isotopes for groundwater flow analysis in basinal structures*: In Proceedings, Vienna Symposium on Application of Tracers in Arid Hydrology, Vienna, Austria.

[74] Strickland, T. and Korleski C. (2007). Groundwater Flow and Fate and Transport Modeling. Technical Guidance Manual for Groundwater Investigations. EPA, Ohio.

[75] Mercer, J. and Faust, C. R. (1980). Ground-Water modelling: An Overview. *Ground Water*, *18*(2):108-115

[76] Faust, C. R. and Mercer, J. W. (1980). *Ground-water modelling*: Recent Developments. *Ground Water*, *18*(6): 569-577

[77] Punmia, B. C., Ashok, K. J. and Arun, K. J. (1995). *Water Supply Engineering*. Mehra Offset Press, Delhi, India.

[78] De Marsily, G. (1986). *Quantitative Hydrogeology*. Academic Press, London, UK.

[79] ASTM D5979-96 (2008). *Standard guide for conceptualization and characterization of groundwater systems*. American Society of Testing Material Standards, Pennsylvania, USA.

[80] Kumar, C. P. and Ish, F. (2003). Basic Guidelines for Groundwater Modelling Studies. *Ish Journal of Hydraulic Engineering*, *9(*2): 11-21

[81] Istock, J. (1989). Groundwater modelling by finite element method. American Geophysics Union, Washington DC.

[82] Stroud, K. A. and Dexter, J. B. (2007), Engineering Mathematics, Palgrave Macmillan, 6th edition, New York, USA.

[83] Stroud, K. A. and Dexter, J. B. (2011), Advanced Engineering Mathematics, Palgrave Macmillan, 5th edition, New York, USA.

[84] Faust, C. R. and J. W. Mercer. (1980). *Ground-water modelling*: Numerical Models. *Ground Water*, *18*(4): 395-365

[85] Eymard, R., Gallouet, T., Herbin, R., (1997), Finite Volume Methods, Handbook of Numerical Analysis, *P. G. Ciarlet, J. L. Lions (eds),* Vol. 7, pp. 713-1020

[86] Versteeg, H. K. and Malalasekera, W. (2007). An introduction to computational fluid dynamics. The Finite Volume Method (2nd ed.). Pearson Educational Limited, Prentice Hall, Harlow, England.

[87] What Is MatLab. Retrieved November 1, 2014 from http://cimss.ssec.wisc.edu/wxwise/class/aos340/spr00/whatismatlab.htm

[88] Burke, K. (1969). The Akwapim Fault, a recent fault in Ghana and related faults of the Guinea Coast. *J. Min. and Geol.*, V. 4: 29-38

[89] Muff, R., Okla, R., Anokwa, Y. M., Brakohiapa, E., Brown, R., Edifor, D. R., Efa, E., Abel, T. and Leydecker, G. (2006). *Geo-information for land use planning and urban development in the Greater Accra Metropolitan Area*. Ghana-Germany Technical Cooperation Project: Environmental and Engineering Geology for Urban Planning in the Accra-Tema Area, Ghana.

[90] Kankam-Yeboah, K., Dapaah-Siakwan, S., Nishigski, M, and Komatsu, M. (2003). The Hydrogeological Setting of Ghana and the Potential for Underground Dams. *Journal of the Faculty of Environmental Science and Technology, Okayama University*, *8*(1): 39-52

[91] Darko, P. K. (2001). *Quantitative Aspects of Hard Rock Aquifers: Regional Evaluation of Groundwater Resources in Ghana*. Ph.D Thesis, Charles University, Prague, Czech.

[92] Landers, R. A. and Turk, L. J. (1973). Occurrence and quality of groundwater in crystalline rocks of the Llano area, Texas. *Groundwater*, *11*(1): 5-6

[93] Akiti, T. T. (1980). Etudé géochimique et isotopique de quelqués aquifers du Ghana. (Thesis) Univeristé Paris-Sud.

[94] Agyekum, W. A. (2002). *Groundwater resources of Ghana with focus on International shared aquifer boundaries.* CSIR -Water Research Institute, Accra, Ghana. Proceedings of the International Workshop Tripoli, Libya, 2-4 June 2002.

[95] Anokwa, Y., Brown, R., Adifor, D., Amponsah, P., Leydecker, G., Muff, R., and Martin, N. (2006). Environmental and Engineering Map of Greater Accra Area, Geohazard Map, Ghana.

[96] Glynn, P. D. and Plummer, L. N. (2005). Geochemistry and the understanding of groundwater systems: *Hydrogeology Journal*, *13*(1), 263-287.

[97] Ganyaglo, S. Y. (2014). *Hydrogeochemical and isotopic studies of groundwater in coastal aquifers of Ghana*. PhD Thesis, University of Ghana.

[98] Kortatsi, B. K. (2006). Hydrochemical characterization of groundwater in the Accra plain of Ghana. *Environmental Geology Journal*, Vol. 50 pp 299-311

[99] Chapuis, R. P. (1992). Using Cooper-Jacob Approximation to take account of pumping well pipe storage effects in early drawdown data of a confined aquifer. *Ground Water*. *30*(3): 331-337.

[100] U.S. EPA. (1996a). *Documenting ground-water flow modelling at sites contaminated with radioactive substances*. EPA 540-R-96-003. United States Environmental Protection Agency. Washington DC, USA.

[101] Orr, S. (1996). *Evaluation of conceptual models for flow in fractured rocks as applied to the Florence in-situ project*. Retrieved December 3, 2014, from https://portal.azoah.com/oedf

[102] Jussila, P. (2000). Geosphere transport of radionuclides in safety assessment of spent fuel disposal. *STUK-YTO-TR 164*, Helsinki.

[103] Wexler, E. J. (1992). Review of analytical solutions for one, two, and three dimensional solute transport in groundwater systems with uniform flow. *Techniques of Water Resources Investigations of the United States Geological Survey*, USA.

[104] Carslaw, H.S. and Jaeger, J.C. (1959), Conduction of heat in solids 2nd edition, Clarendon Press, Oxford.

[105] ASTM D5609-94 (2002). *Standard guide for defining boundary conditions in ground-water flow modelling.* American Society of Testing Material Standards, West Conshohocken, Pennsylvania, USA.

[106] McWorter and Sunada (1977). Representative total porosity and effective porosity of schist, retrieved May 6, 2015, from http://web.ead.anl.gov/resrad/datacoll/porosity.htm.

[107] UNESCO (1984). *Groundwater in hard rocks*. Project 8.6 of the International Hydrological Programme. Studies and Reports in Hydrology No 23.

[108] Pelig-Ba, K. B. (2009). Analysis of Stable Isotope Contents of Surface and Underground Water in Two Main Geological Formations in the Northern Region of Ghana. *West Africa Journal of Applied Ecology*, *15*(1).

[109] Chrysikopoulos, C. V., Kitanidis, P. K. and Roberts, P.V. (1990). Analysis of One-Dimensional Solute Transport Through Porous Media with Spatially Variable Retardation Factor. *Water Resources Research, 26(2):* 437-446

[110] Wels, C., Mackie, D., and Scibek, J. (2012). Guidelines for groundwater modelling to assess impacts of proposed natural resource development activities. BC MOE Report No. 194001

[111] Šimůnek, J., van Genuchten, M. T., and Šejna, M. (2005), *The HYDRUS-1D Software Package for Simulating the One-Dimensional Movement of Water, Heat, and Multiple Solutes in Variably-Saturated Media*. Department of

Environmental Sciences, University Of California Riverside, Riverside, California, USA.

[112] Johnson, R. H. and Bush, P. W. (ND). Summary of the Hydrogeology of the Floridan Aquifer System in Florida and in Parts of Georgia, South Carolina and Alabama. Professional paper 1403-A. Storage Coefficient.

APPENDIX A: Stratigraphy diagrams extracted for boreholes used

Figures A1, A2, and A3 show extracted stratigraphy of the study area developed from the borehole logs data of boreholes used in this research

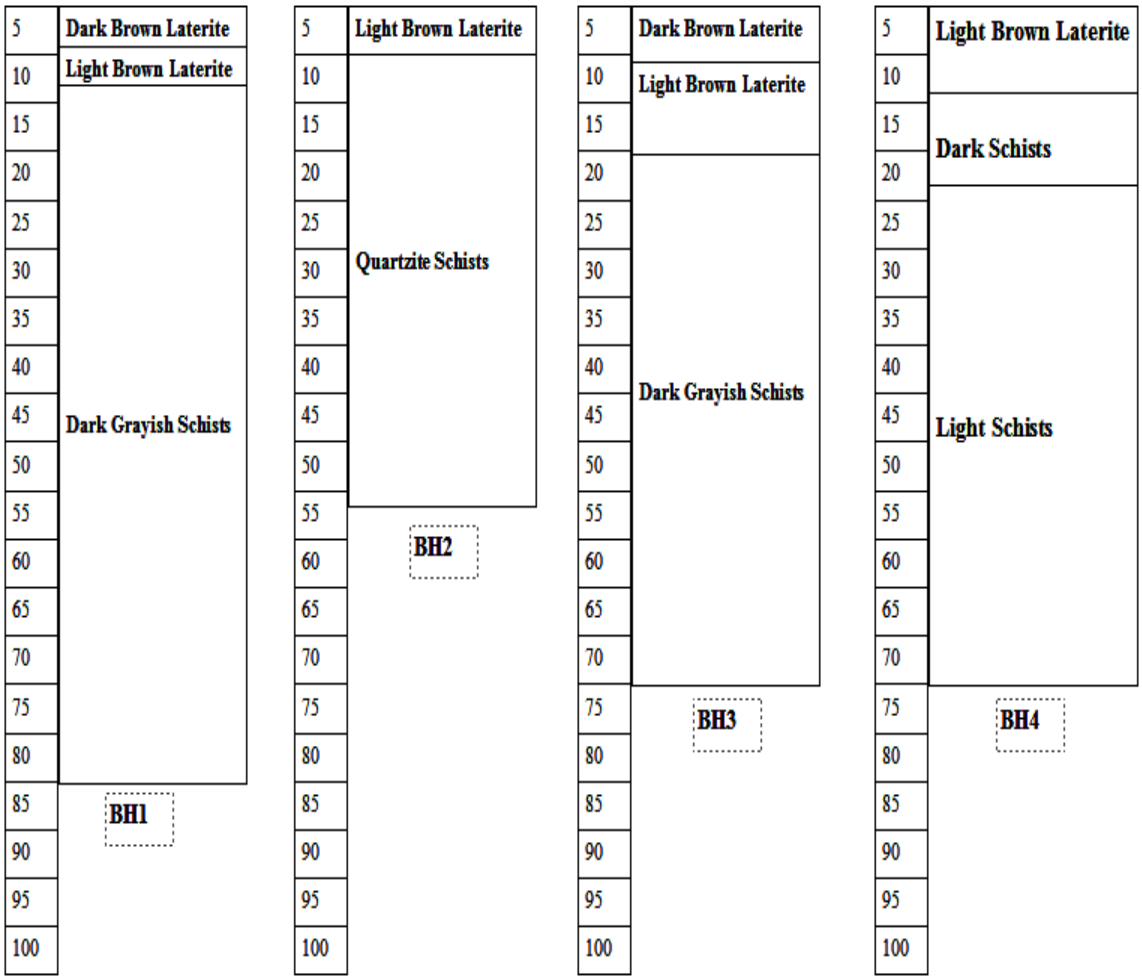

Figures A1: The lithology of boreholes in study area (BH1, BH2, BH3, BH4)

In Figure A1, BH1, no fracture was indicated and BH3, 4 fractures were encountered in dark grayish schists with 2 fractures for BH2 and 3 fractures for BH4 occurring in quartzite schists and light schists respectively. Average groundwater temperature for these boreholes was 26.5^{o}C.

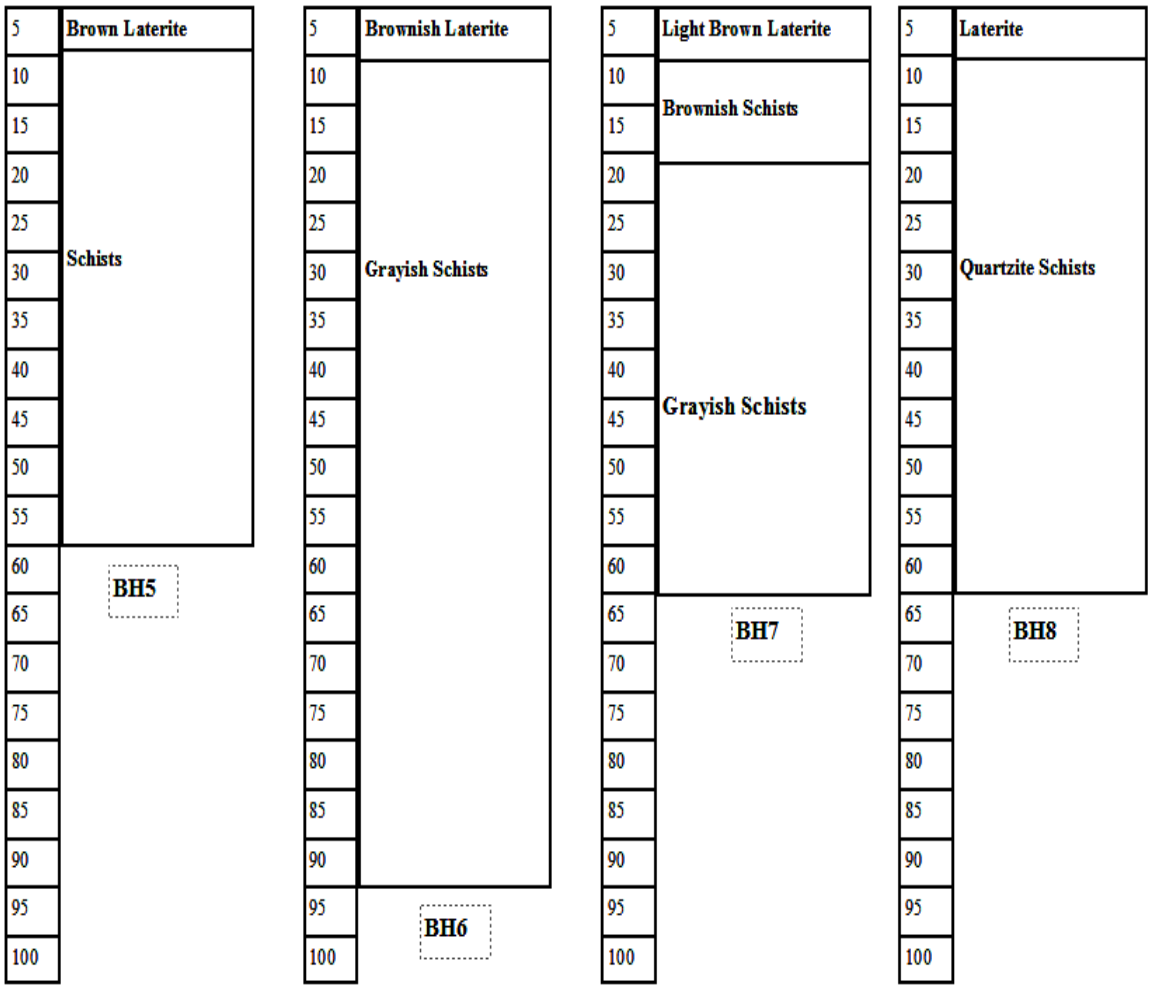

Figure A2: The lithology of boreholes in the study area (BH5, BH6, BH7, BH8)

In Figure A2, 2 fracture aquifers were encountered in schists for BH5. No fracture aquifers were indicated for BH6 and 2 fracture aquifers indicated for BH7 and both were in grayish schists. Three fracture aquifers were found in quartzite schists for BH8. The average groundwater temperature in these boreholes was 26.5^{o}C.

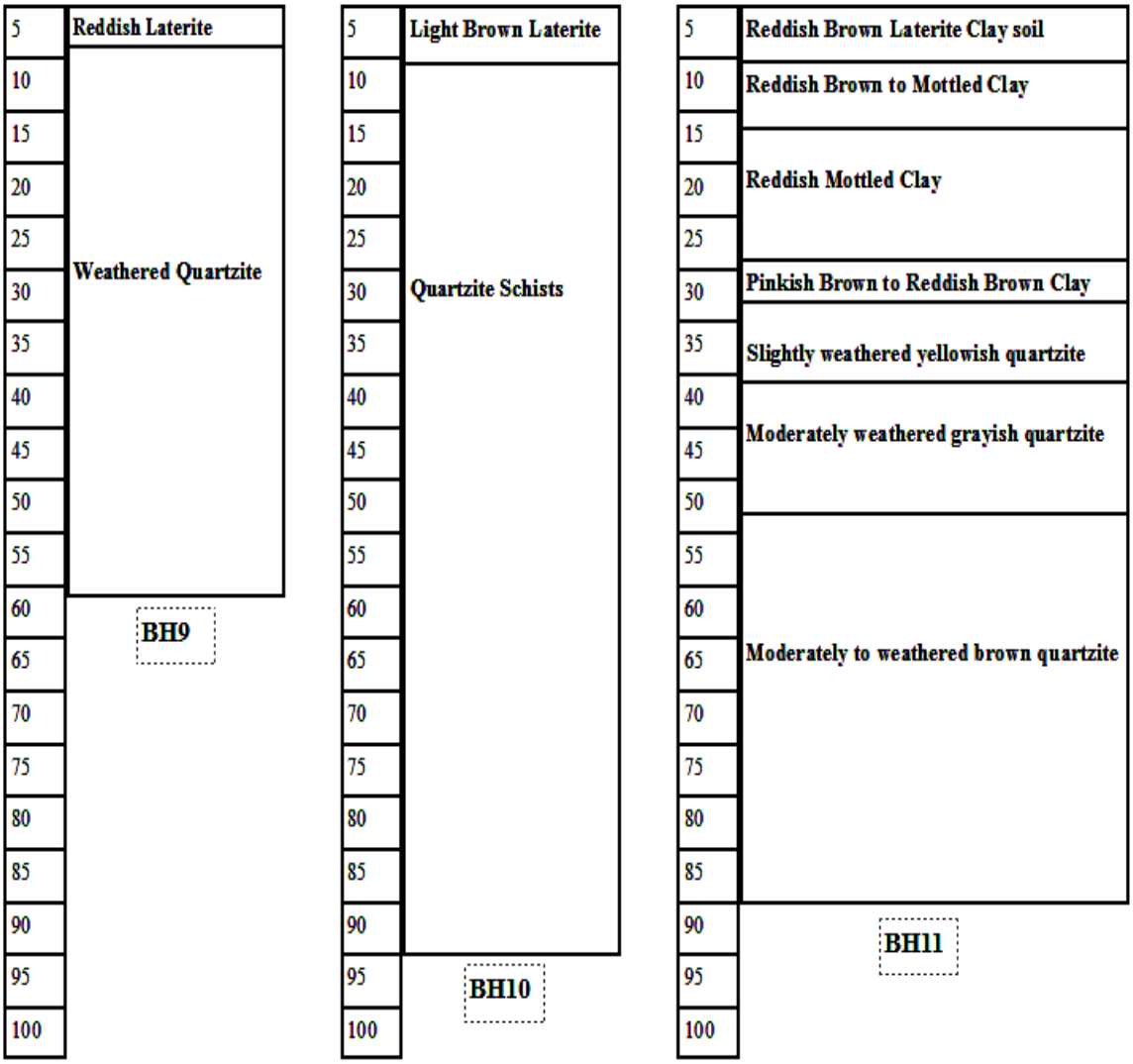

Figure A3: The lithology of boreholes in the study area (BH9, BH10, BH11)

In Figure A3, 3 fracture aquifers were encountered for BH9 in weathered quartzite, no fracture aquifers indicated for BH10 in quartzite schists and fracture aquifers for BH11 were encountered in moderately weathered schists. Borehole BH11 has a monitoring well and was used to calculate storativity that was used as a guide. The average groundwater temperature in these boreholes too was 26.5^{o}C

APPENDIX B: Time-drawdown plots done for boreholes used

Graphs A – J show Time-Drawdown plots developed for Boreholes used

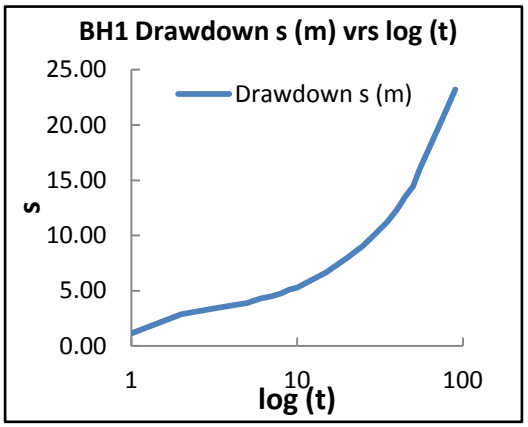

A. Graph of Borehole BH1

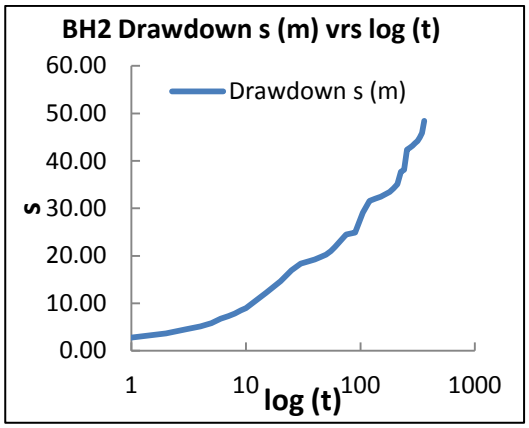

B. Graph of Borehole BH2

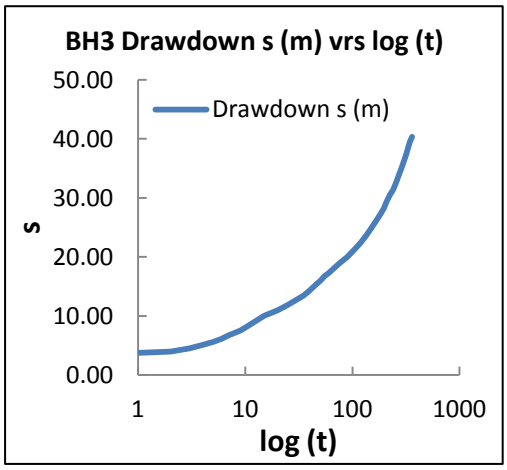

C. Graph of Borehole BH3

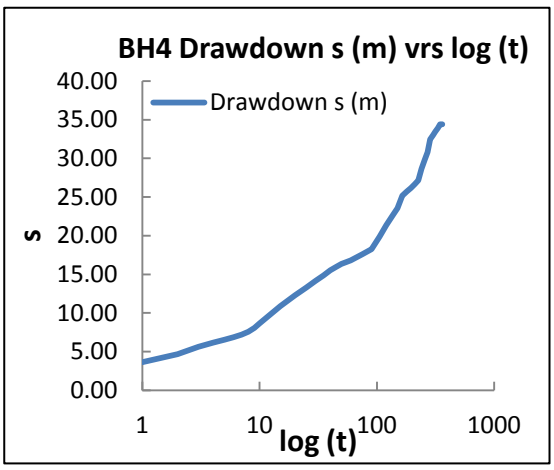

D. Graph of Borehole BH4

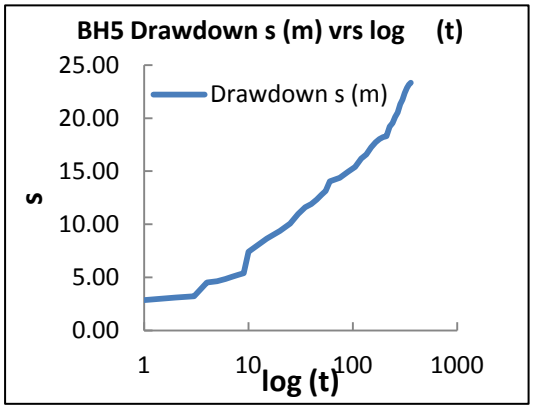

E. Graph of Borehole BH5

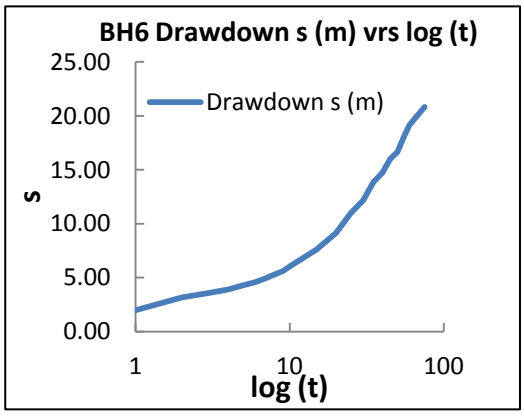

F. Graph of Borehole BH6

Figure B1: A, B, C, D E and F Semi-log plots of drawdown versus log of time.

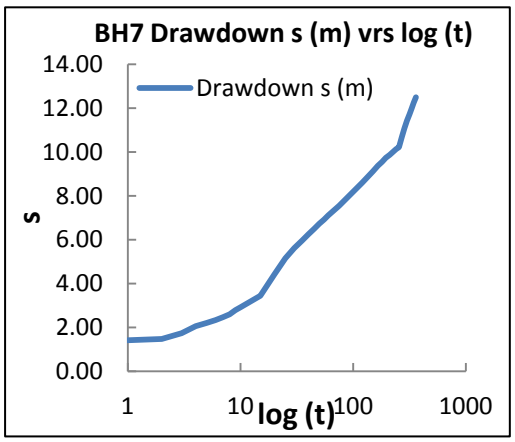

G. Graph of Borehole BH7

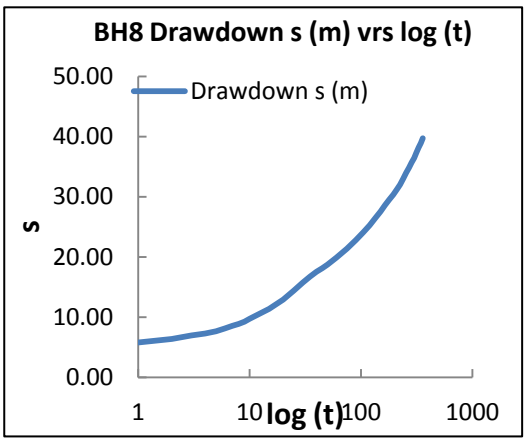

H. Graph of Borehole BH8

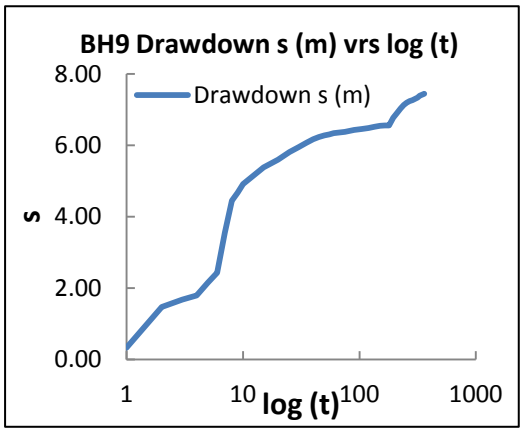

I. Graph of Borehole BH9

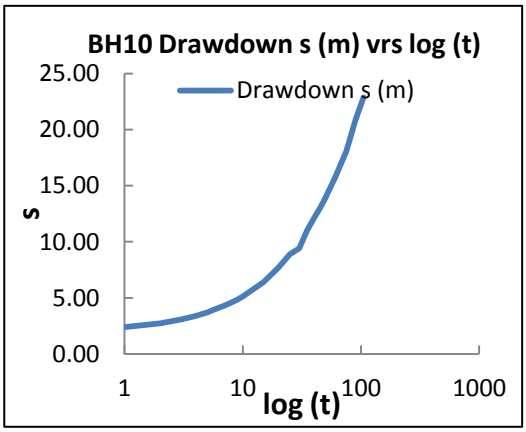

J. Graph of Borehole BH10

Figure B1: E, F, G, H, I, and J Semi-log plots of drawdown against log of time.

APPENDIX C: Primary data of boreholes used

Tables C1 and C2 present summary of boreholes data used in this research.

Table C1: Field data of boreholes drilled in the study area

Community	Ref. No.	Well Depth (m)	Top of Screen (m)	Yield Q (l/min)	SWL (m)	DWL (m)	Specific Capacity (l/min/m)
Sakora	BH1	80	-	5	35.00	58.2	-
Fafraha West	BH2	57	38	10	1.00	49.42	0.21
Kwabenya	BH3	70	39	10	10.69	51.03	0.25
Bethel Presby	BH4	70	38	12	4.36	38.77	0.35
Madina New Mkt	BH5	55	33	12	13.18	36.52	0.51
Babayara Sch	BH6	90	-	7	38.01	58.85	-
Boshye	BH7	60	33	50	2.38	14.88	4.00
Agape Home	BH8	60	30	10	6.33	46.05	0.25
Ashongmang	BH9	56	26	60	2.43	9.88	8.05
Haatso Calvary	BH10	90	-	5	34.01	56.89	-
Abokobi*	BH11		47.6	800			

Source: Community Water and Sanitation Agency, Accra

* Indicates that the borehole was inaccessible by thick bush and GPS coordinate not taken.

Table C2: Primary and secondary data used in plotting hydrogeologic chart

Borehole Ref.	Elevation above sea level (m)	BH depth from sea level (m)	Top of aquifer screen (m)	Static water level (m)	Dynamic water level (m)
BH3	112	42	73	101.31	60.97
BH4	176	106	138	171.64	137.23
BH7	53	-7	20	50.62	38.12
BH9	53	-3	27	50.57	43.12
BH10	66	-14	-	31.00	9.11
BH1	92	32	-	85.67	33.80
BH8	58	-32	28	23.99	11.95
BH5	92	37	59	78.82	55.48
BH2	74	17	36	73.00	24.58
BH6	66	-24	-	28.99	7.15

APPENDIX D: Parameters determined for study area

Table D: Parameters determined for Dahomeyan System of the Accra Plains

Property	Values	Units	Values	SI Units
Aquifer Length			500.0000	m
Aquifer thickness			25.0000	m
Transmissivity in x direction (Tx)	3.7234	m^2/day	4.31E-05	m^2/s
Transmissivity in x direction (Ty)	4.0061	m^2/day	4.64E-05	m^2/s
Hyd. Conductivity in x (Kx)	0.1527	m/day	1.77E-06	m/s
Hyd. Conductivity in x (Ky)	0.1531	m/day	1.77E-06	m/s
Total porosity			0.2700	
Effective porosity			0.1100	-
Hyd. Gradient in x direction Ix			0.0184	-
Hyd. Gradient in x direction Iy			0.0066	-
App. Flow rate in x direction	0.0732	m^2/day	8.47E-07	m^2/s
App. Flow rate in y direction	0.0368	m^2/day	4.26E-07	m^2/s
App. Flow velocity in x direction	0.0030	m/day	3.43E-08	m/s
App. Flow velocity in y direction	0.0009	m/day	1.08E-08	m/s
Pore water flow rate in x direction	0.6654	m^2/day	7.70E-06	m^2/s
Pore water vel. in x direction	0.0269	m/day	3.12E-07	m/s
Storativity range	2.2E-6 – 1.8E-4			-
Diffusivity range	10.00 – 0.10			m^2/s
Longitudinal dispersivity			50.0000	m
Transversal dispersivity			5.0000	m
Dispersion coefficient in x direction	1.3473	m^2/day	1.56E-05	m^2/s
Dispersion coefficient in y direction	0.1347	m^2/day	1.56E-06	m^2/s
Temp. of groundwater of the domain			26.5000	^oC
Temp. (De Smedt, 2009)			20.0000	^oC
Water density(De Smedt, 2009)			998.2000	kg/m^3
Dynamic viscosity(De Smedt, 2009)			1.002E-04	Pa.s
Kinematic viscosity(De Smedt, 2009)			1.004E-07	m^2/s
Gravity (De Smedt, 2009)			9.8000	m/s^2
Permeability			1.62E-13	m^2

APPENDIX E: Properties of selected aquifers materials

Table E: Properties of selected aquifers materials

Material	Hydraulic Conductivity, K (m/s)	Specific Storage, S_s* (m^{-1})	Porosity, n	Bulk Density, ρ_b (kg/m^3)
Gravel	10^{0} - 10^{-3}	0.1 - 0.3	0.20 - 0.40	1200 - 1800
Sand	10^{-2} - 10^{-6}	0.1 - 0.4	0.25 - 0.55	1300 - 1900
Silt	10^{-3} - 10^{-7}	0.2 - 0.4	0.35 - 0.60	1200 - 1800
Clay	10^{-7} - 10^{-10}	0.05 - 0.2	0.35 - 0.55	1000 - 1600
Sandstone	10^{-6} - 10^{-10}	0.01 - 0.2	0.25 - 0.50	2000 - 2400
Siltstone	10^{-8} - 10^{-12}	0.01 - 0.2	0.20 - 0.40	2000 - 2400
Shale	10^{-9} - 10^{-13}	0.01 - 0.08	0.01 - 0.10	2000 - 2400
Limestone				
(No solution cavities)	10^{-6} - 10^{-10}	0.01 - 0.05	0.01 - 0.20	2000 - 2500
(solution cavities)	10^{-2} - 10^{-6}	0.01 - 0.20	0 05 - 0.55	1800 - 2000
Igneous & Metamorphic				
(fractured)	10^{-4} - 10^{-8}	0.01 - 0.05	0.05 - 0.15	2000 - 2500
(unfractured)	10^{-10} - 10^{-14}	~0	0.01 - 0.05	2400 - 3000
Basalt				
(fractured)	10^{-2} - 10^{-7}	0.01 - 0.20	0.05 - 0.35	2000 - 2400
(unfractured)	10^{-10} - 10^{-14}	~0	0.01 - 0.10	2400 - 2800
Tuff/Breccia	10^{-5} - 10^{-9}	0.01 - 0.05	0.05 - 0.25	2000 - 2400

Source: (Istock, 1989)
*These values are for unconfined aquifers and the values for confined aquifers will be 100 to 1000 times smaller.

APPENDIX F: Analytical MatLab code developed for 2D ADDE

Carbon-14 Transport Code: Contran Code

```
% This program solves a 2D ADDE for Radionuclide Transport
% in Dahomeyan System
% Program Title: ConTran Code for Carbon-14
% Author: Kafui Tsoeke Agbevanu
% ID: 10008512
% Institution: University of Ghana
% Department: Department of Nuclear Engineering
% Faculty: Computational Nuclear Sciences & Engineering
% Date: 20th June 2015
% Software Used: MatLab R2013a
close all
clear all
clc
% Initialize parameters
xv=0.0269; % average pore water velocity in x direction
xD=1.3473; % dispersion coefficient in x direction
yD=0.1347; % dispersion coefficient in y direction
decay=0.00000046; % decay constant of Carbon-14
kd=0.0001; % distribution coefficient
rhob=2400;% the bulk density of the domain is between 2000 - 2500
prs=0.11; % secondary porosity
R=(1+(kd*rhob)/prs); % retardation factor
vx=xv/R; % damped pore-water velocity
Dx=xD/R; % damped dispersion coefficient in x direction
Dy=yD/R; % damped dispersion coefficient in y direction
y1=0; % lower point of contaminant source
y2=0.00125; % upper point of contaminant source
W=1000; % width of the domain
pi=3.142; % constant pi
L=0.5;
P=(y2-y1)/W;
c0=1; % initial concentration of contaminant
t=36500; %t = 30*365, 100*365
[X,Y]=meshgrid(0:10:300,0:10:300);
 n=0;
 nu=(n*pi)/W;
 B=sqrt((vx)^2+4*(Dx)*((nu)^2*(Dy)+ (decay)));
 M=exp(X*((vx)-B)/(2*(Dx)))*erfc(X-(B*t))/(2*sqrt((Dx)*t));
 N=exp(X*((vx)+B)/(2*(Dx)))*erfc((X+(B*t))/(2*sqrt((Dx)*t)));
 Z1=c0*(L*(P*(cos(nu*(Y)))))*(M+N);
 for n=1:3
    nu=(n*pi)/W;
    P=(sin(nu*y2)-sin(nu*y1))/(n*pi);
    B=sqrt((vx)^2+4*(Dx)*((nu)^2*(Dy)+ (decay)));
    Z2=c0*(L*(P*(cos(nu*(Y)))))*(M+N);
 end
Z=Z1+Z2;
%surface plot of concentration and how it spreads in x and y
directions
figure
surf(X,Y,Z)
xlabel('X, (m)')
ylabel('Y, (m)')
zlabel('C, (kg/m^3)')
legend(' 2D Analytical Solution')
hold on
```

```
%plot of advection distance against concentration
figure
plot(X, Z)
xlabel('X, (m)')
ylabel('C, (kg/m^3)')
legend('1D Analytical Solution')
hold on
%plot of dispersion distance against concentration
figure
Y=0:10:300;
plot(Y, Z)
xlabel('Y, (m)')
ylabel('C, (kg/m^3)')
legend('1D Analytical Solution')
```

Strontium-90 Transport Code

```
% This program solves a 2D ADDE for Radionuclide Transport
% in Dahomeyan System
% Program Title: ConTran Code for Strontium-90
% Author: Kafui Tsoeke Agbevanu
% ID: 10008512
% Institution: University of Ghana
% Department: Department of Nuclear Engineering
% Faculty: Computational Nuclear Sciences & Engineering
% Date: 20th June 2015
% Software Used: MatLab R2013a
close all
clear all
clc
% Initialize parameters
xv=0.0269; % average pore water velocity in x direction
xD=1.3473; % dispersion coefficient in x direction
yD=0.1347; % dispersion coefficient in y direction
decay=0.000094; % decay constant of Strontium-90
kd=0.0001; % distribution coefficient
rhob=2400;% the bulk density of the domain is between 2000 - 2500
prs=0.11; % secondary porosity
R=(1+(kd*rhob)/prs); % retardation factor
vx=xv/R; % damped porewater velocity
Dx=xD/R; % damped dispersion coefficient in x direction
Dy=yD/R; % damped dispersion coefficient in y direction
y1=0; % lower point of contaminant source
y2=0.00125; % upper point of contaminant source
W=1000; % width of the domain
pi=3.142; % constant pi
L=0.5;
P=(y2-y1)/W;
c0=1; % initial concentration of contaminant
t=36500; %t = 30*365, 100*365
[X,Y]=meshgrid(0:10:300,0:10:300);
 n=0;
 nu=(n*pi)/W;
 B=sqrt((vx)^2+4*(Dx)*((nu)^2*(Dy)+ (decay)));
 M=exp(X*((vx)-B)/(2*(Dx)))*erfc(X-(B*t))/(2*sqrt((Dx)*t));
 N=exp(X*((vx)+B)/(2*(Dx)))*erfc((X+(B*t))/(2*sqrt((Dx)*t)));
 Z1=c0*(L*(P*(cos(nu*(Y)))))*(M+N);
 for n=1:3
```

```
    nu=(n*pi)/W;
    P=(sin(nu*y2)-sin(nu*y1))/(n*pi);
    B=sqrt((vx)^2+4*(Dx)*((nu)^2*(Dy)+ (decay)));
    Z2=c0*(L*(P*(cos(nu*(Y)))))*(M+N);
 end
Z=Z1+Z2;
%surface plot of concentration and how it spreads in x and y
directions
figure
surf(X,Y,Z)
xlabel('X, (m)')
ylabel('Y,(m)')
zlabel('C, (kg/m^3)')
legend(' 2D Analytical Solution')
hold on
%plot of advection distance against concentration
figure
plot(X, Z)
xlabel('X, (m)')
ylabel('C, (kg/m^3)')
legend('1D Analytical Solution')
hold on
%plot of dispersion distance against concentration
figure
Y=0:10:300;
plot(Y, Z)
xlabel('Y, (m)')
ylabel('C,(kg/m^3)')
legend('1D Analytical Solution')
```